LITHUANIAN ENERGY INSTITUTE

ANDRIUS TIDIKAS

INVESTIGATION OF NEUTRON TRANSPORT AND RADIOACTIVE PROCESSES IN NUCLEAR FUSION DEVICES

Doctoral Dissertation
Technological Sciences, Energetics and Power Engineering (T 006)

KAUNAS, 2019

Doctoral dissertation has been prepared at the Lithuanian Energy Institute during 2014–2018 at Laboratory of Nuclear Installation Safety. The work was partially funded by the grant from the project “EUROfusion” (Grant agreement no: 633053) and Research Council of Lithuania.

Scientific Supervisor:
Dr. Gediminas STANKŪNAS (Lithuanian Energy Institute, Technological Sciences, Energetics and Power Engineering – T 006).

Interneto svetainė, kurioje skelbiama disertacija, adresas:
http://ktu.edu

Editor:
Jūratė Kulčickytė-Gutaitė (Lithuanian Energy Institute)

The bibliographic information of this issue is available at Martynas Mažvydas National Library of Lithuania National Bibliographic Data Bank (NBDB)

LIETUVOS ENERGETIKOS INSTITUTAS

ANDRIUS TIDIKAS

BRANDUOLIŲ SINTEZĖS ĮRENGINIUOSE VYKSTANČIŲ NEUTRONŲ PERNEŠIMO IR RADIACINIŲ PROCESŲ TYRIMAS

Daktaro disertacija
Technologijos mokslai, energetika ir termoinžinerija (T 006)

KAUNAS, 2019

Disertacija rengta 2014–2018 metais Lietuvos energetikos institute, Branduolinių įrenginių saugos laboratorijoje. Moksliniams tyrimams buvo skirta parama pagal projektą „EUROfusion“ (dotacijos sutartis Nr. 633053). Mokslinius tyrimus rėmė Lietuvos mokslo taryba.

Mokslinis vadovas:
Dr. Gediminas STANKŪNAS (Lietuvos energetikos institutas, technologijos mokslai, energetika ir termoinžinerija – T 006).

Interneto svetainė, kurioje skelbiama disertacija, adresas:
http://ktu.edu

Redagavo:
Jūratė Kulčickytė-Gutaitė (Lietuvos energetikos institutas)

Leidinio bibliografinė informacija pateikiama Lietuvos nacionalinės Martyno Mažvydo bibliotekos Nacionalinės bibliografijos duomenų banke (NBDB).

CONTENTS

Abbreviations

AC – Access Cell
ACP – Activation Corrosion Products
AP – Activation Products
DCLL - Dual Coolant Lead Lithium
DD – Deuterium Deuterium
DEMO - DEMOnstration power plant
DT – Deuterium Tritium
DTE1 – 1st Deuterium Tritium Experiment
DTE2 – 2nd Deuterium Tritium Experiment
DONES - Demo Oriented Neutron Source
FNG – Frascati Neutron Generator
HCLL - Helium Coolant Lead Lithium
HCPB - Helium Coolant Pebble Bed
HFTM – High Flux Test Module
IFMIF - International Fusion Materials Irradiation Facility
ILTIS - Inner Long Term Irradiation Station
ITER - International Thermonuclear Experimental Reactor
JET – Joint European Torus
OLTIS – Outer Long Term Irradiation Station
PbLi – Lithium Lead
TC – Test Cell
TFTR - Tokamak Fusion Test Reactor
TM – Test Module
TT – Tritium Tritium
TTE – Tritium Trace Experiment
WCLL - Water Coolant Lead Lithium

Notations

AR – Armor
BP – Backplate
BZ – Breeder Zone
CP – Caps
FW – First Wall
IB - Inboard
MF – Manifold
OB – Outboard

INTRODUCTION

As for 2015 (European Union 2017), 1627 million tonnes of oil equivalent were consumed within the European Union in order to fulfill the energy demand. Over 50 % of total energy consumed was produced from the solid fuels and petroleum. Subsequently natural gas was responsible for 22 %, nuclear for 14 % and renewables for 13 % shares of total energy consumed. So far EU is heavily reliant on the energy that is exhaustible and can cause pollution and damage to the environment. While EU set goals (European Commision 2014) to reduce general energy consumption and to migrate to cleaner and more sustainable production of energy, such measures might not be sufficient enough with regard to the global energy market. It is projected (U.S. Energy Information Administration 2017) that between 2017 and 2040 yearly energy demand worldwide will increase by 28 %, mostly in the developing countries.

In order to fulfill future energy demands technological breakthrough and development of alternative fuels is a necessity. One of the most promising sources of relatively clean and sustainable energy is nuclear fusion. While nuclear fusion already governs energy production in the Sun, harnessing fusion energy on Earth is still a challenging task. European Union in 2012 (Romanelli et al. 2012) set a goal to produce electricity from nuclear fusion by 2050 as part of broader strategy to achieve a low-carbon society. In 2014 EUROfusion (EURATOM 2014) consortium was established in order to manage European fusion research within Horizon 2020 framework. So far EU allocated almost 850 million euros for EUROfusion in order to proceed to carry on fusion research strategy specified in EFDA roadmap (Romanelli et al. 2012).

Presently, fusion technologies are still in the early stages of development. Many engineering and physics related issues have to be resolved, while technological and legislative basis must be provided as well in order to achieve sustainable and safe energy production. Nuclear fusion devices based on magnetic plasma confinement currently are considered to be the best suited for such task with deuterium and tritium as the fuel for future fusion reactors (Federici et al. 2016).

Unlike fossil fuel based power plants, fusion reactors do not produce carbon dioxide emissions or any other greenhouse gases. Also it does not produce transuranic and other long-lived radioactive waste such as conventional fission reactors. However, fusion reactors are still capable of producing radioactive waste. Part of it is related to the deuterium-tritium fuel. Although the amount of tritium during the operation of the reactor is quite low (Paul et al. 2017), a fraction of it still can get trapped inside the reactor structural materials. Furthermore, during the fusion reaction a high neutron flux is being produced. Neutrons, while being the main heat carriers in the reactor, play an essential part in activation processes, thus making materials they interact with, radioactive.

Such materials are potential hazards to the environment and the reactor itself. Current fusion devices do not produce significant amount of activated materials, however in the future, for large fusion reactors such as ITER or DEMO, material

activation is an unavoidable factor concerning device operation and decommissioning (Federici et al. 2016).

This thesis is devoted for neutron transport and material activation analysis in fusion devices designed towards the goal of enabling clean and sustainable energy production out of nuclear fusion. Material selection is a significant issue in fusion applications and is yet to be resolved. Due to unique conditions present in nuclear fusion reactors, material testing is required in order to evaluate their feasibility. Currently, only *Joint European Torus* (JET) reactor can provide neutron emissions from deuterium-tritium plasma source with particle energies and fluxes relevant for nuclear fusion production. Compared to planned nuclear fusion power plants, JET is a small scale device with short irradiation times. However, JET operation modes and particle energies are pertinent to larger scale fusion devices as well, hence the material for fusion application experiments are set in place. Future nuclear fusion power plants will have to withstand much higher neutron fluxes for significantly longer exposure times so the experience gained at JET might not be sufficient. This issue in material testing leads to the realization of *International Fusion Materials Irradiation Facility DEMO oriented neutron source* (IFMIF-DONES). IFMIF-DONES is deuteron lithium source based accelerator facility with purpose to test fusion relevant materials under long neutron exposure. In comparison to nuclear fusion reactors, neutron energies at IFMIF-DONES should be significantly higher in order to accelerate the material testing process. Material testing at IFMIF-DONES will result in much larger activation inventories compared to JET and similar to those produced in nuclear fusion power plants. Finally, experience gained from JET and IFMIF material testing should be used in realization of *demonstration power plant* DEMO (Federici et al. 2016). In this work material activation in planned JET experiments, anticipated IFMIF operation and in preliminary DEMO operation were analyzed.

Aim of this work

To investigate neutron transport processes and activation characteristics in the nuclear fusion reactor components located near the radiation source.

The tasks of this work

1. Investigation of material activation in JET long term irradiation station after deuterium-deuterium and deuterium-tritium fusion caused neutron irradiation and determination of deuterium-deuterium and deuterium-tritium activation response to different irradiation scenarios.
2. Investigation of neutron reactions and induced activities in IFMIF-DONES Test Cell facility biological shielding structures and DEMO breeder blanket.
3. Determination of DEMO WCLL breeder blanket module activation characteristics.
4. Determination of DEMO fusion power and vacuum vessel volume change influence on WCLL breeder blanket module activation characteristics

5. Investigation of PbLi flow cycle in WCLL blanket module in terms of material activation.

6. Investigation of DEMO neutron spectra influence on structural steel activation.

Defensive propositions of the work.

1. Deuterium-tritium fusion reactions at JET cause significantly larger material activation than deuterium-deuterium reactions. Deuterium-deuterium fusion response to irradiation scenario adjustment in terms of material activation is greater than deuterium-tritium fusion response.

2. In IFMIF-DONES structural steels neutron reactions (n, p) and (n, 2n) are responsible for majority of material activation while in DEMO (n, g) reactions are more common. Materials irradiated at IFMIF-DONES retain relative activity longer than materials irradiated in DEMO environment.

3. Activity inventories in water cooled lithium lead blanket module are dominated by EUROFER 97-3 constituents in afterheat period with exception of tungsten that is more relevant within a year after the end of irradiation. PbLi radionuclides are mainly relevant during the device operation.

4. Increase in fusion power and vacuum vessel size has greater effect on farthest parts of breeder blanket module such as manifold and backplate.

5. Exclusion of PbLi cycle from irradiation scenario does not increase overall activity values in breeder blanket module.

6. Most impactful neutron energy groups for DEMO breeder blanket EUROFER-97 steel correspond to the 4^{th} period metal resonance peaks and 4^{th} period metal (n, p) and (n,2n) reaction peaks.

Practical importance of work.

Neutron interaction with structural and functional materials can cause gamma or secondary particle emissions as well as turn stable nuclei radioactive. Neutrons can also greatly affect mechanical integrity of materials. These processes can be estimated by performing activation analysis. Activation analysis can determine the design and operation limits of nuclear fusion devices. More so, collation of experimental data of nuclear fusion devices and activation analysis are instrumental for validation of nuclear data libraries and neutron transport codes.

The novelty of the work

In this work neutron activation calculation methodology was extended in order to aggregate complex irradiation scenarios for nuclear fusion devices.

A novel approach utilizing sensitivity analysis was presented in order to investigate neutron spectra.

Scope and structure of the dissertation

Thesis consists of introduction, 4 chapters (literature review, methodology, results and conclusions) and lists of publications, conferences and references. Main

thesis material is presented in 90 pages and contain 7 tables and 65 figures. There is also 10 page long annex comprised of 6 tables and 12 figures. 114 works are referred in this thesis.

1.LITERATURE REVIEW

1.1 Nuclear Fusion

Nuclear fusion is a reaction between atomic nuclei, where two or more nuclei presented in close enough distance can fuse into new nucleus. During such reaction a substantial amount of energy can be released. Such energy corresponds to the binding energy of the newly produced nucleus as according to Einstein relationship the mass of an atomic nucleus is less than the sum of the individual the masses of the free protons and neutrons. Nuclear fusion process is governed by Nuclear and Coulomb forces. Nuclear force binds neutrons and protons in a nucleus while Coulomb force makes protons repel each other as they have the same charge. For light nuclei nuclear force is much stronger than Coulomb force hence excess energy can be released after the fusion reaction. Fusion reaction is exothermic until it reaches iron group elements (fig 1.1.), after that the effects of electromagnetic forces turn fusion reaction into endothermic reaction (Martin 2009).

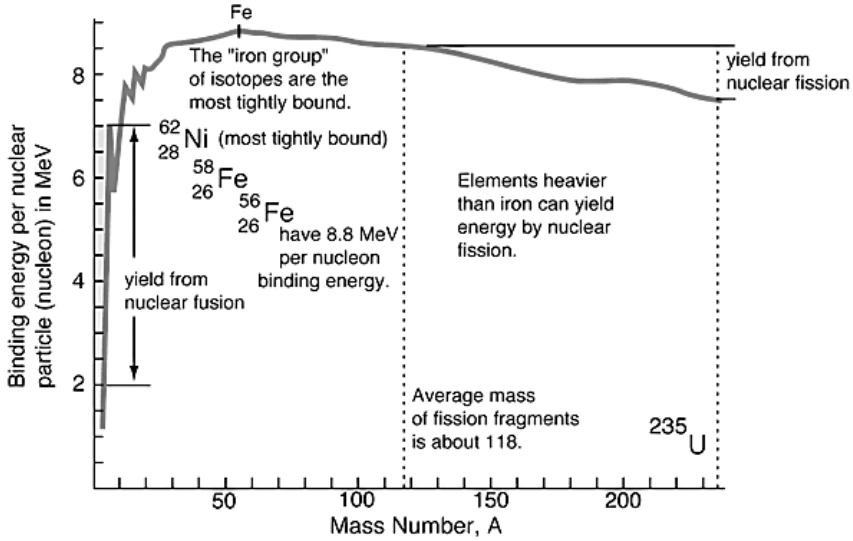

Fig. 1.1. Binding energy curve (Nave 2002)

Naturally nuclear fusion occurs in the stars and it is a primary process responsible for the production of energy. Technological interest in producing fusion reactions on earth rose from the discovery of mass–energy equivalence principle and determination of light nuclei masses. Soon after many attempts followed to exploit newly attained knowledge in order to enable controlled thermonuclear fusion.

1.2 Nuclear Fusion Reactions

While the upper fusion limits are determined by the prevalence of electromagnetic forces, not every light nucleus is suitable for controlled fusion. Plentitude of aspects need to be considered including reaction cross-section, particle energy, material abundance, byproducts, etc.. On the sun the dominant reaction is a proton-proton chain reaction where two protons fuse into unstable He-2 isotope. Subsequently He-2 has a very tiny possibility to decay into deuteron releasing positron and neutrino in the process. However, most of the time He2 decays back into two protons without much energy gain. Other reactions (Bosh ir Hale 1992) proved to be much more energy efficient as well as having much larger reaction cross-section (Fig. 1.2). For controlled fusion Deuterium-Deuterium (DD), Deuterium-Tritium (DT), Tritium-Tritium (TT) and reactions with He-3 are the most employable (Fig 1.2.).

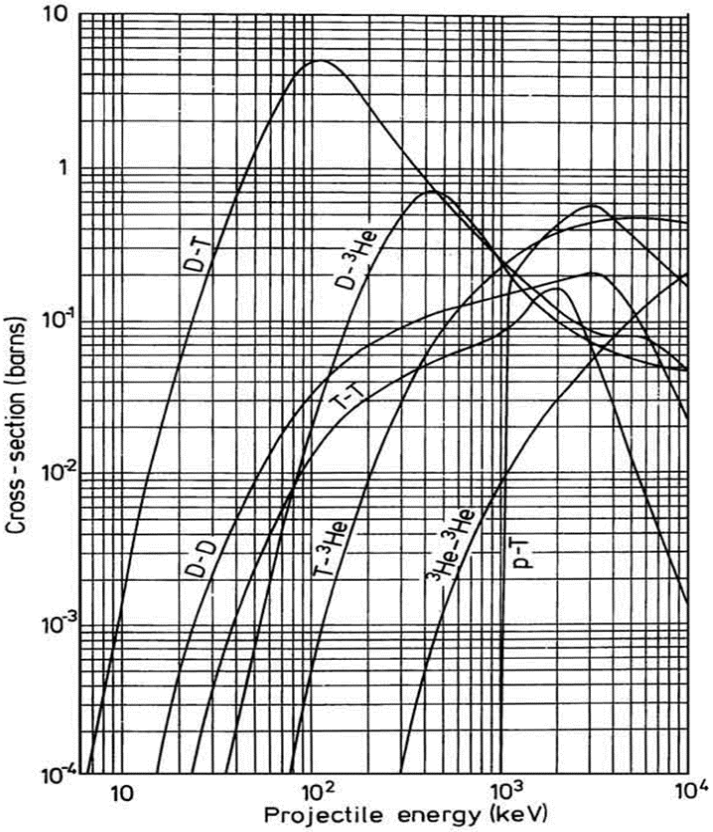

Fig. 1.2. Fusion reaction cross-sections (Bosh ir Hale 1992)

Deuterium-Deuterium reaction is the most commonly used reaction in current experimental fusion devices as the fuel is relatively abundant in nature. Two outcomes of DD fusion are equally possible: reaction in eq. 1.1 results in tritium and proton with 3.022 MeV energy. Proton usually stays in the magnetic confinement

while Tritium might be used in subsequent fusion reactions. Other outcome Eq. 1.2 results in He-3 and neutron with 2.449 MeV energy production.

$$D + D \rightarrow T + p \quad (1.1)$$
$$D + D \rightarrow He3 + n \, (1.2)$$

Among tritium fusion reactions, Deuterium-Tritium (Eq. 1. 3) reaction looks most promising so far as it has relatively high reaction cross section and can be achieved in temperatures between 10 and 1000 keV. Such reaction produces He-4 and 14.029 MeV energy neutron. He-4 is stable and doesn't fuse with any other particles in typical fusion device. More so it is considered a waste and impairs further fusion reactions. However, neutron energy can be harnessed in collision events within fusion device structural material. If temperature is high enough (above 1000 keV) tritium can fuse with proton (Eq. 1.4) producing He-3 and a neutron, however the reaction is endothermic and consumes the excess of 764 keV. Tritium-Tritium is another desirable reaction (Eq. 1.5) to have in a fusion device as apart from He-4 and pair of neutrons it releases majority of energy in terms of electromagnetic radiation (11.332 MeV).

$$D + T \rightarrow He4 + n \, (1.3)$$
$$p + T \rightarrow He3 + n \, (1.4)$$
$$T + T \rightarrow He4 + 2n \, (1.5)$$

Current available Tritium reserves would not be sufficient in case of operation of one large scale fusion reactor (Ni et al. 2013). There are two solutions. Reactor could run on DD plasma until enough Tritium is being produced for subsequent DT operation. This would impair the effectiveness of reactor as DD operation would not yield net electricity in current designs. Other solution would include tritium breeding technologies. Tritium could be breed from lithium (Eq. 1.6-7). Li-6 can produce tritium by interacting with any energy neutron resulting in exothermal reaction. Li-7 can produce tritium in endothermic reaction by interacting with fast neutrons. For breeder technologies in fusion reactors Li-6 is more desirable, however in nature lithium 6 usually makes up less than 8 percent of stable lithium isotopes.

$$Li6 + n \rightarrow He4 + T \quad (1.6)$$
$$Li7 + n \rightarrow He4 + T + n \, (1.7)$$

While mixture of tritium and deuterium is the primary fuel for near future fusion devices, He-3 reactions also are in need of consideration. Firstly as byproducts of hydrogen isotope fusion reactions. He-3 can fuse with deuterium (Eq. 1.8) where He-4 and 14.641 MeV proton is produced or it can fuse with tritium in two possible ways (Eq. 1.9-10). After tritium and He3 fusion there is ~59% chance to produce He-4, neutron and proton (12.096 MeV energy is mostly released in the

form of electromagnetic radiation). 41% percent of T-He-3 fusion outcomes will result in He-4 and deuterium production.

$$D + He3 \rightarrow He4 + p \quad (1.8)$$
$$T + He3 \rightarrow He4 + n + p \quad (1.9)$$
$$T + He3 \rightarrow He4 + D \quad (1.10)$$

He3 can also fuse with another He-3 nucleus (Eq. 1.11), resulting in production of He-4 and a proton pair. Energy in He-3-He-3 reaction is released mostly by electromagnetic radiation (12.860 MeV). Such reaction is very attractive as it doesn't produce any neutrons and the reactions between protons or He-4 are very unlikely. On the other hand, such reaction requires better confinement and the He-3 reserves are rather scarce on earth.

$$He3 + He3 \rightarrow He4 + 2p \quad (1.11)$$

Reaction rate between two ion species with densities n_i and n_j in plasma is defined by:

$$R = \mathrm{n}_i \mathrm{n}_j (1 + \delta_{ij})^{-1} \langle \sigma v \rangle \quad (1.12)$$

Where $\langle \sigma v \rangle$ is average fusion cross-section σ over velocities v and δ_{ij} is Kronecker delta function. Considering Maxwellian nature of ion energy distribution *N(E)* in plasma (Brysk 1973):

$$N(E) = 2\pi^{-\frac{1}{2}}\theta - \frac{3}{2}E^{-\frac{1}{2}}\exp(-\frac{E}{\theta}) \quad (1.13)$$

Where E is relative energy, while θ is kT. So $\langle \sigma v \rangle$ can be expressed as:

$$\langle \sigma v \rangle = N(E) = \left(\frac{8}{\pi}\right)^{\frac{1}{2}} m^{-\frac{1}{2}} \theta^{-\frac{3}{2}} \int_0^\infty E\sigma\, E\exp(-\frac{E}{\theta}) dE \quad (1.14)$$

In Maxwellian plasma consisting of two types of ions with a temperature θ the mean kinetic energy is defined by subsequent expression:

$$\langle K \rangle = \theta^2 \left(\frac{d}{d\theta}\right) \left[\ln(\theta^{\frac{3}{2}} \langle \sigma v \rangle)\right] \quad (1.15)$$

Majority of applicable fusion reactions lead to a neutron emission, hence the average energy of neutron produced in fusion Deuterium-Tritium reaction is equal:

$$\langle E_n \rangle = \frac{1}{2} m_n \langle V^2 \rangle + \frac{m_a}{m_n + m_a} (Q + \langle K \rangle) \quad (1.16)$$

Where Q is energy released from nuclear reaction, V is motion of the system center of mass and m_a, m_n are the masses of D-T reaction products (neutrons and alpha particles).

Neutron spectra is defined by Gaussian distribution of neutron energies:

$$f(E_n)dE_n = dE_n exp\left[-(E_n - \langle E_n \rangle)^2 / \frac{4m_n \theta \langle E_n \rangle}{m_n + m_a}\right] \quad (1.17)$$

1.3 Conditions for Nuclear Fusion

In order to achieve nuclear fusion some conditions need to be fulfilled. For D-T fusion deuteron energy must be large enough to overcome repelling Coulomb force. Maximum reaction cross section is reached when temperature T is around 100 keV. In addition to that quantum tunneling through the coulomb barrier is also possible so 20 keV temperature is sufficient for the reaction. However, reaction cross-section σ is rather low so most of the particles do not interact with each other. Energy is being lost by the kinetic collisions and bremsstrahlung radiation through slowing down processes. Low cross-section issues can be solved by increasing density n of the particles. Electron density n_e at typical fusion device is around 10^{20} m^{-3}. At 20 keV D-T fuel is fully ionized, charged particles due to coulomb forces start to migrate. This leads to decrease in density so plasma starts to cool down by losing more energy to environment due to radiation and discontinuation of further fusion reactions while some particles start to interact with a reactor vessel. From this process another important fusion property can be derived – confinement time τ_E. Confinement time describes the rate at which a system loses energy to its environment. $n_e T \tau_E$ is called fusion triple product and is used to estimate the performance of fusion devices. Confinement time and ion density estimate is called Lawson's Criterion (Lawson 1957).

1.4 Nuclear Fusion Devices

Requirements for making an efficient fusion device can be determined from the fusion triple product $n_e T \tau_E$. There are a few possible approaches to design fusion device. Inertial confinement fusion and magnetic confinement fusion are two primary concepts. Inertial confinement fusion is laser based technology that converges the beams on the D-T target achieving extremely high temperatures and densities. However confinement time is very short and at the moment such technology is far from being suited for energy production. In comparison magnetic confinement fusion devices while having lower temperatures and densities can provide much better confinement time. Ideally continuous operation can be achieved. In these devices plasma is confined by strong magnetic fields. The charged particles are gyrating around the magnetic field lines in relation to strong magnetic field that confines the plasma in the direction perpendicular to the field. As

charged particles are moving along the field lines, full plasma confinement can be achieved, if magnetic field lines correspond to toroidal shape (Fig 1.3.). Toroidal plasma confinement device is called tokamak (Wesson 1999).

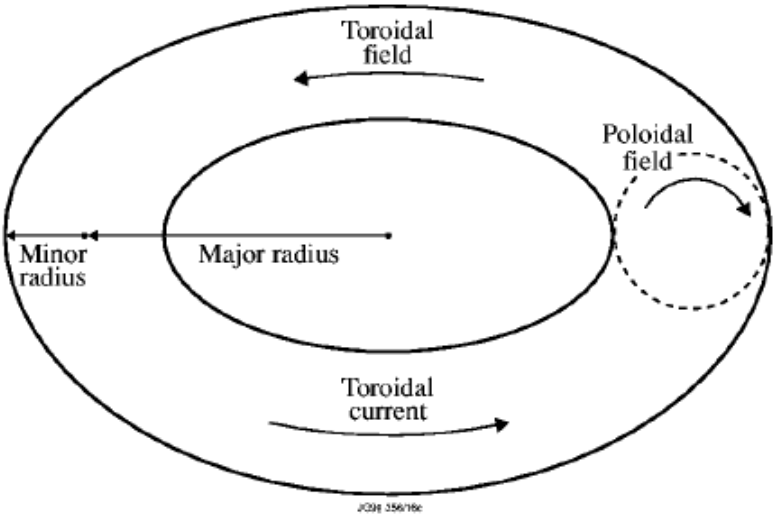

Fig. 1.3. The currents and fields in tokamak plasma. (Wesson 1999)

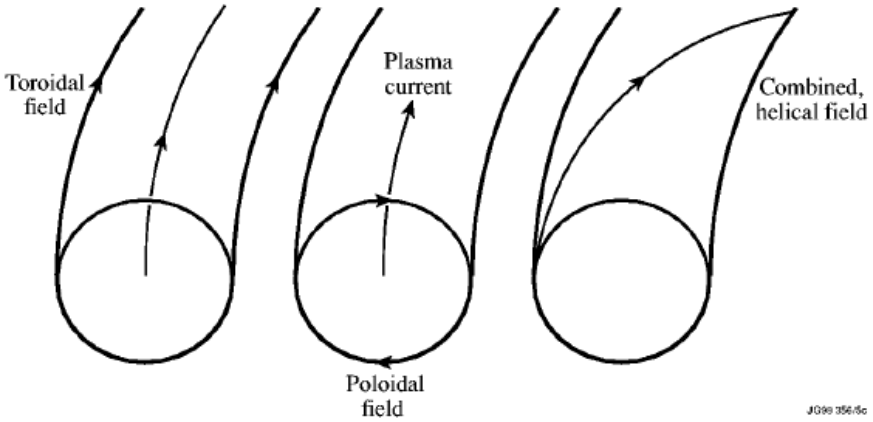

Fig. 1.4. The tokamaks toroidal magnetic field combines with the poloidal field with the plasma current to produce magnetic field with helical field lines (Wesson 1999)

The principal magnetic field component is in the toroidal direction and is generated by the external toroidal field coils. A current flowing through the plasma is induced by a transformer with the plasma forming the secondary winding. This plasma current produces a poloidal magnetic field, which when combined with the dominant toroidal field results in a helical magnetic field (Fig. 1.4.). The charged particles are confined to gyrate around these helical magnetic field lines, and consequently the transport coefficients parallel to the magnetic field are much larger

than the perpendicular transport coefficients. This means that the density and pressure are approximately constant along a flux surface, although large perpendicular gradients can exist.

1.4.1 Joint European Torus

Joint European Torus (JET) is currently the largest operating nuclear fusion reactor situated near Culham, United Kingdom. It started to operate in 1983 with initial goals aimed at plasma-wall interaction investigation, plasma heating, alpha particle production and plasma confinement studies. More so the most important task of JET was to test the scaling law of fusion devices. Since the start of operation JET undergo variety of upgrades designed to improve its performance as well as to test the technologies and scenarios necessary for future fusion reactors. At the moment JET is the only machine in the world suitable for deuterium and tritium operations. Last deuterium tritium campaign was held at JET in 1997 (Keilhacker, M. 1999), while the new campaign is set for 2019/2020 (Horton L. et al. 2016).

In the most recent configuration plasma in JET is confined by strong magnetic fields induced by copper magnet system and plasma currents, respectively up to 4 T and 5 MA. The major plasma radius reaches Major plasma radius inside the reactor reaches 3 meters while minor 0.9 meters. JET has beryllium based first wall and tungsten based divertor system. During JET DTE1 campaign, device produced 16 MW of fusion power with total input heating power reaching 24 MW (Q=0.67) [8].

1.4.2 International Thermonuclear Experimental Reactor

International Thermonuclear Experimental Reactor (ITER) is a massive experimental fusion reactor currently being built in Caradache, France. The device is a successor to JET (Litaudon 2017) and it has much more ambitious goals (IAEA 2001):

- reach Q larger than 10 in inductive Deuterium-Tritium operation with pulses lasting for 300-500s.
- To reach Q larger than 5 in quasi-stationary operation with non-inductive current drive.
- To demonstrate necessary fusion technologies
- To test components of future fusion reactor.
- To test tritium breeding concepts.
- To ITER is set to be the first fusion device capable to reach fusion power and external heating ratio sufficient enough for effective energy production, however the facility itself is not designed to produce electricity.

The main advantages of ITER reactor is its high plasma volume with major and minor radiuses reaching 6.2 and 2 meters respectively. Nb_3Sn superconducting magnet system will allow to reach magnetic fields as strong as 11.8 T inside the

reactor vessel. Reactor will be capable to produce 500 MW of fusion Power with 50 MW of total input heating power (Holtkamp 2009).

1.4.3 Demonstration Fusion Power Reactor

Demonstration Fusion Power Reactor (DEMO) is a follow up to ITER and is considered to be the first reactor to produce net electricity power. Currently DEMO reactor is in development stage and final configuration is yet to be set and will most likely be influenced by the results of ITER and IFMIF-DONES. As for 2017 total fusion power is expected to be around 2000 MW with major and minor radiuses to be around 9 and 2.9 meters respectively. Device should be also able to provide 500 MW net electricity to the grid. DEMO will be equipped with superconducting magnet system as well as fully integrated breeding blanket technology for tritium production and better efficiency. The plasma facing materials most likely will be produced from Tungsten alloy (Bachmann et al. 2018).

Compared to ITER, DEMO is not equipped with plentitude of diagnostic and other auxiliary systems designed to carry out experiments. DEMO objectives revolve around providing net electricity to the power grid and to demonstrate sufficient reliability and availability of fusion technology (Federici et al. 2016).

1.4.4 Wendelstein 7-X

Wendelstein 7-X (W7-X) is a stellarator type fusion device built in Greifswald, Germany. It produced the first plasma in 2015 (Pedersen et al. 2015). In terms of technological applicability to produce energy from fusion it is somewhat close to JET. Currently device is not suited to withstand high heat or neutron fluxes and has no tritium breeding capabilities. Deuterium tritium experiments are also not being planned. Due to unique coil configuration, stellarators can avoid plasma instabilities that occur in tokamaks due to large current flows in the plasma. Furthermore, stellarators by design should be able to work in continuous operation.

Wendelstein 7-X was built to demonstrate the suitability of stellarator type devices for a power plant design. If projects like ITER or DEMO fail to perform due to plasma instabilities, stellarator concept might become principal design in further fusion energy research.

The current main objective of W7-X project is to confine ~10 keV hot plasma for up to 30 minutes for a single discharge as well as to reach quasi-stationary mode of operation. Besides this, there are many goals related to further development of stellarator technologies (Gasparotto et al. 2014).

1.4.5 Breeding Blanket Modules

Breeding blanket technology at the moment is regarded as one of the most important issue in development of sustainable nuclear fusion power plant. Breeding blanket is modular construction inside the fusion reactor vacuum vessel. In ITER

only few blanket modules will be installed at port locations in order to investigate different concepts and general capability to successfully operate in reactor environment, while DEMO will be almost entirely covered by a breeding blanket. In general breeding blanket has few purposes in fusion devices. The major one is to breed tritium out of lithium via neutron interactions as it was shown in the section 1.2. Its efficiency is described by tritium breeding ratio (TBR) which should be slightly higher than 1 (at least to produce as much tritium as it is consumed by fusion reactions inside the plasma) in order to sustain the continuous stream of tritium into device and thus maintain the continuous operation (Cismondi et al. 2018).

Breeding blanket module as a plasma facing component must also be able to endure high heat and neutron fluxes and retain structural integrity. Neutron fluxes are volumetric while core radiation and plasma interactions mostly affect the surface which is protected by a layer of tungsten. More so module itself is a heat transfer element with a cooling piping subsystem that provides thermal power for further generation of electricity. Thermohydraulics is another important aspect that needs to be considered in effective blanket model design.

Breeder blanket also acts as radiation barrier, so it is also need to be assessed in order to prevent radiation leakage from the reactor, as well as to prevent the irradiation of sensitive components or structures that in some way might get in contact with the personnel of fusion power plant. Many blanket concepts have neutron multiplying features, where newly formed neutrons in breeder zone both propagate further production of tritium and also transfer additional heat to the system.

There are four primary concepts of breeding blanket modules that are currently under immense investigation and development for European DEMO reactor.

Water Cooled Lithium Lead blanket

Water Cooled Lithium Lead blanket (WCLL) (fig. 1.5.) is design based on water cooling, WCLL uses EUROFER 97 reduced activation ferritic martensitic steel as structural material and lithium Such blanket modules are formed by directly cooled steel, utilizing C shape double-walled tubing in which the water coolant circulates. The water flows downstream in the tubes near the first wall and upstream near the back plate of the module. The first wall is cooled by pressurized water flowing in horizontal channels. Tubing is 5 millimeter in diameter, coolant velocity is close to 5m/s and pressure is 15.5 MPa. Coolant temperature can vary between 285 and 325 ^{0}C for inlet and outlet respectively (Del Nevo et al. 2017).

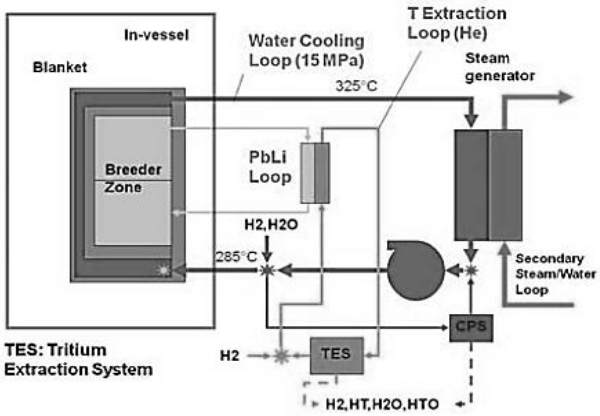

Fig. 1.5. Schematic configuration of WCLL (Boccaccini 2014)

Dual Coolant Lithium Lead

Dual Coolant Lithium Lead (DCLL) (fig. 1.6.) uses lithium lead mixture as main coolant, neutron multiplier and tritium breeder. Helium is being used to cool parts exposed to higher temperatures such as fist wall. EUROFER 97 is being used as structural material. Outlet temperatures for PbLi and for helium are designed to be 548 and 445 ^{0}C, respectively (Rapisarda et al. 2017).

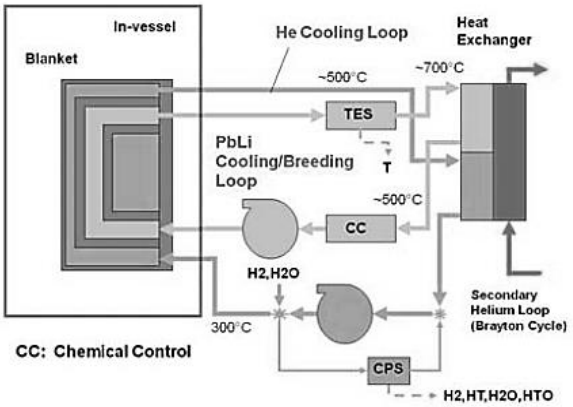

Fig. 1.6. Schematic configuration of DCLL (Boccaccini 2014)

Helium Cooled Lithium Lead

Helium Cooled Lithium Lead (HCLL) (Fig. 1.7.) is helium cooled design made of EUROFER 97 structural material. Breeder zone is made of lead that is being used for neutron multiplication function and lithium (enriched to 90% lithium 6) as tritium breeder. Helium coolant flows at 8 MPa pressure and has 300 and 500 ^{0}C temperatures at inlet/outlet respectively (Aubert et al. 2018).

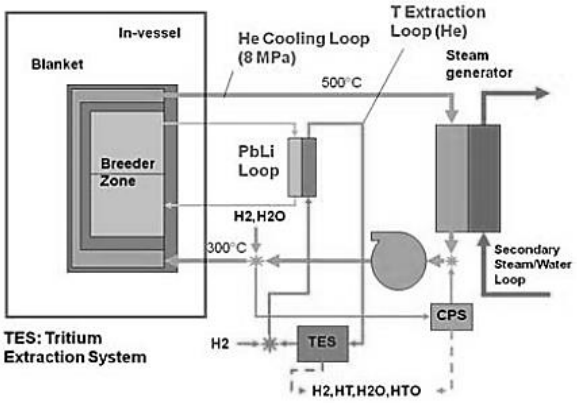

Fig. 1.7. Schematic configuration of HCLL (Boccaccini 2014)

Helium Cooled Pebble Bed

Helium Cooled Pebble Bed (HCPB) (Fig. 1.8.) breeder blanket is helium cooled design. Its most distinct feature is the breeder zone which is made of pebble bed of a Li4SiO4 with 60% lithium 6 enrichment as a tritium breeder and beryllium as neutron multiplier. Breeder zone layers are separated by cooling plates. Prime structural material is EUROFER 97 steel. Helium coolant which flows at 8 MPa pressure at 300 and 500 ^{0}C for inlet and outlet, respectively. For tritium purging from pebble bed separate low pressure helium stream is used (Hernández et al. 2017).

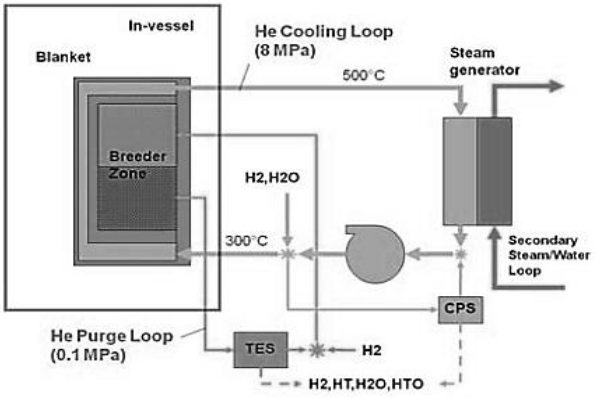

Fig. 1.8. Schematic configuration of HCPB (Boccaccini 2014)

1.4.6 International Fusion Materials Irradiation Facility

International Fusion Materials Irradiation Facility-Demo Oriented Neutron Source (IFMIF-DONES) is an accelerator based neutron source designed to reproduce the neutron irradiation conditions that could be present in the future

fusion power plants. So far the device is still in the development stage. Preliminary construction site should be located near Granada, Spain. IFMIF planned to have one 125 mA deuteron beam guiding 40 MeV particles to the lithium target, where neutrons are being produced at 5.5 10^{16} s^{-1} rate. Neutrons produced at D-Li source should have high energies, even up to 55 MeV. Facility will also be upgradable to the former IFMIF-EVEDA design that provides extra accelerator and auxiliary research facilities. (Ibarra et al. 2014) (Knaster et al. 2016) (Tian et al. 2018).

1.5 Research of Neutronics in Nuclear Fusion

Application of neutron transport calculation in nuclear fusion was introduced from the fission research experience with primary focus on fission-fusion hybrid reactors. Due to complexity of the fusion devices, first models were simplified and codes were designed to solve transport equation in one-dimensional plane (Seki and Iida 1980). The interest in nuclear waste production and material activation rose in 70s after the successful operation of Soviet Union T-3 tokamak as it showed the possible viability of the fusion technology (Peacock et al. 1969). Many studies were conducted on fusion waste production, however the methodology for computation was not developed yet and therefore estimations were not considering heterogeneity of the device and neutron transport in detail. In 1977 scientists at Oak Ridge National Laboratory developed computation method for the nuclear fusion activation estimation by using ANSIN neutron transport and ORIGEN activation inventory codes (Smith and Parish 1977). Between late 1970s and early 1980s interest in fusion research peaked, TFTR and JET tokamaks were under construction with scheduled tritium experiments, more so, the idea of ITER (at time ITER was intended to be fully functional power plant) was already in consideration. Such rapid progress in fusion research led to increased interest in nuclear safety of fusion devices that primarily dealt with tritium handling and neutron activation. However at time neutron activation wasn't considered particularly important issue due to different radiation protection standards (Hirsch and Rice 1974). Desire to use tritium as fusion fuel presented new challenges as estimated available sources of tritium production was not sufficient for the propagation of nuclear fusion power plants (Ni et al. 2013). In order to solve tritium problem lithium based breeder blanket concept was suggested (Rosen and Stewart 1962). Breeder blanket design required nuclear analysis in order to precisely determine the performance and tritium breeding ratio. Neutron transport and activation inventory codes were developed and nuclear data libraries compiled in order to address these issues.

Deuterium-Tritium fusion provides unique irradiation settings with high energies and high neutron fluxes, therefore existing experimental data is not complete yet and some material activation yield certain uncertainty (Forrest, 2011), (Fischer et al., 2005). There are two main approaches for benchmarking materials in fusion relevant conditions: fusion neutron streaming experiments and accelerator based material qualification. Both directions are grounded in activation analysis and recreation of conditions relevant to nuclear fusion.

Neutron streaming in fusion relies on existing fusion devices that can operate with deuterium-deuterium or deuterium-tritium fuel. So far only two significant experiments with tritium took place. First deuterium-deuterium neutron streaming experiment was held at TFTR. Gamma and neutron emissions were calculated with MCNP code. Calculation results were 20-40 % higher than the readings of the dosimeters placed in TFTR (Liew et al., 1986). At JET two tritium experiments followed: preliminary tritium experiment (PTE) in 1991 and first deuterium tritium experiment (DTE1) in 1997. During PTE and DTE1 neutron streaming experiments were not considered (Rebut et al. 1992), (Keilhacker and Watkins, 1999). The next deuterium-tritium experiment (DTE2) should take place in 2019 or later at JET (Villari et al. 2016). DTE2 neutron streaming experiment will consist of three parts: neutron flux determination, shutdown dose rate estimation and material sampling. Neutron streaming experiments as well as shutdown dose rate measurements were already performed in JET deuterium-deuterium campaigns from 2012 till 2014 (Batistoni et al., 2015). Neutron streaming experiments resulted in satisfying agreement between MCNP calculations and thermoluminescent detectors used for the measurements. Shutdown dose rate measurements performed in deuterium-deuterium 2012 campaign were affected by significant experimental uncertainties (up to 30%). Plentitude of uncertainty sources were identified including energy and anisotropy responses, low activation, detector calibration and placement. All named aspects set to be improved/evaluated for the upcoming deuterium-tritium shutdown dose rate measurements. Measurements will be performed by monitoring decay gamma emissions during reactor downtime with ionizing chambers and thermoluminescent detectors inside and outside the reactor vessel (Villari et al. 2016). New addition to the previous experiments will be the placement of material samples inside the reactor vacuum vessel. Material samples will be placed inside irradiation station where high neutron flux is expected. The purpose of sampling is to have better understanding of radiation damage, nuclear heating and activation. The advantage over the previous shutdown dose rate measurements is that samples can be recovered after the end of irradiation and examined under laboratory conditions, allowing more in-depth analyses and the reduction of environmental factors (Lengar and et. al 2016). Some EUROFER 97-3 steel samples were irradiated during JET Tritium Trace Experiment (TTE) in 2013, where activities of medium half-life isotopes were evaluated and experiment data coincided with activation calculation results within acceptable uncertainty limits (Angelone et al., 2006). DTE2 activation calculations performed for JET irradiation station samples are subject of this thesis and are presented in section 3.1.

Accelerator based material qualification aims at recreating neutron flux or/and heat relevant to nuclear fusion. Number of nuclear data library benchmark experiments were performed with 14-MeV Frascati neutron generator (FNG), however the accelerator is only capable to deliver ~5.10^{11} n/s to the material specimens and for limited exposure (Martone, Angelone and Pillon 1994), (Pillon, Angelone and Sandri 2011). So far the largest and most capable IFMIF-DONES facility is under development. While IFMIF idea first surged in 1988 (Mann, 1989)

and project was launched in 1994, only in 2007 primary specifications and technologies were confirmed and later realized at IFMIF-EVEDA facility (located in Rokkasho, Japan) and currently are set for testing (Yamanishi et al. 2016). During IFMIF-DONES operation number of material specimens will be irradiated and subjected up to 15 displacement per atom per year. While material degradation investigation is the primary focus of the irradiation facility, nuclear safety issues also play a substantial role. Activation analysis is part of nuclear safety assessment. So far number of neutronic studies were conducted for the IFMIF facility, however majority of publications cover different aspects and setups while sharing only the model and McDeLicious source term as commonality (Fischer et al. 2019). McDeLicious code was developed for MCNP in order to describe D-Li neutron source term (Simakov et al. 2012). IFMIF neutronic studies include neutron fluence, shielding calculations, dose rate and nuclear heating maps (Kondo et al., 2015) (Qiu and et al. 2019) (Kondo et al., 2014) (Mota and Molla 2016). In section 3.3 activation analysis for IFMIF biological shielding is presented.

Numerical methods are widely used in order to estimate possible activation inventories in irradiated materials. There is a bilateral relation between experiments and numerical methods as the former provide the nuclear data for the later and numerical methods are extensively used in designing experiments and experimental setups. While IFMIF-DONES can reproduce comparable to nuclear fusion reactor type of neutron flux, there are still more many differences between the two. Nuclear fusion reactor neutron production depends on the energy confinement mode that can transition spontaneously. More so, the edges of the confinement tend to be unstable. There is also a difference in neutron spectrum as accelerator based source neutron energy range tend to significantly extend beyond 14 MeV. Moreover fusion reactor vessel itself is a rather complex scattering source. While IFMIF can give clues on material selection and tritium breeding it can't warrant the functionality of actual fusion reactor. However, HCPB and HCLL breeder blanket module mockups were irradiated at FNG in order to test the tritium production rates. Total uncertainty between measures and experiments was estimated to be lower than 5.9%, where 3 % were due to cross-section data (Batistoni and et al., Neutronics experiments for uncertainty assessment of tritium breeding in HCPB and HCLL blanket mock-ups irradiated with 14 MeV neutrons 2012). DEMO is considered to be the first functional European fusion power plant, however its development is far from over. Preceding ITER and IFMIF-DONES experiments should determine it is final design. With regards to neutronics, current European DEMO development is based primarily on numerical methods. Applications of such methods was firstly used for the first wall and breeding blanket calculations as it was a priority to ensure tritium breeding and heat transfer performances as well as to evaluate exposed structural materials. It shortly became a standard method for the whole device assessment including diagnostic, control and heating systems. With the improvement of computational power, shut down dose rate calculations for the extended surroundings of the fusion devices became a common practice and were implemented for the preparation planning of operation (Leichtle and et al., Global

shutdown dose rate maps for a DEMO conceptual design 2015). Extensive shutdown dose rate calculations utilize a rigid two step (R2S) method where subsidiary codes bridge neutron transport and activation calculation codes (Fischer et al. 2017). So far in preparation for ITER activation values for safety considerations are assumed to be up to 10 times larger than calculated. More so the latest development in ITER numerical models showed that the more detailed reconstruction of model might have significant impact on the overall results (Leichtle et al. 2018). For breeder blanket activation calculations few approaches are utilized with regards to the model used for neutron transport. Model can either be depicted as full reactor vessel or just use a slice of it that describes repeating structures (e.g. breeder blanket port). Model can contain auxiliary structures in a certain detail, such as divertor, neutral beam injector, central solenoid and others. Breeder blanket module itself can be represented as a homogenized structure, multi module segment or single module segment (Fischer et al. 2005), (Tassone et al. 2018), (Eade et al. 2017). Neutron source can be presented as a simple point source or series of surfaces. Some more advanced solutions are possible by utilizing supplementary codes (Eriksson et al. 2016). Neutronic breeder blanket calculations often deal with tritium self-sufficiency, shielding and radiation streaming, irradiation damage and nuclear heating density (Moro et al. 2018), (Federici et al. 2019).

1.6 Neutron Transport

Radiation transport plays a principal role in safety and operation of fusion devices. Deuterium-Tritium fusion relies on neutrons to transfer the fusion energy in a form that can be harnessed on the grounds of electricity production. Neutrons act as heat carriers in the system, on top of that they could be potentially used to breed tritium. However neutrons also cause many problems as their kinetic interactions can cause damage to the sensitive equipment and in locations where neutron flux is high enough it can disintegrate structural materials or severely detriment mechanical integrity. On top of that material activation process due to neutrons is critical for safety of the devices. The activated materials after device operation require remote handling and need to be safely stored for at least 50-100 years.

Current and near future nuclear fusion devices are classified as nuclear objects. There are several possible types of directly and indirectly ionizing radiation sources:

- fusion plasma itself consist of energetic charged particles;
- charged particles in plasma cause Bremsstrahlung radiation;
- fusion fuel tritium is unstable beta emitter with a tendency to permeate into other materials;
- fusion reaction results in neutron and gamma production;
- material interaction with neutrons makes it radioactive.

Neutron transport deterministic methods are based on the neutron flux concept $\psi(r, \Omega, E)$. Neutron flux is six-dimensional density-like function (eq. 1.18) describing collective behavior of the neutron population.

$$\frac{1}{v}\frac{\partial y}{\partial x}\psi(r,\Omega,E,t) + \Omega\nabla\psi(\mathrm{r},\Omega,\mathrm{E},\mathrm{t}) + \sum(r,E)\psi(r,\Omega,E,t) = Q + S + F \quad (1.18)$$

Where Q is external source, S is scattering source and F is fission source. If we assume that reaction cross sections are not dependent on flux, the equation can be considered being linear. However, complexity and heterogeneity of geometry, cross-section dependence on neutron energy and the angular dependence on streaming and scattering source term is difficult to compute.

In general, deterministic transport methods rely on at least three fundamental approximations:

- Discretization and homogenization of geometry and materials.
- Discretization of energy functions.
- Angular and directional dependence representation by functional expansions.

Empirically neutron flux can be defined as physical reaction rates (Eq. 1.19):

$$R_x = \int_V \int_\Omega \int_E \sum(r,E)\psi(r,\Omega,E,t)\, dV d\Omega dE \quad (1.19)$$

1.6.1 Neutron Interactions

Neutron transport is a neutron diffusion process through matter. Neutron diffusion can be described by 3 major interactions: nuclear fission, absorption and scattering.

Elastic and Inelastic Scattering

During the elastic scattering event a neutron and nucleus collision result in no change in the structure of the target nucleus the nucleus recoils instead and the neutron changes direction and speed. The neutron and nucleus exchange kinetic energy. Total kinetic energy of the system stays as it was before the elastic collision.

Inelastic scattering occurs when incident neutron after collision with the target nucleus leave it in an excited state. Excited nucleus decays to the ground state with the follow-up of gamma ray emission. Inelastic scattering is threshold reaction. For it to occur, incident neutron should have energy greater than the excitation state of the nucleus. After such collision part of the kinetic energy is transformed into electromagnetic radiation while incident neutron changes speed and direction.

Absorption

Absorption in neutron transport describes neutron capture (Eq. 1.20) and other reactions leading to neutron absorption. Neutron capture (n, g) is a two stage process. Firstly, nearby neutron is being captured by a nucleus. Due to the change in

nucleus structure some energy states become excited. Excited nucleus decays to the ground state and some energy is being released by electromagnetic gamma radiation.

$$n + {}^{A}_{Z}X \rightarrow {}^{A+1}_{Z}X^{*} \rightarrow {}^{A+1}_{Z}X + \gamma \quad (1.20)$$

Besides neutron capture (n, g) reaction there are plentitude of other reactions that can occur during neutron interaction event. Generally such reactions are marked as (projectile, ejectile) and their cross sections correspond to the energies of projectile and target nucleus. Nuclear fission (n, f) is another category of nuclear absorption events.

Nuclear fission

Nuclear fission (Eq. 1.21) is a phenomenon where heavy nucleus due to reaction with neutron splits into two smaller nuclei. Such event is usually followed by additional neutron and gamma emission.

$$n + {}^{A1}_{Z1}X \rightarrow {}^{A2}_{Z2}X + {}^{A3}_{Z3}X + n \quad (1.21)$$

In fusion reaction fission reactions are not desirable and on large scale is eliminated by the selection of the materials. However tiny fractions of these elements in form of impurities can still be present in reactor materials and cause a significant increase in the activation of inventory values.

1.6.2 Neutron Activation

Neutron absorption can lead to neutron activation, where nuclei with captured neutrons form nuclei with excited states. Such nucleus usually decays in very short time period emitting gamma rays, subatomic particles or fission products. After this capture event stable nucleus can turn into unstable. These newly formed unstable nuclei are called activation products.

Activity

Activity describes the number of decays per unit time occurring in material. It is an important characteristic used to measure the radioactivity of a material. The activity of a nuclide i, represented by Ai, is equal to the product of the number of nuclides Ni and its decay constant λ_i, that is,

$$A_i = \frac{dN_i}{dt} = \lambda_i N_i \quad (1.22)$$

The activity of a material equals to the sum of the activities of all radioactive nuclides in the material. The variation of a material's activity with time obeys the exponential decay law. The unit of activity is the Becquerel (Bq). 1 Bq is one nucleus decaying per second.

Specific activity is usually used to characterize the radioactivity of the material and is defined as the ratio of the activity to the mass, in units of Bq/kg. The specific activity can be directly measured, and the activity can be calculated as the product of the specific activity and the mass.

Decay Heat

Decay heat corresponds to a thermal energy output of activated material. Decay heat is being produced during the decay event when photon or other decay product transfers its kinetic energy to the surrounding nuclei.

The decay heat P_i produced by the nuclide i in the material can be expressed as:

$$P_i = A_i E_i = \lambda_i N_i E_i \quad (1.23)$$

Where E_i is the average energy released in each decay of nuclide i. The material's decay heat equals to the sum of the decay heat of all radioactive nuclides in the material (ICRP 1991).

According to IAEA waste classification system (IAEA 2007) if decay heat is below 10 W/m^3, no active cooling is required, for waste between 10 W/m^3 and 2 kW/m^3 dry cooling is recommended and for waste with decay heat above 2 kW/m^3 wet cooling is necessary

1.6.3 Radiation Protection Characteristics

Absorbed and equivalent dose rates

Absorbed dose is a physical quantity characterizing the mean energy $\tilde{E}$ conveyed by ionizing radiation in a volume element and the mass m. It is expressed in Jkg^{-1} or grays (Gy).

$$D = \frac{d\tilde{E}}{dm} = \lambda_i N_i E_i \quad (1.24)$$

Dose equivalent is a physical quantity for the relative biological effectiveness of an absorbed dose of ionizing radiation. It is expressed in sieverts (Sv). Different types of radiations r are defined by specific weighting factors w_r.

$$H = \sum_r w_r D_r \quad (1.25)$$

If exposure from the source (the contact dose rate) is lower than 10μSv/hour hand handling is permissible, if the dose rate is in between 10μSv/h and 2 mSv/h shielded handling is needed and for dose rates higher than 2 mSv/h remote handling is required (IAEA 2007).

1.7 Author Contribution to the Field of Research

Doctoral thesis material was featured in 10 publications: 7 in journals referred in “Clarivate Analytics – Web of Science Core Collection” database and 3 in the proceedings of international conferences. Doctoral thesis material was also presented in 10 international conferences.

Three different cases of activation calculation application connected to the nuclear fusion power plant prototype development are presented in result section.

For JET OLTIS sample box calculations (section 3.1), author of the thesis performed activation calculations with FISPACT code and result analysis.

For the IFMIF-DONES calculations (section 3.2) author of the thesis performed neutron transport calculations with MCNP code and performed activation calculations with FISPACT code and subsequent result analysis.

For European DEMO 2014/2015/2017 breeder blanket calculations (section 3.3) author of the thesis performed neutron transport calculations with MCNP code and performed activation calculations with FISPACT code and subsequent result analysis. Dr. Tadas Kaliatka helped with SUSA calculations in section 3.3.6.

2.METHODOLOGY

This section is dedicated for the overview of tools, methods and other affiliated subjects used in the conductance of numerical experiments and obtainment of the results. Schematic representation is presented in fig 2.1.

Standard activation calculation procedure begins with neutron transport. Neutron transport calculations provide neutron flux densities for segments where activation analysis is desired to be performed. Neutron transport calculations referred in this thesis were performed with MCNP code (more details in section 2.1). For neutron transport calculations it is necessary to specify experiment geometry and source as well as to provide material information including compositions and densities. Finally, tallies are required in order to specify what sort of information should be retrieved from the neutron transport calculation results. Such information can be described in single or multiple input files. Variety of variance reduction techniques can also be described in input files with a purpose to save computation time as well as to make results more accurate. Typical baseline DEMO model input contains thousands of lines, hence MCNP inputs will not be provided in this thesis. Standard version of MCNP code comes with ENDF/B-VI nuclear data library (section 2.2.1). Nuclear data is described in ACE format, so in order to use different data libraries that are more endorsed by European fusion research community (e.g. JEFF, FENDL), third party nuclear data processing tool NJOY is used (MacFarlane and R.E. Kahler 2010).

After flux densities in discrete energy groups are acquired via neutron transport calculations or other means (e.g. neutron streaming experiments), neutron spectra can be prepared. Spectrum describes neutron number in every discrete

energy group. Determination of neutron amount depends on experimental data as well as the model used. Neutron production in fusion as well as reaction rates were described in section 1.2. Usually the neutron amount is just an estimate as so far it is rather difficult to predict plasma behavior inside the reactor. Estimation of neutrons produced during long term device operation is called budget. For example European DEMO 2017 device is assumed to have 1998 MW fusion power, with another assumption that DT neutron has energy equal to 14.1 MeV and produced Helium atom has 3.5 MeV we can calculate that whole reactor produces ~$6.7 \cdot 10^{20}$ neutrons per second. While such approach is not particulary accurate, as neutron energies vary due to collisions and different possible reactions in reactors, it is still a commonly used practice in fusion calculations.

After neutron spectrum preparation activation calculations can be performed. Activation calculations presented in this thesis were perfomed with FISPACT code (more details in section 2.2). For FISPACT one input file is required. The file contains material information (Mass, density, composition, number of atoms) and irradiation scenario where multiple neutron spectrum or flux density files can be referenced. Lastly, time intervals for cooling times are specified in the input file. The execution of FISPACT results in output file generation that contains all the information on the activation. However variety of sorting/data manipulation/auxiliary operations and additional data extraction are possible by inclusion of tallying and other key codes in input file.

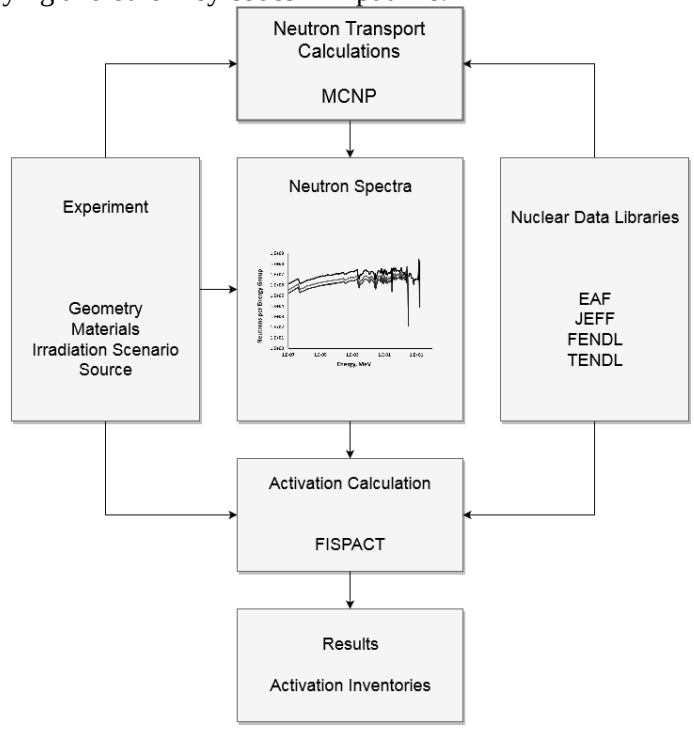

Fig. 2.1. Block diagram representing the process of activation inventory calculation

2.1 The Monte Carlo Codes

Unlike the deterministic methods mentioned in section 1.5, the Monte Carlo method approach is based on individual neutron transport instead of the entire neutron population (flux). Each particle has its own simulated random history, in which probabilities of each random events depends on the position and the energy of the transported particle. The interactions are described by probability distributions. These distributions correspond to empirical data of physical phenomena, however the outcome is randomly sampled. Usually generation of 10^8 or 10^9 particle histories gives satisfactory results of the simulated experiment. Further increment of particle histories provides better accuracy and lower uncertainties, however the process can become redundant in relation to the computation time. Furthermore the estimated results represent the summation of simulated histories.

Monte Carlo method itself does not provide the solution for transport equation, but provides the statistical estimators for integrals of the form

$$\int_V \int_\Omega \int_E f(r, \Omega, E)\psi(r, \Omega, E)\, dV d\Omega dE \quad (2.1)$$

Where f is an arbitrary response function depending on neutron coordinates in the six dimensional phase space (a cross section in most cases).

Compared to deterministic methods, Monte Carlo methods do not require integration of flux or the energy due to discretization.

The Monte Carlo method is commonly used for complicated linear problems, where the problem can be split up into several much simpler tasks. Likewise solution of transport equation can be obtained by simulating individual particle histories. Typically Monte Carlo codes dedicated for neutron or any other particle transport consists of tracking routine which defines particle movement and geometry of experimental setup by the means of linear algebra and vector calculus, physics routine which include the description of physical phenomena and corresponding data bases, and processing routine which apply statistical methods on the desirable results.

Neutron transport calculations have been widely employed in the nuclear fusion field. Currently, the most common codes for neutron transport in fusion systems are based on the Monte Carlo method. Most relevant Monte Carlo transport simulation codes dealing with neutron transport are presented below.

MCNP

MCNP, a General Monte Carlo N-Particle Transport Code, was developed by Los Alamos National Laboratory (LANL) in the USA. It was coded using the FORTRAN and C programming languages, and the latest version is MCNP6, which

combines the features of both MCNP5 and MCNPX. MCNP6 can be used to perform transport computations of heavy charged particles and has been widely applied in nuclear fusion calculations. It supports transport simulations of neutrons, photons, electrons and heavy charged particles and can perform eigenvalue and fixed-source calculations. Simulations of neutrons with energies ranging from 10^{-5} eV to 150 MeV and photons with energies ranging from 1 keV to 100 GeV are supported. In the latest version of MCNP6, multi-type descriptions of sources, various tallies and variance reduction techniques are included. MCNP has been applied in the neutronics analysis of JET/ITER/DEMO/IFMIF, including calculations of neutron wall loading, neutron/photon fluence rate and nuclear heat deposition. (Pelowitz 2013)

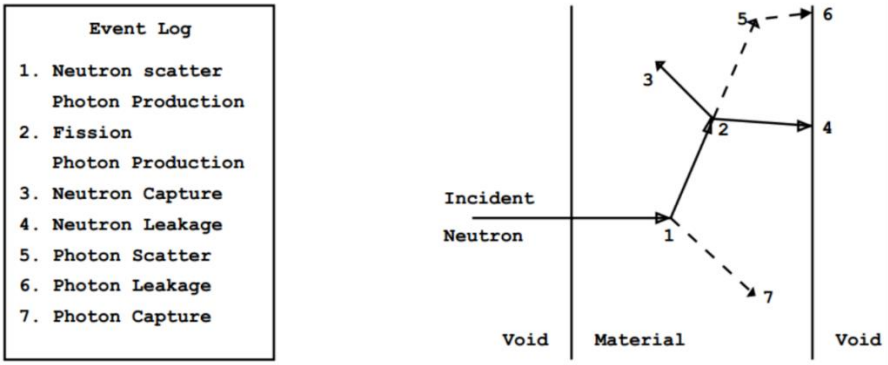

Fig. 2.2. MCNP neutron history. (Pelowitz 2013)

Source

There are four ways to define a source in MCNP. The most standard procedure is to define source by general source variables (SDEF), which includes a source geometry description (either aligned to the existing cell volume, surface or existing as a point source and defined by the coordinates of position), anisotropy/isotropy description and description of particle energy, weight and type. Source information parameter provides discrete source variable values for a description of energy spectrum. Source probability is another multivariable parameter that defines source by providing distribution functions. Source bias is used to provide a probability distribution for sampling that is different from distribution function. There are three other ways to define the source Surface Source Read (SSR) method import the source obtained from preceding MCNP calculation, KCODE is defines critically source and there is also an option for individual source subroutines. Individual source subroutines and source information parameters are most commonly applied in fusion neutronic calculations.

Tracking

Tracking (Fig. 2.2.) describes the particle movement inside the geometrical system constructed for the experiment. Tracking includes sampling of path length till the next collision event, transporting particle to collision point and sampling

interaction. Tracking is heavily affected by the geometry as particle path is stopped at every surface intersection and the sampling probabilities are being re-estimated. In homogenous medium the probability of a first collision for a particle between distance l and dl is given as:

$$p(l)dl = e^{-\Sigma_t l}\Sigma_t dl \quad (2.2)$$

Where Σ_t is a macroscopic total cross-section. Given that there are two possible outcomes 0 or 1 defined by ξ, probability can be rewritten as:

$$\xi = \int_0^l e^{-\Sigma_t l}\Sigma_t dl = 1 - e^{-\Sigma_t l} \quad (2.3)$$

Hence the distance to collision l can be expressed as:

$$\mathrm{l} = -\frac{1}{\Sigma_t}\ln(\xi) \quad (2.4)$$

Collisions

Collision events are defined by physics routines of the code and nuclear data libraries used for calculations.

Tallies

Tallies are used in order to obtain the desired characteristics from the calculation. There are 8 major tallies that describe surface current, surface flux, track length estimate of cell flux, flux at a point, track length estimate of energy depositions, track length estimate of fission energy depositions and energy distribution of pulses created in a detector. For each tally the type of particle needs to be specified.

Variance reduction

Variance reduction is an important aspect of Monte Carlo calculations that can both speed up the computation time and decrease statistical errors. Most commonly used variance reduction techniques in MCNP can be classified into collision event based (absorption weighting, forced collisions), history based (splitting, Russian roulette), direction based (exponential transform, DXTRAN sphere), geometry based (cell weighting and weight windows) and source biasing. Collision based variance reduction might either force or delay collision events, thus either terminating or prolonging the particle walk. History based variance reduction techniques are for the particle population control, where histories might be multiplied or weight of the particle increased upon collision event. Direction based techniques provides direction bias that will increase particle population in specified location in the geometry. Geometry based variance reduction techniques specifies certain cell to have higher or lower importance. Source biasing is heuristic variance reduction method

MCNP model for Joint European Torus and spectra calculations

Neutron fluxes for JET outer long term irradiation station (OLTIS) activation analysis were provided by Sean Conroy (Uppsala University) and Igor Lengar (Jožef Stefan Institute) who performed the MCNP calculations with generic MCNP model for JET (Gatu Johnson et al. 2010) (Fig. 2.3.). Model contains full 360^0 vacuum vessel with the torus hall and supporting structures.

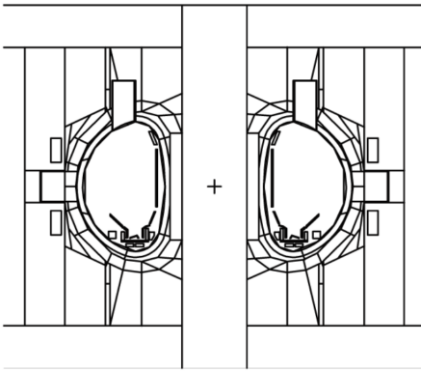

Fig. 2.3. MCNP JET model cross-section (Gatu Johnson et al. 2010)

Generic DEMO MCNP model

Generic European DEMO model is primarily being developed by Max Planck Plasma Physics Institute in Garching (Wenninger et al. 2016). Compared to JET and ITER (Leichtle et al. 2018) models generic DEMO model is significantly less complex. It only contains the vacuum vessel with homogenized structural elements instead of full device. It represents only 11.25° section as seen in Fig. 2.4. In this work three different evolved baseline DEMO models were examined: DEMO2014, DEMO2015 and DEMO 2017. For each model specific WCLL blanket module configuration (Del Nevo et al. 2017) (Moro et al.2018) was integrated.

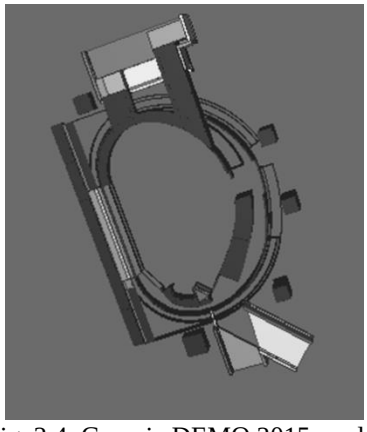

Fig. 2.4. Generic DEMO 2015 model

MCNP calculations for 2014/2015/2017 baseline designs were used in this work in order to obtain neutron spectra for breeding blanket segments and were performed in Lithuanian Energy Institute. The complete analysis was performed by means of MCNP using JEFF 3.1.2 nuclear data library coupled with FISPACT. The statistical error of Monte Carlo calculation results of the neutron flux and energy spectrum is less than 10% with 10^9 particles histories.

IFMIF-DONES model

IFMIF Test Cell model was developed by Karlsruhe Institute of Technology. Model integrates set of cooling pipes with a simplified TC wall. Neutron flux and energy distribution for each TC material and water pipe cell were calculated at Lithuanian Energy Institute. The complete analysis was performed by means of MCNP5 + McDeliciuous with JEFF-3.1.2 nuclear data library. The statistical error of Monte Carlo calculation is about 0.1% with 10^9 particles histories.

Monte Carlo codes relevant for nuclear fusion research and their applications

TRIPOLI (Both et al. 2003) is general-purpose continuous-energy Monte Carlo transport code developed by French Alternative Energies and Atomic Energy Commission (CEA). It is widely used in neutronics analyses of fusion systems, most notably ITER (Lee 2018) and for DEMO breeder blanket calculations (Jaboulay et al. 2018). *TRIPOLI* code is endorsed by European fusion research community and usage should increase in fusion related applications in the future.

FLUKA (Fasso et al. 2011) is a fully integrated particle physics Monte Carlo simulation package developed by CERN and the Italian Institute for Nuclear Physics (INFN). At the moment *FLUKA* application in fusion is limited to subsidiary calculations, however code is being successfully used for Far East CFTR fusion reactor (Chen et al. 2016) neutronic calculations.

Geant4 is a toolkit for the simulation of the passage of particles through matter that was developed by the European Organization for Nuclear Research (CERN). *Geant4* has been applied for design activities and neutronic analysis of fusion systems. (Allison et al. 2003)

Serpent 2 (Leppänen et al. 2015) is a multi-purpose three-dimensional continuous-energy Monte Carlo reactor physics burnup calculation code developed by the National Technical Research Center of Finland (VTT). Currently the code is being adjusted to accommodate nuclear fusion experiments better, however it has very promising source term description capabilities (Leppänen and Kaltiaisenaho 2016).

2.2 Activation Inventory Codes

FISPACT

FISPACT is a transmutation and activation calculation code developed by the UKAEA, with the latest version being FISPACT-II. FISPACT-II can perform transmutation, activation and burnup calculations for neutrons, protons, alphas, deuterons and photons. FISPACT-II solves the Bateman equations with the LSODE ordinary differential equation solver, developed by Lawrence Livermore National Laboratory. FISPACT-II supports the calculation of the activity, decay heat, dose rate, biological hazard potential and decay gamma spectrum, and it also provides many auxiliary calculation functions such as pathway analysis, sensitivity analysis and uncertainty calculation. The nuclear libraries of TENDL-2014, ENDF/BII.1, JENDL-4.0 and JEFF-3.2 are supported in FISPACT-II. FISPACT-II can be applied to reactor physics, fuel and waste management, radiation shielding, etc. (Forest 2007) (Sublet et al. 2016)

European Activation System: Easy-2007 was used as an interface program for the determination of dominant radionuclides in structural materials after irradiation. FISPACT code is being utilized for simulation of irradiation process. Model of irradiation is simplified: infinite and infinitely dilute slab of homogeneous material is being irradiated by time-dependent neutron projectile flux in sequences corresponding to operation of fusion device. Evolution of nuclides is described by set of rate equations (Sublet et al. 2017) (Eq. 2.5):

$$\frac{dN_i}{dt} = \sum_j \left(\lambda_i^j + \sigma_i^j \phi^{int}(t)\right) N_j \qquad (2.5)$$

Where N_i = number of nuclide i at time t, ϕ^{int} (cm^{-2}s^{-1}) projectile flux. And for λ_i^j (s^{-1}) decay constant of nuclide j producing i, σ_i^j (cm^2) reaction cross-section for reactions on j producing i. If $j = i$ then $\lambda_i^j = -\lambda_j^j$ and represent total decay constant of nuclide j and $\sigma_i^j = -\sigma_j^j$ and represents total cross-section for reactions on j. Processes in described Eq. 2.5 can be portrayed by flow graph (Fig. 2.5.):

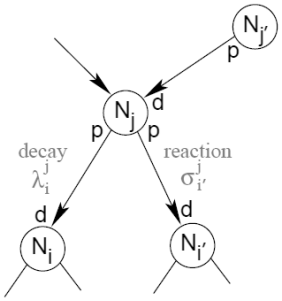

Fig. 2.5. Flow graph representation of reactions and decays. (Subletet al. 2016)

Reaction cross-sections are projectile energy dependent and are described by the nuclear data libraries (section 2.2.1). Some nuclear data libraries also offer data for specific energy target nuclei. Projectile energies are limited to energy groups (section 2.2.2). Effective cross-section in FISPACT is calculated as average cross-section weighted by projectile fluxes in each energy group (Eq. 2.6):

$$\sigma_i^j = \sum_k \sigma'^j_i (E_k)\, \phi_n(E_k) / \sum_k \phi_n(E_k) \quad (2.6)$$

Where $\sigma'^j_i(E_k)$ the cross-section of projectile energy group k is, $\phi_n(E_k)$ is the integrated projectile flux in energy group k.

In FISPACT projectile flux is not modified by the reactions and decays in the target material and the decay rates and cross-sections are not dependent on of the nuclide numbers. As a result rate equations can be rewritten as (Eq. 2.7):

$$\frac{dN}{dt} = NA \quad (2.7)$$

Where A is inventory N independent matrix. As projectile flux is constant at given irradiation sequence the matrix A is a piece-wise constant in time.

Dose rates in FISPACT can be calculated either as a contact dose rate from the surface of a semi-infinite slab or as a dose rate from a point source at a given distance.

Contact dose rate is calculated by following equation:

$$D = C \frac{B}{2} \sum_{i=1}^{N_\gamma} \frac{\mu_{a(E_i)}}{\mu_{m(E_i)}} S_\gamma(E_i) \quad (2.8)$$

Where D is surface γ dose rate (Sv/h), N_γ number of spectrum energy bins, E_i mean energy of *i*-th bin, μ_α mass energy absorption coefficient for air, μ_m mass energy attenuation coefficient for the material, *B* buildup factor, S_γ rate of γ emission, *C* unit conversion factor.

Dose rate from a point source is calculated:

$$D = C \sum_{i=1}^{N_\gamma} \frac{\mu_{a(E_i)}}{4\pi r^2} e^{\mu_{(E_i)} r} m_s S_\gamma(E_i)\, C \quad (2.9)$$

Where m_s is mass of source, r distance from source, μ energy attenuation coefficient for the air.

Input data consists of irradiated material compositions and densities Mass can be expressed either as the percentage of elemental composition or as a number of atoms of each nuclide. Irradiation scenarios can be specified as separate neutron spectra files or be weighted according to existing spectra profile given the total amount of neutrons.

Materials investigated in this thesis are presented below.

For JET DTE2 experiment:

- Functional materials: Sapphire (Al2O3), YAG, ZnS, Spinel, KUI1, KS-4V, ALON (Al22O30N2), ALON-23 (Al23O28N5), ALON-67 (Al67O87N9), ALON-68 (Al68O64N12), Al-Bronze, Alloy 660, Be(S-65C), CuCrZr, JJ1, Nb3Sn, NbTi, OF-CU, SS-304 (Borated), SS316L(N), SS316L(N)-IG, SS316L, XM-19, ZrO2. (Stork ir Zinkle, Introduction to the special issue on the technical status of materials for a fusion reactor 2017) (Packer et al., 2017)
- Pure material foils: Al, Co, Fe, In, Mn, Ni, Sc, Ta, Ti, Y. (Packer et al., 2017)
- Structural materials: 316L(N)-IG, 316LN, 316L, Alloy 660, Alloy 660 div, Al-Bronze, CuCrZr, EUROFER 97-3, INCONEL 718, SS304, W, XM-19 (Packer ir et al 2018).

For DEMO operation simulation:

- Material mixtures for WCLL Breeder Blanket: EUROFER 97-3, Tungsten, PbLi, Water (Stork et al., 2014) (Fusion for Energy 2008).
- Reduced activation steels: EUROFER 97, F82H, F82-IAE, JLF-1, Manet, Manet II, Optifer 1a, Optifer II, la12lc, la12talc, T91 (Danon ir et al. 2003) (Stork et al. 2014) (Chen ir al. 2012) (Gaganidze and Aktaa 2013) (Kimura 2005) (Youssef et al. 1998).
- Type 316 stainless steels: 316, 316H, 316L, 316LN, 316LVM, 316N, 3162Ti (Lee ir et al. 2014).

For IMFIF-DONES operation simulation:

- Biological shielding and cooling system materials: SS316L(N)-IG steel, sodium depleted magnetite concrete, PbLi, Water

Material compositions and densities are presented in annex.

Activation inventory codes relevant for nuclear fusion research and their applications

ACAB (ACtivation ABacus Inventory Code for Nuclear Applications) is a computer code designed to perform activation and transmutation calculations for nuclear applications. *ACAB* has been used to simulate realistic operational scenarios of very different nuclear systems: inertial fusion, magnetic fusion, accelerator driven systems, fission reactors. It was developed by National University of Distance Education and Technical University of Madrid. *ACAB* uses EAF-2007 nuclear data library (Sanz et al. 2008). Currently code is used for fusion specific tasks such as analyses of breeder blanket designs (Palermo et al. 2017) (Palermo et al. 2017), analyses of divertor (Palermo et al. 2018) and vacuum vessel ports (Kolšek et al. 2018). Code is also used in JET DTE campaign (Villari et al. 2016).

ORIGEN is a computer isotope generation and depletion code designed for the buildup, decay calculations and processing of radioactive materials. The code originated in Oak Ridge National Laboratory (Ludwig 2002). *ORIGEN* application for fusion reactor calculations are uncommon, however it is still used for burnup fission-fusion calculations.

ALARA (Analytic and Laplacian Adaptive Radioactivity Analysis code) is designed to calculate the induced activation caused by neutron irradiation throughout a nuclear system (including fission reactors, fusion reactors, and accelerators). (Wilson n.d.) *ANITA* code computes the radioactive inventory of a material subject to neutron irradiation, continuous or stepwise. (Cepraga, et al. 1998) Both codes uses outdated EAF-2001 nuclear data libraries and are currently rarely used.

2.2.1 Nuclear Data Libraries

The underlying constituent of all the neutron transport and activation calculation codes are nuclear data libraries. In general nuclear data libraries act as foundation of nuclear science. In form of numerical values of reaction cross-sections, energy and angular distributions, properties of atoms and radioactive decay chains nuclear data binds physical processes with empirical observations thus enabling accurate predictions.

With regards to the application and data sources, nuclear data libraries are divided into three categories: experimental nuclear data libraries, evaluated nuclear data libraries and application nuclear data libraries.

Experimental nuclear data libraries include nuclear reaction cross-sections obtained during variety of experiments consisting of neutron source measurements. The most extensive experimental data library is EXFOR (Otuka et al. 2014). EXFOR is being developed and maintained by Nuclear Data Section of IAEA currently data from 22189 experiments and it contains cross section and nuclear reaction data obtained from neutron, charged-particle and photon irradiation. The EXFOR nuclear data library has a solid coverage for reactions induced by low and intermediate energy neutrons, however higher energy reactions, that are relevant for fusion application could be still improved. This is due to the absence of high energy and high volume neutron experiments as many fusion relevant materials have rather low reaction cross-sections resulting in inconclusive information.

Evaluated nuclear data libraries were introduced in order to compensate the absence of experimental data as well to estimate the available data as not every conducted experiment provided equally reliable results. It does so by reprocessing experimental data with theoretical based models of nuclear reactions. (Fischer et al. 2018)

Application nuclear data libraries include evaluated nuclear data reprocessed for specific application related to certain nuclear technologies. Such data libraries usually are compiled in order to reduce the size of the data subsequently increasing the computation times. For example some application nuclear data libraries deal exclusively with nuclear decommissioning, photonuclear reactions, accelerators or fusion technologies.

European Activation File

European Activation File (EAF) is application neutron nuclear data library designed for activation and transmutation phenomena. The most recent version

EAF-2010 includes 816 target isotopes for neutron energy ranging from 10^{-5} eV to 60 MeV. EAF-2010 has original library format, however it is also available inENDF-6 format. (J. C. Sublet 2010)

TALYS-based evaluated nuclear data library

TALYS-based evaluated nuclear data library (TENDL) is a nuclear data library which provides in ENDF format the output of the TALYS nuclear model code system for direct use in both basic physics and applications. The TENDL library is based on both default and adjusted TALYS calculations and is complemented by data from other sources whenever required, e.g. in the resolved resonance region. (Koning et al. 2015)

The Joint Evaluated Fission and Fusion File

The Joint Evaluated Fission and Fusion File is an evaluated library produced via an international collaboration of Data Bank member countries coordinated by the JEFF Scientific Co-ordination Group, under the auspices of the NEA Data Bank. The JEFF-3.2 general purpose library has been released in 2014 and contains incident neutron data for 472 nuclides or elements from H-1 to Fm-255. (Koning et al. 2006)

Fusion Evaluated Nuclear Data Library

Fusion Evaluated Nuclear Data Library (FENDL) is application neutron nuclear data library designed for fusion technologies. It contains data in ENDF-6 format. FENDL includes 180 fusion relevant nuclides with a given reaction energies up to 150 MeV. (Lopez and Capote 2011)

Japanese Evaluated Neutron Data Library

Japanese Evaluated Neutron Data Library (JENDL) uses ENDF-6 format and contains data for 406 materials from H-1 to Fm-255. Latest version 4.0 was released in 2010 and slightly updated in 2012. JENDL is also a basis for numerous application neutron data libraries (Shibata et al. 2011)

Evaluated Nuclear Data File

Evaluated Nuclear Data File B-VIII.0 (ENDF/B-VIII.0) is evaluated nuclear data base made in United States. It is originator of ENDF format that contains data for evaluated cross sections, spectra, angular distributions, fission product yields, photo-atomic and thermal scattering law data, with emphasis on neutron induced reactions. Nuclear data library contains information for 557 nuclides. (Brown et al. 2018)

2.2.2 Energy Group Structures

Energy group structures resulted from the necessity of energy discretization for computational applications. It is favorable to select different groups for different types of nuclear devices. Regarding the neutron energy groups the selection of structure should be based on the following principles (Wu 2017):

- Group boundaries should correspond to the important threshold energies for the nuclear reactions.
- Group boundaries should correspond to abrupt change in reaction cross section.
- Most prominent reaction resonance peaks should be located in different energy groups.
- The energy group width should not exceed the maximum energy loss by elastic scattering
- The energy group width should be aligned to neutron lethargy width

For fusion applications it is important to have a high resolution in 14 MeV neutron energy range, so the energy group structure should be denser in this region. Neutron energies ranging from 100 keV to 10 MeV are also very important for calculations of fusion neutronics as such energy neutrons have significant populations as well as are reactive with commonly used structural materials. In this work three specific energy groups were used:

- Vitamin J 175 (Sartori 1985) energy group structure specifically designed for nuclear fusion blanket calculations, however it is used also for other fusion reactor structures that are close next to the neutron source. 175 neutron groups cover energy range from 0.1 eV to 19.6 MeV.
- Vitamin J+ 211 energy group structure was designed as extension of Vitamin J 175 group. It has 211 energy groups covering neutron energies from 0.1 eV to 55 MeV.
- CCFE - 709 (Hodgson et al. 2015) is a more modern energy group structure designed for variety of fusion applications. It was developed with respect to the TALYS-based evaluated nuclear data library. 709 energy groups cover neutron energies from 10^{-5} eV to 10^{9} eV.

3.RESULTS AND DISCUSSION

3.1 Material Activation Calculations in JET Long Term Irradiation Station

This section describes the activation characteristic calculations performed for Joint European Torus Long Term Irradiation Station. Such characteristics include activities and dose rates of materials irradiated in the Outer Long Term Irradiation Station O-LTIS during deuterium, tritium and DTE2 campaigns. Variety of nuclear fusion relevant material samples will be irradiated during the deuterium and tritium campaigns. Such samples include functional materials used in diagnostics and heating systems for radiation damage studies, structural steels and alloys and pure material foils.

The Joint European Torus is playing an important role in preparing the operations on the future world's largest tokomak, ITER. A new Deuterium-Tritium campaign is proposed at JET in 2019-2020 (DTE2 in Fig. 3.1.). The proposed 14 MeV neutron budget for the DTE2 is nearly an order of magnitude higher than any previous DT campaigns (in JET or TFTR) and with this proposed budget, the achievable neutron fluence on the first wall of JET will be up to 10^{20} n/m^2. This fluence is much higher than practically achievable at existing 14 MeV irradiation facility and, also important, it can be obtained in larger volumes thanks to the volume plasma neutron source.

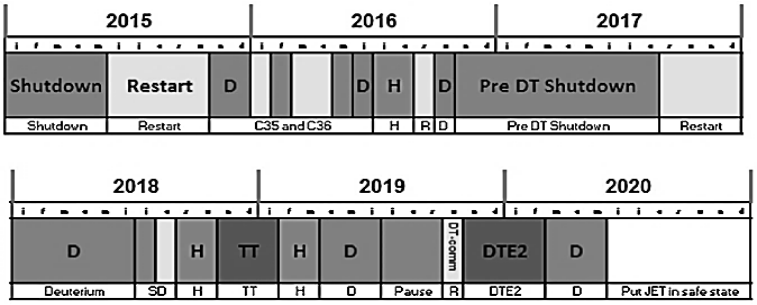

Fig. 3.1. JET operation plan and DTE campaigns.

Materials (annex) will be irradiated all during deuterium and tritium campaigns in a Long Term Irradiation Station (LTIS) that will be located inside the JET vessel, at outboard midplane where the maximum neutron fluence will be achieved, and then retrieved after the campaign. In the first case, the Inner Long Term Irradiation Station (I-LTIS), located inside the vessel at the outboard midplane, is already in use for the 2015 deuterium campaign, but it is not favored for deuterium-tritium operations mainly due to tritium contamination of samples and due to the need to use the remote handling for the installation and removal. The I-LTIS consist of a Tungsten Shim, AISI316 Tray Sample Holder and AISI316 Box Sample Holder. Alternatively, as the second case, the Outer Long Term Irradiation

Station (OLTIS) would be located in a closed lower small horizontal port in Octant 7, and the installation/removal of samples does not require the use of in-vessel remote handling system.

The location of OLTIS in the JET vessel is shown in Fig. 3.2. The objective of the present work is to calculate the activity, contact dose rates of the samples of ITER structural material and of functional materials at the location of OLTIS box. We also calculate the activation of station components as resulting from neutron long-term irradiation after whole deuterium and tritium campaigns.

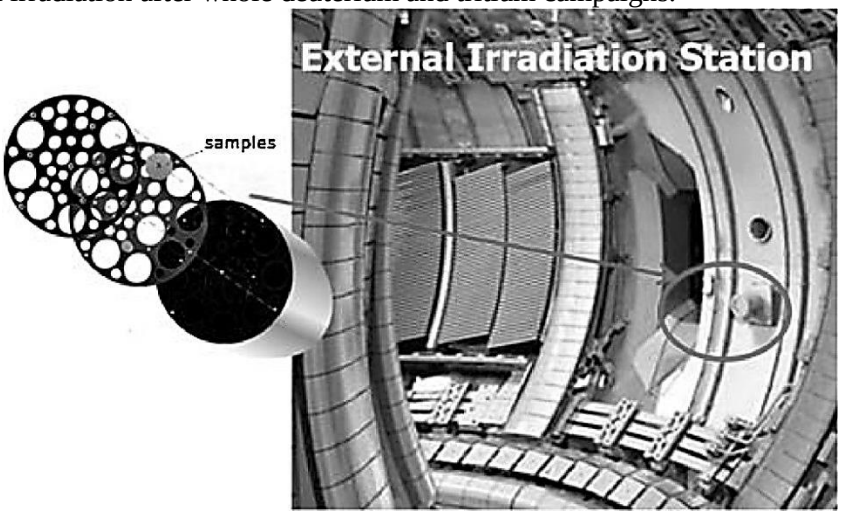

Fig. 3.2. OLTIS and its position in vacuum vessel.

Neutron induced activities and contact dose rates at shutdown are calculated by means of the FISPACT-2010 code with EAF-2010 using the neutron flux densities and spectra (Fig. 3.4-6.) provided by the preceding MCNP neutron transport calculation for LTIS box.

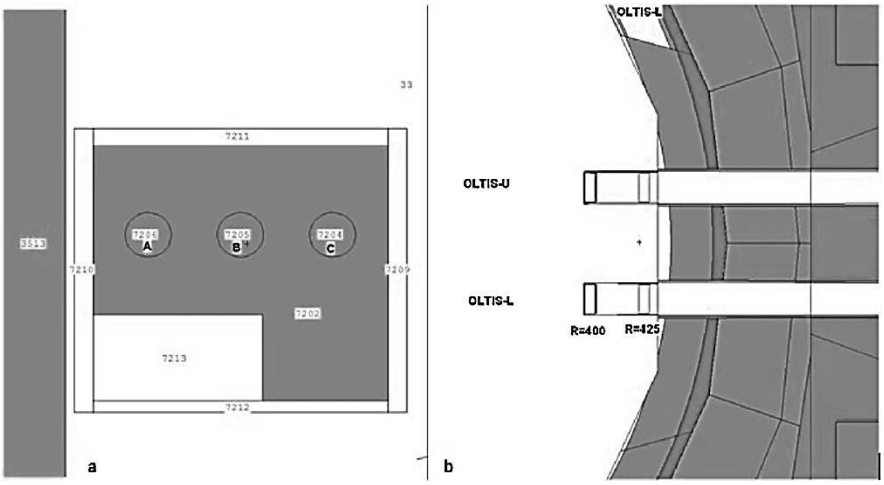

Fig. 3.3. MCNP model of LTIS (a) and position of the OLTIS (b).

The neutron transport calculation for OLTIS was performed with MCNP5 to obtain the neutron fluxes and spectra with the model as illustrated in Fig. 3.3. The calculated local neutron fluences are 6.3 10^{-6} for deuterium-deuterium and 6.23 10^{-6} for deuterium-tritium per source neutron. After the end of irradiation, the activities and dose rates are calculated at the cooling time of 0 and 1 s, 1 h, 1 day, 1 week, 1 month, 1 year.

Deuterium-tritium (DTE2) and deuterium-deuterium activation calculations

For subsequent calculations each campaign was considered separately. Irradiation scenario is assumed to be continuous with 1 MW/m^2 wall load. Material samples were selected with regard for their application in auxiliary equipment that otherwise would not face direct neutron source, but still could be affected by stray radiation. Such materials include samples for diagnostic, cooling, magnet and other systems. Fig. 3.4. shows neutron spectra used for this calculation. Both deuterium-tritium and deuterium-deuterium campaigns assumed to last for 4 months. Deuterium-tritium campaign known as DTE2 will operate with 50% deuterium and 50% tritium fuel.

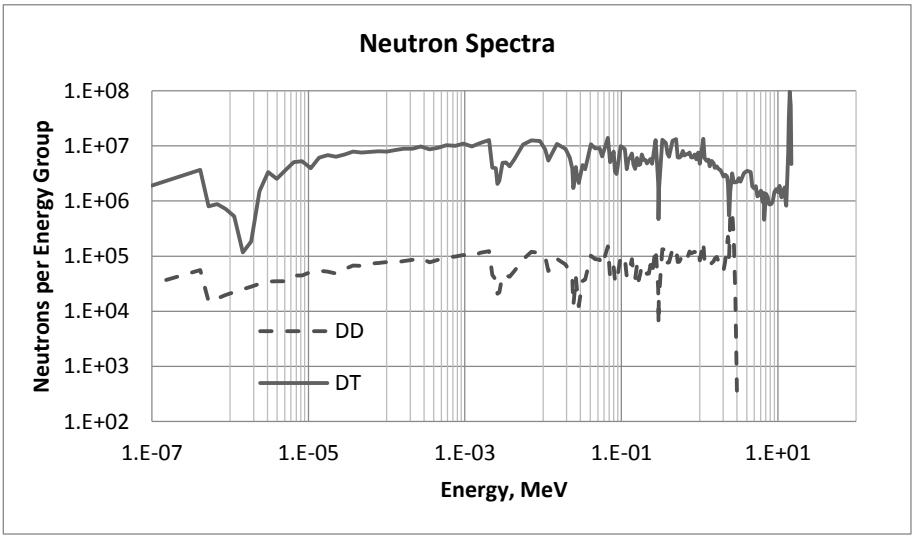

Fig. 3.4. Deuterium-deuterium and deuterium-tritium neutron spectra at OLTIS box.

This section contains neutron induced activities and contact dose rates (together with most contributing isotopes identified) at shutdown and other time intervals using the neutron flux densities.

In Table 3.1. preliminary material samples are examined, most of them are functional materials for in-vessel components including:

- Optical transmission materials for diagnostics can be darkened in case of presence of neutron flux and reflective coatings can also be damaged.

- Insulators and senor materials for diagnostics, where dielectric and electric properties can by altered by irradiation leading to inaccurate measurements and malfunction.
- Superconducting material performance depends on the temperature and structural integrity that can be heavily influenced by irradiation and subsequent decay heat from activation.
- Various alloys for coils, rails, cooling system elements, etc.

Table 3.1. JET deuterium-tritium and deuterium-deuterium irradiation calculation results.

Material	DD n-flux				DT n-flux				Princ. Radionucl.
	Activity		Dose rates		Activity		Dose rates		
	1 month	1 year	1 month	1 year	1 month	1 year	1 month	1 year	
Sapphire (Al2O3)	< 0.001 Bq/g	< 0.001 Bq/g	-	-	< 0.01Bq/g	< 0.01Bq/g	-	-	14C
YAG	~3 Bq/g	< 0.001 Bq/g	-	-	~ 2 Bq/g	< 0.001 Bq/g	-	-	90Y/14C
ZnS	1.3 kBq/g	0.5 kBq/g	0.2 mSv/Hr	80 μSv/Hr	~ 75 kBq/g	30 kBq/g	12 mSv/Hr	4.6 mSv/Hr	65Zn
Spinel	< 0.001 Bq/g	< 0.001 Bq/g	-	-	< 0.01Bq/g	< 0.01Bq/g	-	-	14C
KUI1	25 Bq/g	25 Bq/g	< 0.1 μSv/Hr	< 0.1 μSv/Hr	~ 1.3 kBq/g	~ 1.2 kBq/g	< 0.1 μSv/Hr	< 0.1 μSv/Hr	3H
KS-4V	40 Bq/g	37 Bq/g	< 0.1 μSv/Hr	< 0.1 μSv/Hr	2 kBq/g	2 kBq/g	< 0.1 μSv/Hr	< 0.1 μSv/Hr	3H
ALON (Al22O30N2)	0.2 Bq/g	0.2 Bq/g	-	-	9 Bq/g	9 Bq/g	-	-	14C
ALON-23 (Al23O28N5)	0.4 Bq/g	0.4 Bq/g	-	-	22 Bq/g	22 Bq/g	-	-	14C
ALON-67 (Al67O87N9)	0.25 Bq/g	0.25 Bq/g	-	-	14 Bq/g	14 Bq/g	-	-	14C
ALON-68 (Al68O64N12)	0.3.5 Bq/g	0.3.5 Bq/g	-	-	18 Bq/g	18 Bq/g	-	-	14C
Al-Bronze	30 Bq/g	24 Bq/g	13 μSv/Hr	11 μSv/Hr	1.5 kBq/g	1.25 kBq/g	0.7 mSv/Hr	0.6 mSv/Hr	60Co
Alloy 660	1.3 kBq/g	0.1 kBq/g	10 μSv/Hr	< 0.1 μSv/Hr	70 kBq/g	6 kBq/g	0.7 mSv/Hr	3 μSv/Hr	55Fe
Be(S-65C)	1 Bq/g	1 Bq/g	< 0.1 μSv/Hr	< 0.1 μSv/Hr	8 Bq/g	6 Bq/g	< 0.1 μSv/Hr	< 0.1 μSv/Hr	55Fe
CuCrZr	60 Bq/g	< 0.1 Bq/g	< 0.1 μSv/Hr	< 0.1 μSv/Hr	3 kBq/g	1 Bq/g	20 μSv/Hr	< 0.1 μSv/Hr	51Cr
JI1	1 kBq/g	0.1 kBq/g	25 mSv/Hr	10 mSv/Hr	60 kBq/g	7 kBq/g	1.4 mSv/Hr	0.6 mSv/Hr	51Cr/55Fe
Nb3Sn	40 kBq/g	0.55 kBq/g	1.4 mSv/Hr	0.2 mSv/Hr	0.3 MBq/g	0.04 MBq/g	0.1 Sv/Hr	0.014 Sv/Hr	182Ta
NbTi	1.5 Bq/g	0.3 Bq/g	< 0.1 μSv/Hr	< 0.1 μSv/Hr	0.4 kBq/g	0.3 kBq/g	40 μSv/Hr	7.5 μSv/Hr	182Ta/93mNb
OF-CU	0.01 Bq/g	0.01 Bq/g	-	-	0.1 Bq/g	0.1 Bq/g	< 0.1 μSv/Hr	< 0.1 μSv/Hr	63Ni
SS-304 (Borated)	1.7 kBq/g	0.14 kBq/g	30 μSv/Hr	10 μSv/Hr	90 kBq/g	7.6 kBq/g	1.7 mSv/Hr	0.6 mSv/Hr	51Cr/55Fe
SS316L(N)	1.5 kBq/g	0.14 kBq/g	30 μSv/Hr	10 μSv/Hr	80 kBq/g	7.6 kBq/g	1.5 mSv/Hr	0.6 mSv/Hr	51Cr/55Fe
SS316L(N)-IG	1.6 kBq/g	0.15 kBq/g	30 μSv/Hr	10 μSv/Hr	82 kBq/g	7.7 kBq/g	1.6 mSv/Hr	0.6 mSv/Hr	51Cr/55Fe
SS316L	1.7 kBq/g	0.2 kBq/g	100 μSv/Hr	50 μSv/Hr	92 kBq/g	11 kBq/g	6.2 mSv/Hr	2.7 mSv/Hr	51Cr/55Fe
XM-19	1.9 kBq/g	0.13 kBq/g	32 μSv/Hr	14 μSv/Hr	100 kBq/g	6.9 kBq/g	1.75 mSv/Hr	0.6 mSv/Hr	51Cr/55Fe
ZrO2	100 Bq/g	4 Bq/g	17 μSv/Hr	0.7 μSv/Hr	8.4 kBq/g	0.34 kBq/g	1.5 mSv/Hr	0.6 mSv/Hr	95Zr/95Nb

Activation calculations for aggregate deuterium-tritium and deuterium-deuterium scenario

In this section aggregate scenario is considered where total activities and dose rate are calculated after multiple campaigns (Table 3.2.). This scenario is comprised of the 1st deuterium-deuterium (DD1) and 2nd deuterium-deuterium (DD2) campaigns, two hydrogen campaigns (H1 and H2), where no neutrons are assumed

and Tritium Tritium (TT). Tritium Tritium campaign will be operating with 99% and 1 percent of deuterium, however due to massive difference in reaction cross-sections deuterium-tritium reaction will still be the main source of neutrons in this campaign. Here pure material foils were investigated in terms of activity and dose rate after irradiation. Together with the contact dose rate, dose rate at 30 cm distance was also calculated. Neutron spectra are presented in Fig. 3.5.

Table 3.2. Campaigns at JET.

DD1	**H1**	**TT**	**H2**	**DD2**
180 days	60 days	90 days	60 days	90 days

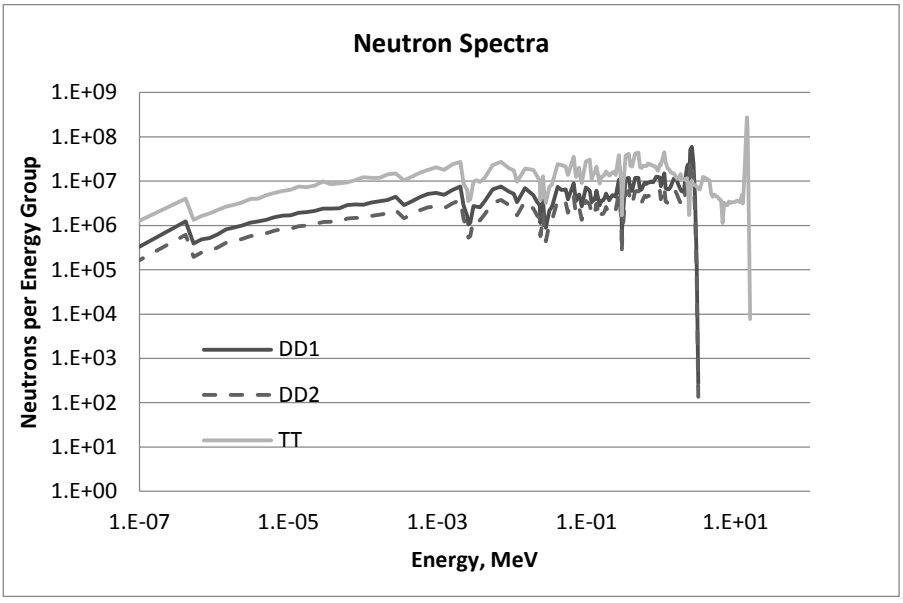

Fig. 3.5. OLTIS neutron spectra used for calculation of pure material foils.

Table 3.3. JET aggregated irradiation scenario calculation results.

Material	Activity			Contact dose rate			Dose rate at 30 cm			Princ. Radionuclide		
	1 second	1 month	1 year	1 second	1 month	1 year	1 second	1 month	1 year	1 second	1 month	1 year
Al	~ 1.1 MBq/g	-	-	~ 0.64 Sv/Hr	-	-	2.5 uSv/Hr	-	-	Al 28	-	-
Co	~ 65 MBq/g	~ 13 MBq/g	~ 11 MBq/g	~ 9.4 Sv/Hr	~ 9 Sv/Hr	~ 8 Sv/Hr	100 uSv/Hr	43 uSv/Hr	38 uSv/Hr	Co 60m	Co 60	Co 60
Fe	~ 85 kBq/g	~ 80 kBq/g	~ 60 kBq/g	~ 3.7 mSv/Hr	~ 1.8 mSv/Hr	~ 0.22 mSv/Hr	77 nSv/Hr	67 nSv/Hr	47 nSv/Hr	Fe 55	Fe 55	Fe 55
In	~ 3 GBq/g	~ 2.1 MBq/g	~ 21 kBq/g	~ 1200 Sv/Hr	~ 12 mSv/Hr	~ 0.11 mSv/Hr	6 mSv/Hr	307 nSv/Hr	3 nSv/Hr	In116m	In 114/In 114m	In 114/In 114m
Mn	~ 30 MBq/g	-	-	~ 17 Sv/Hr	-	-	75 uSv/Hr	-	-	Mn 56	-	-
Ni	~ 110 kBq/g	~ 43 kBq/g	~ 11 kBq/g	~ 15 mSv/Hr	~ 7.8 mSv/Hr	~ 0.37 mSv/Hr	140 nSv/Hr	73 nSv/Hr	4 nSv/Hr	Co 58	Co 58	Ni 63
Sc	~ 93 MBq/g	~ 46 MBq/g	~ 2.9 MBq/g	~ 32 Sv/Hr	~ 25 Sv/Hr	~ 1.5 Sv/Hr	175 uSv/Hr	130 uSv/Hr	8uSv/Hr	Sc 46	Sc 46	Sc 46
Ta	~ 47 MBq/g	~ 40 MBq/g	~ 5.3 MBq/g	~ 15 Sv/Hr	~ 12.5 Sv/Hr	~ 1.7 Sv/Hr	130 uSv/Hr	110 uSv/Hr	14.5 uSv/Hr	Ta 182	Ta 182	Ta 182
Ti	~ 29 kBq/g	~ 1 kBq/g	~ 77 Bq/g	~ 2.8 mSv/Hr	~ 515 uSv/Hr	~ 32 uSv/Hr	19 nSv/Hr	3 nSv/Hr	-	Ti 51	Sc 46	Sc 46
Y	~ 3.5 MBq/g	~ 1 kBq/g	~ 1.5 Bq/g	~ 23 mSv/Hr	~ 15 mSv/Hr	-	125 nSv/Hr	-	-	Y 90	Y 90	Sr 89

Activation calculations for detailed tritium-tritium scenario

In this section structural steels and other alloys were investigated. In addition to previous scenario (Table 3.2.), TT campaign was also specified (Fig. 3.6.) Neutron spectra used for calculation are presented in Fig. 3.5.).

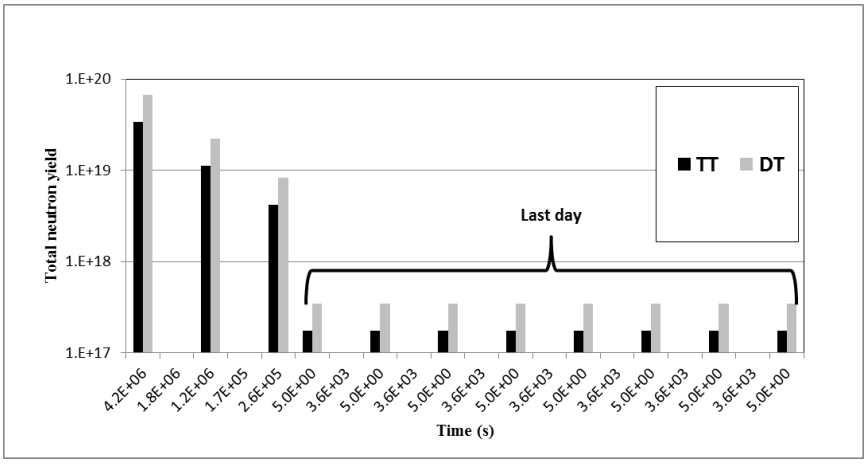

Fig. 3.6. Irradiation scenario for DT campaign.

Table 3.4. JET detailed irradiation scenario calculation results.

Material	Activity			Contact dose rate			Dose rate at 30 cm			Princ. Radionuclide		
	1 second	1 month	1 year	1 second	1 month	1 year	1 second	1 month	1 year	1 second	1 month	1 year
316L(N)-IG	49 MBq/kg	18 MBq/kg	4 MBq/kg	11.7 mSv/h	4.0 mSv/h	0.8 mSv/h	83 nSv/h	36 nSv/h	7 nSv/h	Co 58	Co 58	Mn 54
316LN	48 MBq/kg	18 MBq/kg	4 MBq/kg	11.4 mSv/h	3.8 mSv/h	0.8 mSv/h	80 nSv/h	34 nSv/h	7 nSv/h	Co 58	Co 58	Mn 54
316L	48 MBq/kg	18 MBq/kg	4 MBq/kg	11.6 mSv/h	4.0 mSv/h	1.0 mSv/h	81 nSv/h	35 nSv/h	7 nSv/h	Co 58	Co 58	Mn 54
Alloy 660	61 MBq/kg	27 MBq/kg	3 MBq/kg	13.4 mSv/h	5.9 mSv/h	0.5 mSv/h	107 nSv/h	55 nSv/h	5 nSv/h	Co 58	Co 58	Mn 54
Alloy 660 div	64 MBq/kg	27 MBq/kg	3 MBq/kg	15.1 mSv/h	5.9 mSv/h	0.5 mSv/h	115 nSv/h	55 nSv/h	5 nSv/h	Co 58	Co 58	Mn 54
Al-Bronze	289 MBq/kg	5 MBq/kg	1 MBq/kg	13.3 mSv/h	1.1 mSv/h	0.1 mSv/h	223 nSv/h	10 nSv/h	1 nSv/h	Cu 64	Co 58	Ni 63
CuCrZr	337 MBq/kg	0.43 MBq/kg	0.35 MBq/kg	12.3 mSv/h	0.004 mSv/h	~10 nSv/h	244 nSv/h	~0	~0	Cu 64	Ni 63	Ni 63
EUROFER 97-3	57 MBq/kg	22 MBq/kg	6 MBq/kg	10.6 mSv/h	5.5 mSv/h	1.1 mSv/h	96 nSv/h	47 nSv/h	10 nSv/h	W 187	Ta 182	Mn 54
INCONEL 718	152 MBq/kg	60 MBq/kg	13 MBq/kg	23.6 mSv/h	18.1 mSv/h	6.7 mSv/h	232 nSv/h	137 nSv/h	35 nSv/h	Co 58	Co 58	Co 60
SS304	35 MBq/kg	18 MBq/kg	4 MBq/kg	7.4 mSv/h	3.8 mSv/h	0.8 mSv/h	61 nSv/h	34 nSv/h	7 nSv/h	Co 58	Co 58	Mn 54
W	2570 MBq/kg	165 MBq/kg	8 MBq/kg	141.0 mSv/h	0.002 mSv/h	~10 nSv/h	2840 nSv/h	6 nSv/h	1 nSv/h	W 187	W 185	W 185
XM-19	72 MBq/kg	19 MBq/kg	4 MBq/kg	22.9 mSv/h	4.1 mSv/h	0.8 mSv/h	134 nSv/h	36 nSv/h	7 nSv/h	Mn 56	Co 58	Mn 54

Activities and dose rates (contact and at the distance of 30 cm) were obtained for the samples of JET long term irradiation station. Firstly samples for potential materials were analyzed (28 samples). Out of these samples 1 month after irradiation 11 (for DD) and 13 (for DT) exhibited larger than 10 μSv contact dose rates. Two samples had higher than 2 mSv contact dose rates. Highest activity was exhibited by Nb3Sn, SS316L, XM-19 samples. Later on selected materials for LTIS were examined (36 samples, including 10 pure material foils). Complex irradiation scenario was applied. 7 foils after irradiation and 1 month of cooling 7 out of 10 foils exceeded 10 μSv contact dose rate, while 6 had larger than 2 mSv dose rate. Management of such materials requires remote handling. Highest dose rate was

exhibited by scandium and highest activity by indium. Out of 11 metal alloy foils 8 exhibited larger than 2 mSv contact dose rate 1 moth after the irradiation.

Irradiation step increment effect on activation from deuterium-deuterium and deuterium-tritium reactions

Increasing the amount of irradiation steps can yield tangible differences in calculation results even though neutron budget and full time irradiation interval remains the same. In general results are more affected by radionuclides with half-lives that correspond to irradiation steps. Decay estimations and possible reactions also differ. In the section irradiation step increment was analyzed for separate deuterium-deuterium (DT) and deuterium-tritium (DT) spectra from DTE2 campaign (Fig 3.4.). DT and DD activation characteristics for detailed scenario presented in (Fig 3.6.) are compared to continuous scenario. Total amount of neutrons are equal for both scenarios.

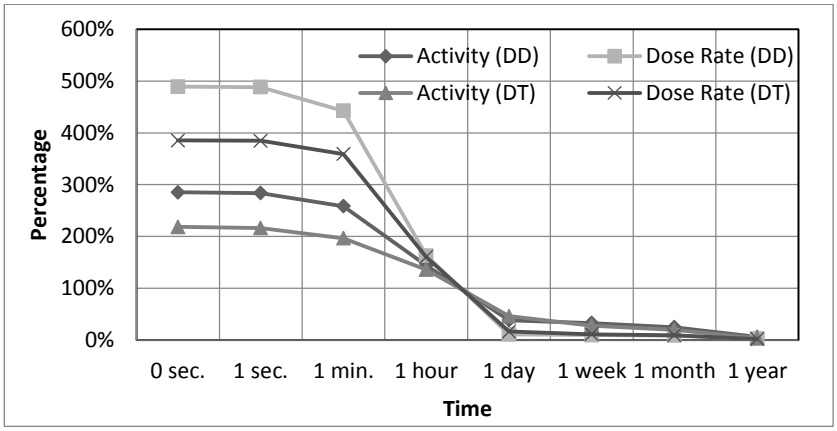

Fig. 3.7. Activity and dose rate differences between continuous irradiation scenario and detailed scenario.

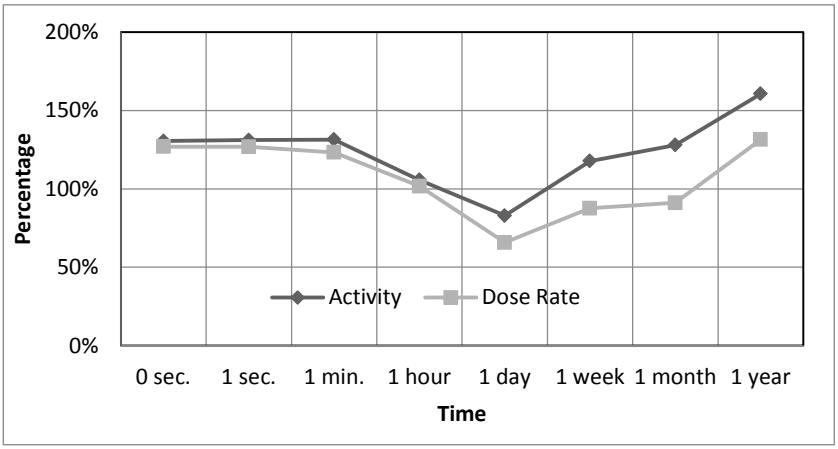

Fig. 3.8. Comparison of differences due to irradiation step increment between DD and DT.

After increment of irradiation steps in irradiation scenarios, dose rates can differ for as much as 4 and 5 times for DT and DD respectively within a minute after operation, while activity can differ for as much as 2 and 3 times (Fig. 3.7.). More so, activities and dose rate drop by as much as magnitude of 10. Comparison of irradiation steps increment influence between DD and DT scenarios shows that dose rate and activity values in DD scenarios are influenced up to 30 percent within first minute after end of irradiation (Fig. 3.8.).

3.2 ACTIVATION CALCULATIONS OF IFMIF-DONES

In this section IFMIF-DONES neutron irradiation effects on test cell facility biological shielding and cooling structure that are close to the neutron source were examined.

IFMIF-DONES is a testing facility equipped with accelerator based d-Li neutron source which aims at reproducing irradiation conditions under DEMO fusion power reactor operation for the qualification of fusion materials. The basis of IFIMIF-DONES is superconducting radio frequency linear accelerator guiding 40 MeV deuterons to the lithium target. The high intensity neutron radiation produced in the liquid lithium target results in a strong material activation in the Test Cell (TC) including the High Flux Test Module (HFTM), housing the irradiation specimens, the TC steel liner and the water cooled concrete walls.

The Test Systems comprise all equipment, primary heat removal systems, and handling equipment for an accurate and safe positioning and handling of test modules and target during beam operation and maintenance. In the TC system deuteron beams converge at the lithium target area to generate high neutron and gamma emissions to irradiate Test Modules (TMs). Subsequently, large amount of radioactive material is being produced. By the design it should be built in Na free concrete with 316 stainless steel liner, therefore main radioactive materials to be considered are: 1) Activation Products (AP) in stainless steel liner, pipes, cables, etc., 2) tritium production in concrete, although it is expected to be negligible and 3) Activated Corrosion Products (ACP) in cooling systems: He stream, Li and water. In general, tritium associated radiological hazards mainly concern the TMs. ACP associated radiological hazards mainly concern gas and liquid cooling system of TMs, Lower Shielding Plug of the TC and TC liner. AP formation related radiological hazards mainly concern stainless and reduced activation steels of TC liner and structural components of the TMs.

Test Cell is surrounded by biological shielding composed of heavy concrete and stainless steel inner liner. Inner layer is an independent closed framework which is covered with liner from inside with a thickness of 8 mm. Between the liner and inner shielding a set of water cooling pipes is placed. The cooling pipes in this setup are responsible for excess heat removal during the irradiation operation as neutrons will deposit significant amount of heat inside the shielding. On top of that, activated

materials will also produce heat via decay processes. The thickness of the inner layer ranges from 1 m at the beam and lateral directions to 0.5 m at the ground direction.

In addition, TC is a blind hot cell with an opening at the top (see Fig. 3.9). The surrounding shielding walls are riveted with a liner which together with the TC upper cover plate provide a vacuum tight enclosure. Inert atmosphere is maintained inside during beam operation. Furthermore liner and cover constitute as containment for the radioactive inventories in the lithium loop and in the cavity with the TMs. Liner and concrete made biological shielding are cooled with chilled water.

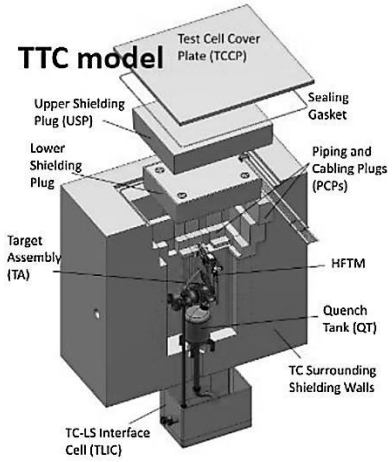

Fig. 3.9. Test Cell with internals and including HTFM

Biological dose rate distribution around the Test Cell, calculated for 345 days operation and one day cooling after shutdown is lower than 7.5 μSv/h in most places of the Access cell (AC). The results show that when both TC shielding plugs have been removed (that is, the Test Cell is full open), the dose rate in the AC will be quite high (more than 1 Sv/h). Due to the activation of the liner and the concrete wall, the residual dose rate is still very high even without all the removable in-cell components.

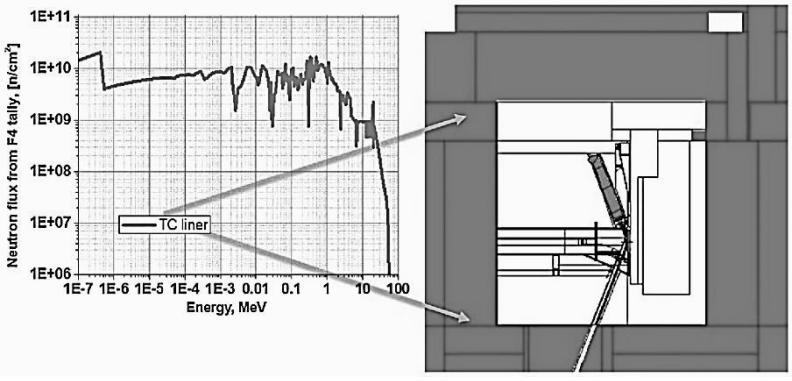

Fig. 3.10. Neutron 211 g spectrum of TC liner for.

Neutron transport calculations with MCNP were used in order to obtain neutron flux distribution in 211 energy group, FISPACT-II was used in order to obtain activation characteristics.

The irradiation scenario is based on the operation scheme specified by DONES project. The scheduled operation runs over 10 calendar years. 345 day full power irradiation (the operation schedule assumes a 345 day irradiation period and a 20 days maintenance period). The decay times considered for the calculation of the activity inventories and the decay heat are as follows: 0 s, 1 s, 5 min, 30 min, 1 h, 3 h, 5 h, 10 h, 1 day, 3 days, 1 week, 2 weeks, 4 weeks, 8 weeks, 6 months, 1 year, 10 years, 50 years, 100 years, 300 years and 1000 years.

The inventory analysis was carried out for the TC liner. Cell based analysis was performed; the liner part consists of 8 cells in the present calculation model (top, bottom, downstream, upstream, two lateral sides and two for TM supports).

The scheduled operation scenario as indicated before was assumed in the activation calculation. Figs. 3.11–13. show activity, decay heat and the contact dose rate calculated for the TC liner on the lateral TM support wall. The differences in the neutron spectra among the 8 cells examined are not significant enough, thus the most dominant nuclides and the decay trends are similar in all the cells of TC liner. In Fig. 3.11. the specific activity for the TC liner on the lateral wall and the total activity calculated for all liner cells are shown. The liner is 10 mm thick.

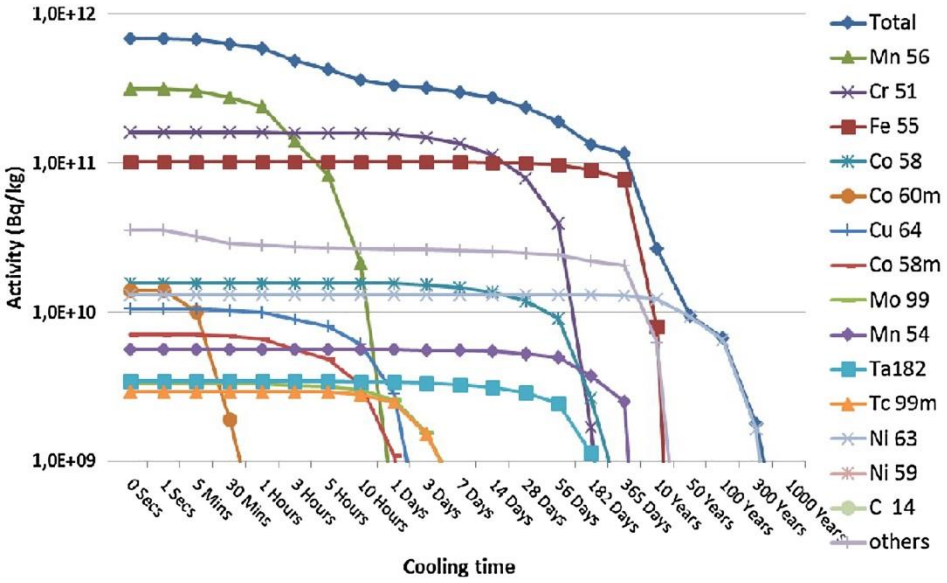

Fig. 3.11. Time evolution of activity induced in the TC liner.

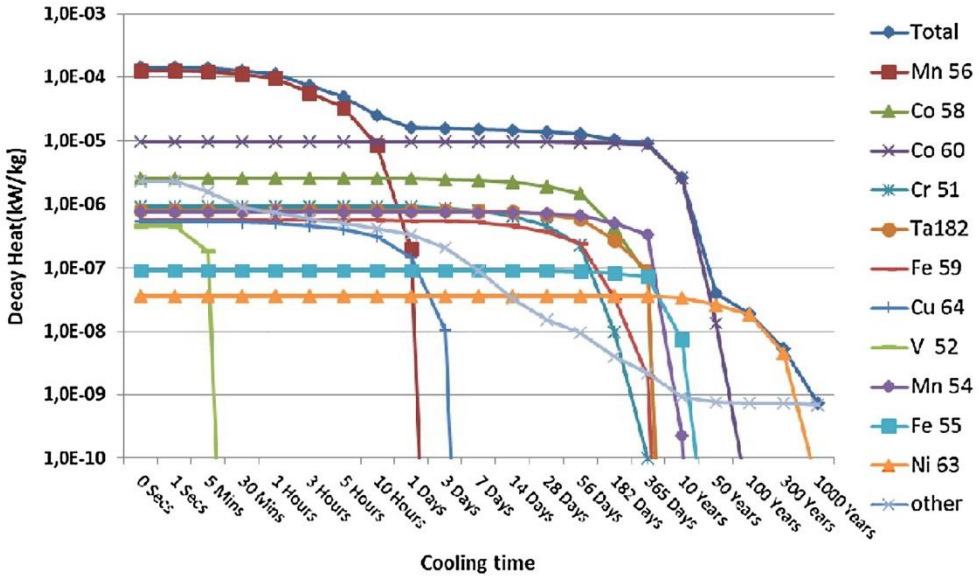

Fig. 3.12. Time evolution of decay heat for the TC liner on the lateral TM support wall after 10 years of operation.

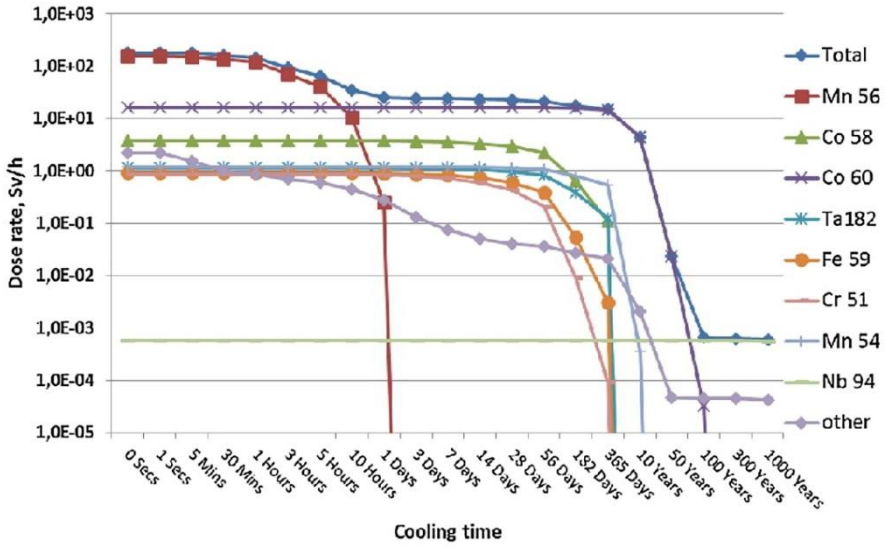

Fig. 3.13. Time evolution of the contact dose rate for the TC liner on the lateral TM support wall after 10 years of operation.

Material activation due to broader neutron energy spectrum is dominated by high energy (n, p) and (n, 2n) reactions in contrast to nuclear fusion devices based on deuterium and tritium fusion. The largest decay heat contributor after the decay of Mn-56 is Co-60 and it stays relevant for about 10 years.

The preliminary activity, decay heat and contact dose rate analysis has been also carried out for the water coolant which is used for the TC biological shielding. Although the detailed structure of the TC cooling network topology has not yet been decided, a rough estimation about water activation using calculated neutron spectrum was performed.

An adjusted TC model, in which water cooling pipes with 10 cm in diameter were considered (as shown in Fig. 3.14), was used to calculate the neutron spectra (Fig. 3.15). Each spectrum was averaged over each layer of pipes.

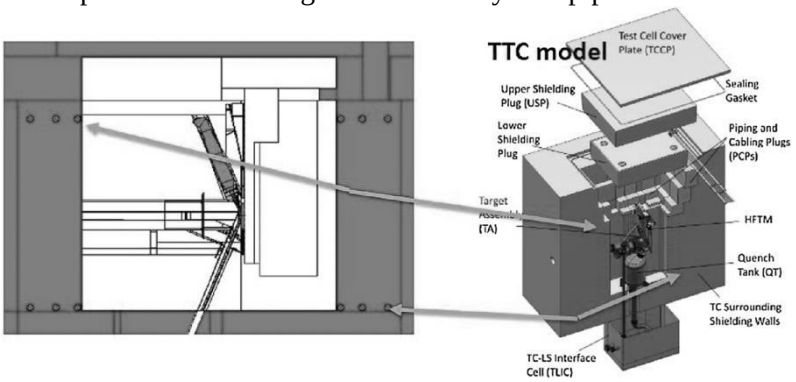

Fig. 3.14. Suggested approach to model water pipes inside the biological shielding.

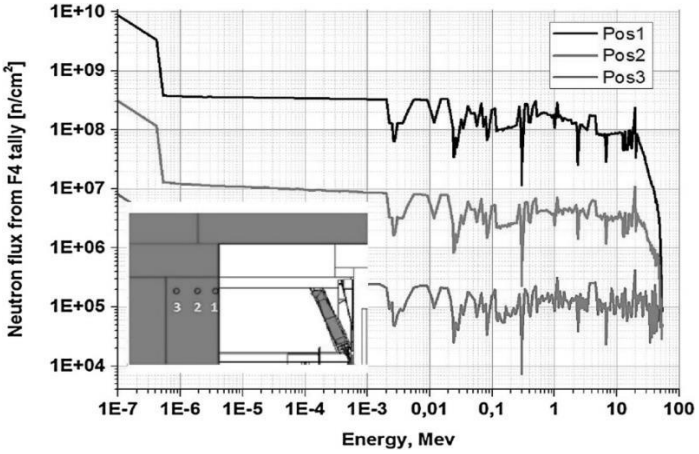

Fig. 3.15. Calculated neutron flux spectrum at three positions inside the biological shielding.

The total amount of water in the biological shielding walls was expected to be about 0.5 m^3. Water circulation was excluded from this study for the reason that utilized tools are not suited for coupling activation calculation with dynamic changes in environment.

Calculated inventory of dominant nuclides after 10 years irradiation is shown in Fig. 3.16. and 3.17. There are several key radionuclides with aggregate half-lives

ranging from 5 to 30 minutes. These nuclides are mostly the products of oxygen isotope reactions. In particular, N-16 (half-life 7.13 sec, 16O(n,p) reaction, β- decay resulting in high energy 6.13-MeV gamma emission) and O-15 (half-life 2.037 min, 16O(n,2n) reaction, β+ decay) constitute almost two orders more than the others within first 5 minutes after end of irradiation. Furthermore they pose radiological risk during whole device operation period and shortly after its shutdown. So for the safe operation, shutdown dose rates should be carefully estimated around the cooling system, more so system itself should be adequately shielded. Closed loops should also prevent activated coolant to leave radiation control zones.

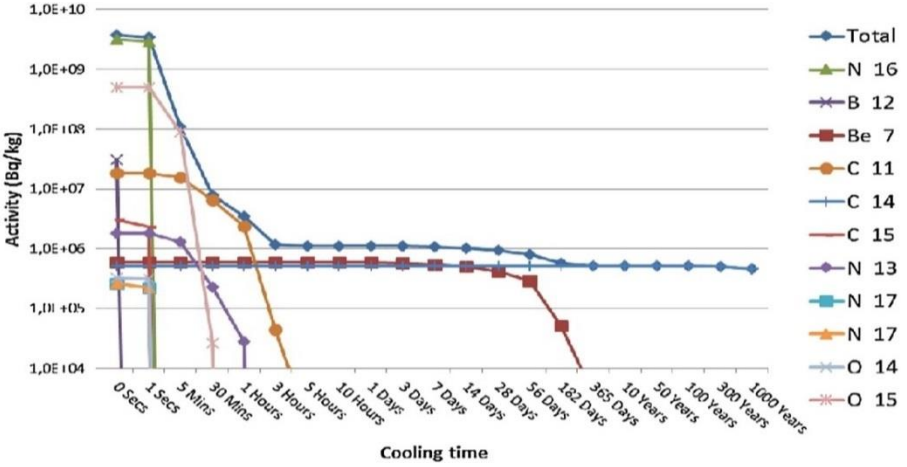

Fig. 3.16. Time evolution of activation calculated for the TC cooling water in the most inner layer (excluding tritium).

Production of N-17 from 18O(n,d) and 17O(n,p) reactions is insignificant (Fig. 3.16-17.) even though former reaction cross-section is larger than 16O(n,p) as O-17 and O-18 isotopes account for less than in percent in natural abundance of oxygen isotopes.

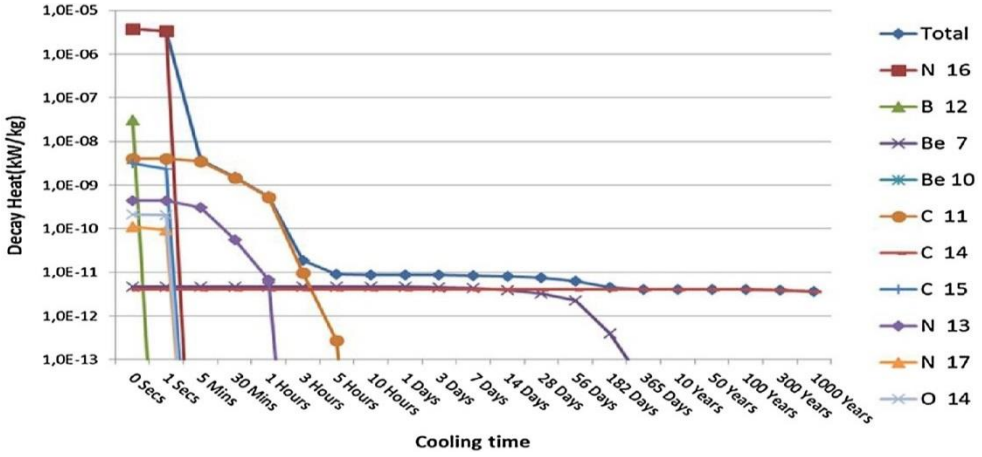

Fig. 3.17. Time evolution of decay heat calculated for the TC cooling water in the most inner layer (excluding tritium).

The total value of the specific decay heat reaches about $5 \cdot 10^{-5}$ kW/kg at the beginning of the cooling time and drops down to the negligible values in approximately 30 min after the beam is off. In addition, the biggest radiological hazard in cooling systems with water as coolant is N-16 nuclide, which is heavy gamma emitter as well as a nuclide responsible for highest activities, dose rates and decay heat for few seconds after the end of irradiation.

Activity inventories and decay heat for waste evaluation and decommissioning are essential parameters for development of any nuclear device. The activities in this field aim to provide the preliminary calculation results and identify the needs for updates to be performed for further development of IFMIF-DONES Test Cell facility.

The specific activity in the TC liner is mainly caused by Mn-56, Cr-51 and Fe-55 radionuclides. The most common radionuclide producing neutron reactions in TC liner steel are Fe-56 (n, p) (~54%) results in Mn-56, Cr-52 (n, 2n) (~67%) results in Cr-51 and Fe-56 (n, 2n) (~92%) results in Fe-55.

The biggest concern in the water cooling systems is N-16 nuclide, which has significant impact on the total value of specific activity and dose rate. Specific decay heat value drops to insignificant value within half an hour and after the end of irradiation (from ~10^{-3} kW/kg reaching 10^{-5} kW/kg).

Activation characteristics were obtained for IFMIF-DONES test cell facility biological shielding and cooling system structures. These structures were mainly composed of SS316L(N)-IG steel, concrete and water. Activated steel exhibits very large contact dose, largely due to Co-60 which is relevant for 50 after the irradiation. The material stays radiologically hazardous for the whole investigated 1000 year period. Due to high decay heat it is recommended to apply 1 year wet cooling for closest compartments and dry cooling for the next 100 years after discontinuation of irradiation. Activation for concrete had no radiological significance. In cement mixture highest activity was exhibited by 4th period metal isotopes. For water activity highest influence had short-lived N-16 and O-15 radionuclides. In subsequent cooling periods activity rapidly drops and carbon isotopes with tritium begin to dominate.

3.3 Activation Calculations of DEMO WCLL Breeder Blanket Module

3.3.1 DEMO 2014 and DEMO 2015 WCLL Breeder Blanket Module

One of the conceptual designs of the breeder blanket for a European DEMO is the Water Cooled Lithium Lead (WCLL) concept. Design development of the WCLL blanket in recent years has undergone evolution of the neutronics model employing the MCNP code, with key changes in radial lengths and thickness as well as dimensional differences in inner structures, such as breeding zone, shielding zones and manifold. Furthermore there has also been a significant increase in projected fusion power. Such changes were made with respect to its nuclear, thermohydraulic and thermomechanical performances. In this work neutronic

characteristics of WCLL modules were analyzed in terms of fusion power increase and dimensional changes of the blanket geometry presented in DEMO 2014 and 2015 models. For comparison, outboard and inboard single segment blanket modules of equatorial region were selected. Investigated neutronic characteristics include activity, decay heat and contact dose rates. Numerical experiment was carried out with MCNP particle transport code and FISPACT/FISPACT-II activation calculation codes with EAF-2010/TENDL-2015 nuclear data libraries.

Table 3.5. DEMO baseline models.

Model	Fusion power [MW]	Major radius [m]	Minor radius [m]
DEMO2014	1570	9.0	2.25
DEMO2015	2037	9.072	2.927
DEMO2017	1998	8.938	2.883

A DEMO reactor might be the first prototype of commercial reactor. Its development and design is constantly being changed with regards to the newly attained knowledge from other fusion projects and the emerging techniques. Crucial component for such a reactor is a module called the breeding blanket. The breeding blanket mainly serves as neutron multiplier and tritium producer. There are few types of breeding blankets, which in principle differ in coolant type and breeder zone compositions. For this study a water-cooled lithium lead breeding blanket was selected for examination.

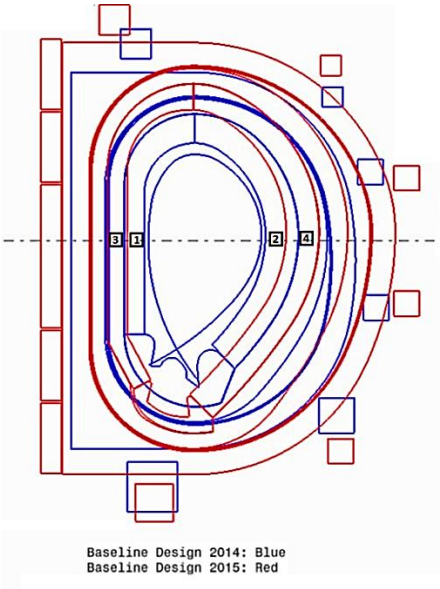

Fig. 3.18. Comparison of reactor vacuum vessel cross section geometric change. 1 and 2 blanket module localizations for 2014 IB and OB modules respectively, 3 and 4 for 2015 IB and OB modules.

Activity inventories and decay heat output of DEMO WCLL equatorial breeding blanket modules were examined in terms of recent changes in reactor nominal power and geometry seen in Fig. 3.18. Compared to the 2014 DEMO baseline, in the 2015 version the fusion power was significantly increased from 1570 MW to 2037 MW. The major radius was changed from 9.0 to 9.072 m. and the minor radius from 2.25 to 2.927 m. For the WCLL module changes were introduced in order to reduce parasitic neutron absorption by blanket structural steels. Parasitic absorption can not only make device less efficient, but also impair tritium breeding in the blanket.

The Water Cooled Lithium Lead blanket design is based on water cooling. Other prominent designs include helium as primary or secondary coolant. With the DEMO reactor advancement, there were also changes made in the blanket geometry.

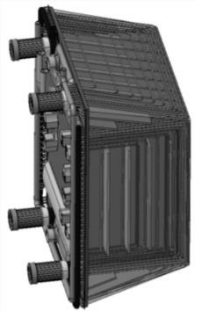

Fig. 3.19. 2015 DEMO WCLL Blanket module. CAD visualization.

There is only a slight variation in the inner structure composition fractions, which for the 2015 model are presented in table 3.5. Investigated WCLL modules were divided into six different segments that correspond to different materials or compositions: armour (AR), first wall (FW), breeder zone (BZ), caps (CP), backplate (BP) and manifold (MF). The armour is made from tungsten alloy and serves as a plasma facing material. The first wall and caps are made from EUROFER steel and act as a cladding and heat exchanger for the module. The core component of the breeder zone is PbLi alloy. It has tritium breeder, neutron multiplier and heat transfer medium functions. The backplate is a EUROFER based support construction and the manifold includes auxiliary structures for cooling and tritium extraction. Volumetric changes between segments are presented in table 3.6. The modules overall became smaller in size largely due to decrement of breeder zone. Such decrement was a result in attempt to bring temperature closer to design limits, thus lessening the need of cooling plates.

Table 3.6. Investigated materials and their compositions.

WCLL DEMO						
VOLUME	ARMOUR	FW	BREEDER MODULE	CAPS	BACKPLATE	MANIFOLD
EUROFER		99.5	18	95.2	100	74.4
WATER		0.5	1.9	4.8		4.2
PBLI (90% LI_6)			80.1			9.2
TUNGSTEN	100					
VOID						11.6

The neutron spectra, in form of VITAMIN-J 175 groups, were calculated for equatorial inboard (IB) and outboard blanket (OB) module localizations for each segment. The OB module is located further from the central axis of the fusion device, while IB is closer. The differences in spectra between breeder zone of 2014 and 2015 models are shown in fig 3.20.

Table 3.7. Volumes of investigated module segments.

Volume, [cm^3]	**Armour**	**FW**	**Breeder module**	**Caps**	**Backplate**	**Manifold**	**Total**
2014 IB	4.63E+03	4.42E+04	5.89E+04	9.67E+05	4.09E+04	5.69E+05	1.68E+06
2015 IB	4.10E+03	5.88E+04	2.06E+04	9.70E+05	5.43E+04	3.21E+04	1.14E+06
2014 OB	5.25E+03	5.26E+04	1.21E+05	2.48E+06	6.72E+04	1.46E+06	4.18E+06
2015 OB	4.49E+03	8.69E+04	2.67E+04	2.16E+06	1.09E+05	4.87E+05	2.87E+06

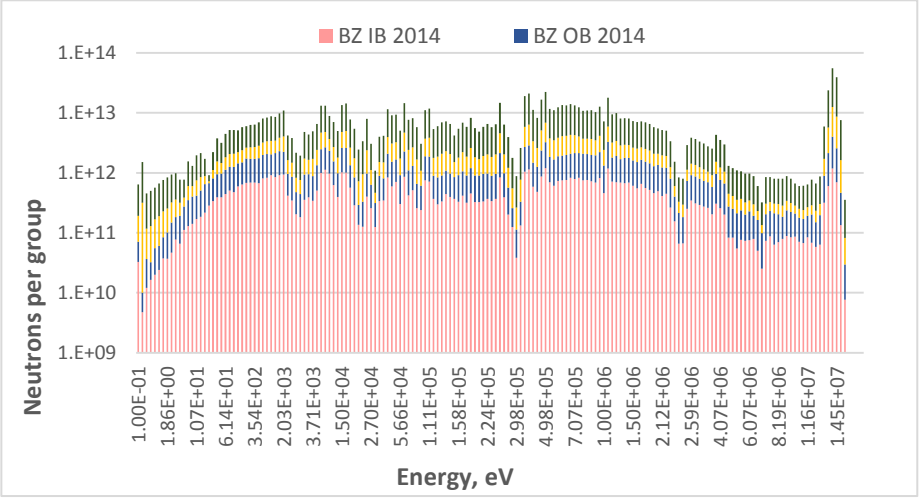

Fig. 3.20. Neutron spectra used for IB and OB breeder zone segments.

The European Activation System: Easy-2007 was used as a primary tool for the determination of dominant radionuclides in structural materials after irradiation together with EAF-2010 nuclear library for 2014 model calculations. Its code

FISPACT utilized for simulation of the irradiation process. The model of irradiation is simplified: material is irradiated by a neutron flux in pulses corresponding to operation of a fusion device. Such simulation is being performed by solving reaction rate equations. Input data consists of composition, density and masses. For the 2015 model same methods were applied with FISPACT-II code and TENDL-2015 nuclear library.

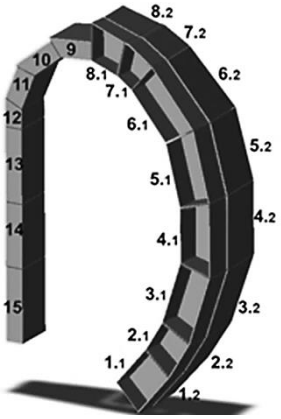

Fig. 3.21. 2015 WCLL blanket localizations.

The first irradiation sequence lasts for 1888 days with 0.3 MW m^{-2} neutron load on the slab surface. Another sequence consists of 48 pulses: material is exposed to 1 MW m^{-2} load for 4 hours. Pulse sequences were performed one after another with one hour delay. It is assumed that after irradiation all activated coolant and tritium is being removed from blanket module, however no assumptions are made to compensate for the possible replacement of depleted blanket during operation. Neutron activation related properties were analyzed for a 1000-year period after the last irradiation sequence starting with zero seconds after the irradiation ends. In the time frame the interval and its change was selected in accordance with different stages of reactor utilization. The period from the very first second after shutdown up to the month later provides data that might be useful during regular power plant operation and maintenance. The subsequent period up to 100 years would correspond to plant decommissioning and material storage. 100 years and up period are dedicated for evaluation of long term radioactive waste presence in the reactor.

Activity and decay heat values for all segments of the 2014 and 2015 models were obtained and are displayed in fig. 3.22-25. Roughly all segments can be lined up by distance from the source. The neutron flux is highest at the armour segment and gradually decline while moving towards manifold construction.

In most cases outboard modules exhibit higher activities and decay heat values than inboard modules. In the early time period of shutdown, such values range within a factor of ~ <2-5 for the 2015 model and within a factor of ~ <3-10 for the 2014 model. The maximum difference applies to armour and first wall segments, however the 2014 model manifold IB/OB segments also have quite significant variance in activation characteristics. These differences might be caused by

geometry flaws present in the model. With the cooling time increment such tendencies remain with only slight shrinkage in differences.

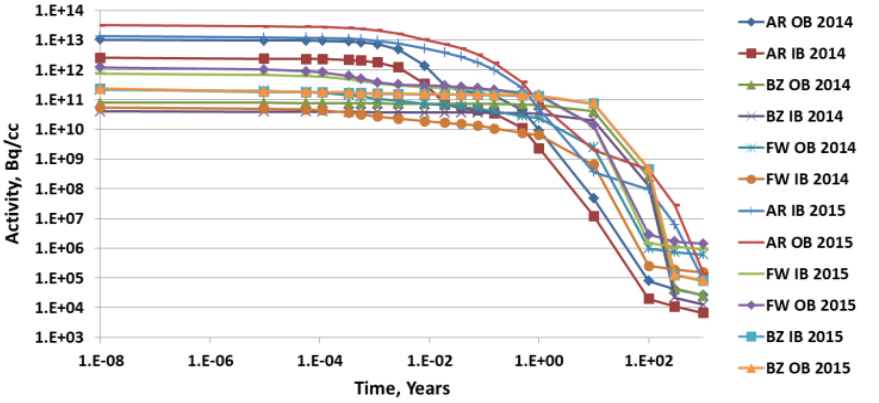

Fig. 3.22. Activity dependences on time after shut down for armor (AR), first wall (FW), breeder zone (BZ).

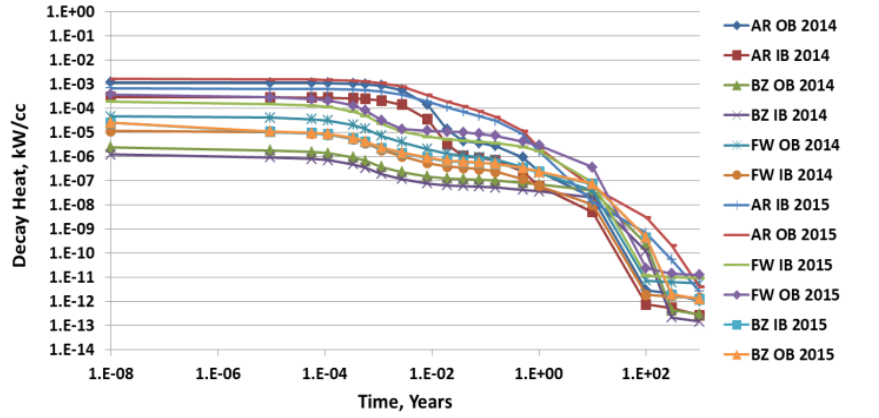

Fig. 3.23. Decay heat dependences on time after shut down for armor (AR), first wall (FW), breeder zone (BZ).

Comparing the 2014 and 2015 models side by side render the following results: all 2015-model obtained values are higher as expected. During the shutdown period, for armour localization it varies by a factors ~3-5, for the first wall by a factor of ~6-15, for the breeder zone by a factor of about ~3-10 and more, for the backplate by a factor of ~50-100, for the caps by a factor of ~10-40 and for the manifold by about 20-100 or more. With increments of time such differences are more pronounced and in parts increase by a factor of 10 up to 10 years cooling period, but not more.

The armour is made of tungsten alloy. Its activity and decay heat characteristics are highly dependent on W-187 and Re-188 isotopes. In the first seven days the influence of these isotopes is comparable with other radionuclides. Later on, the W-185 isotope makes up the largest part of activity inventories for the armour segment. For the first wall, caps, backplate and manifold the principal

radionuclides correspond to the EUROFER 97-3 composition as tritium from water activation is being removed from the module and tritium retention and absorption are not taken into consideration in this study. The key activity and decay heat contributors in EUROFER 97-3 are Mn-56, Cr-51 and V-52. There is a slight variation between these and other radionuclides in hierarchy across the investigated module segments, however these variations are not very significant. In 10 years after shutdown, the most prominent radionuclide is Fe-55, moreover in such a timeframe the overall activity starts to fall rapidly. Radionuclide production in EUROFER 97-3 steel in DEMO is mainly governed by (n, g) type neutron capture reactions.

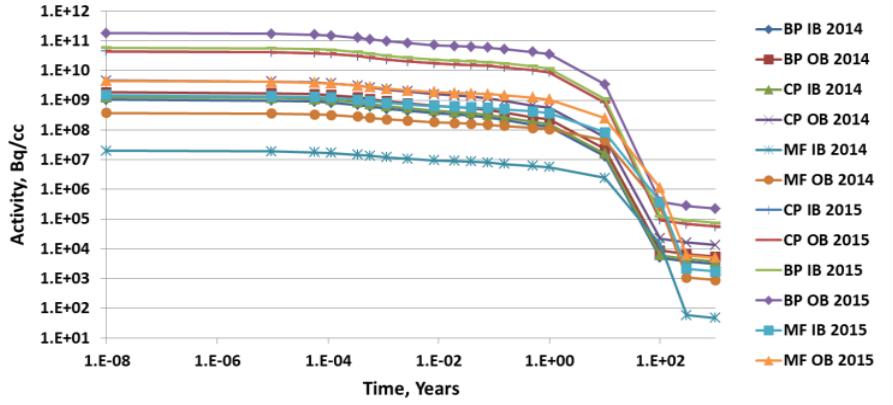

Fig. 3.24. Activity dependences on time after shut down for caps (CP), backplate (BP), manifold (MF).

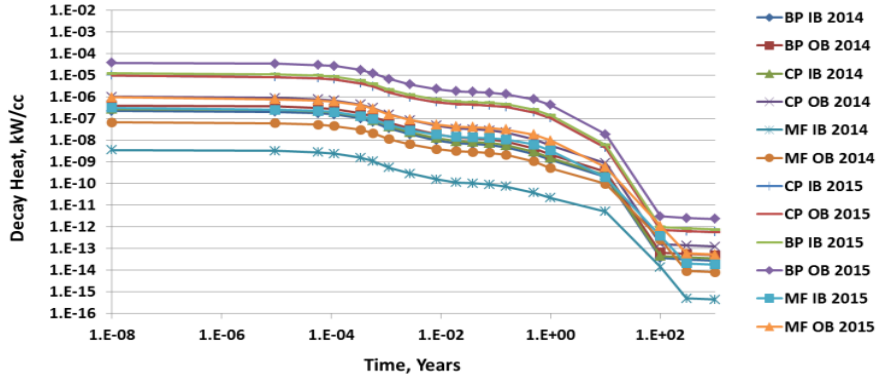

Fig. 3.25. Decay heat dependences on time after shut down for caps (CP), backplate (BP), manifold (MF).

The breeder zone is mostly made of PbLi alloy, however almost all lithium activation products consist of tritium that is removed from the system and of the Li-8 radionuclide with a very short half-life. Lead activation mainly results in production of fast decaying Pb-205m and Pb-203m radionuclides. Essentially, the activity and decay heat of the breeder zone are dominated by EUROFER activation products; nonetheless a significant part is also affected by lead activation products

that become more prominent with the cooling time increment. Such an effect is seen in the manifold segment that has a fraction of PbLi alloy.

Principal radionuclides for DEMO2015 equatorial OB WCLL module in armour, first wall, breeder zone, caps, backplate and manifolds are presented in annex (Fig. 4.1-12).

Regarding dose rates after irradiation, the highest values shortly after shutdown are encountered in the first wall segment and remain the highest contributors for the remaining investigated time period. In the early period dose rates are about 10 times higher compared to values for armour and breeding zone and about 100 times higher compared to the lowest dose rate possessed by the manifold segment. For the Breeder zone the dose rate starts to decrease after one week of shutdown, mostly due to Pb-203 decay.

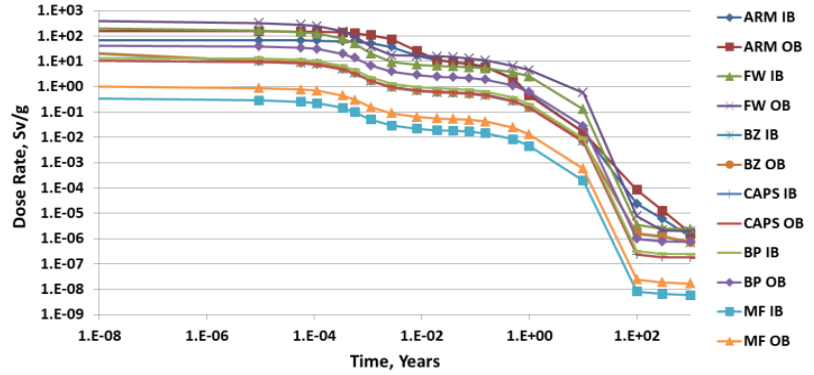

Fig. 3.26. Dose rate dependences on time after shut down for 2015 model.

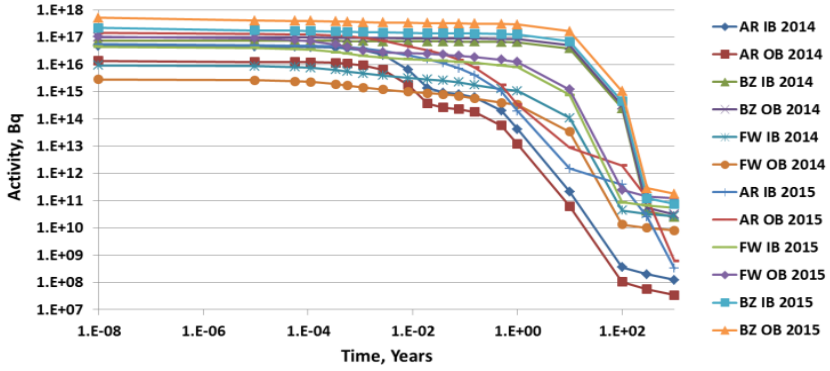

Fig. 3.27. Total activity dependences on time after shut down for armor (AR), first wall (FW), breeder zone (BZ).

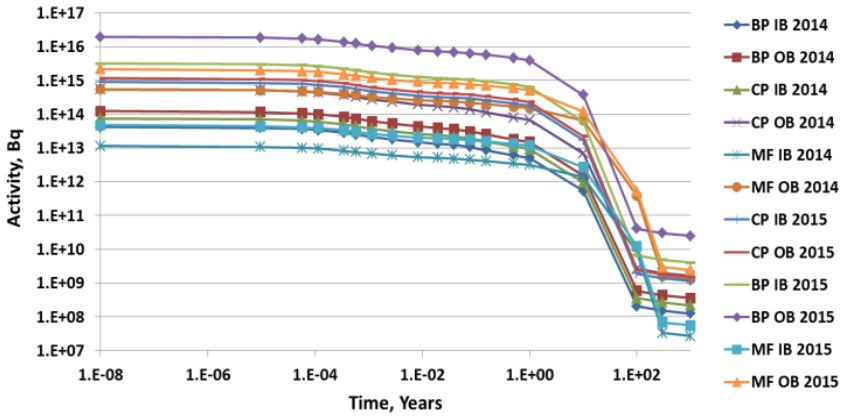

Fig. 3.28. Total activity dependences on time after shut down for caps (CP), backplate (BP), and manifold (MF).

In figures 3.27-28 total activity is presented among the investigated segments. The highest value of activity is present in the breeder zone followed by the armour, first wall, backplate, manifold and caps for the 2015 model during the early period after shutdown. For the 2014 model it is the breeder zone followed by the armour, first wall, backplate, caps and manifold. Similar tendencies remain over the entire investigated period.

After geometry changes and an increase in power from 1570 MW to 2037 MW, activity and decay heat in equatorial inboard and outboard water cooled lithium lead blanket modules have changed substantially. Outboard modules generally have higher activity values than inboard modules. Overall the obtained values using the 2015 model in respective segments were higher by factors ranging from 3 to 15 for armour, first wall and breeder zone segments and from 10 to 100 for backplate, caps and manifold, with a tendency to increase along the radial distance compared to the 2014 model.

Differences among inboard and outboard models range from 2 and lower to 5 times for the 2015 model and from 3 and lower to 10 for the 2014 model. Typical blanket placement in vacuum vessel is shown in fig. 3.28. 1 second after shutdown 2015 OB and IB modules respectively have about ~5.8 and ~2.8 times higher total activity compared to 2014 counterparts.

Radionuclide analysis showed that with the exception of tungsten armour, in all other parts of the module the most significant activation products arise from EUROFER alloy with minor variances. Tungsten armour activity inventories decrease significantly in a week time period after shutdown, while EUROFER-based segments remain relatively steady for a year and more.

3.3.2. DEMO 2017 WCLL Breeder Blanket Module

As for DEMO2017 outboard and inboard equatorial modules were analyzed in terms of activities and decay heats. Unlike previous calculations for DEMO2014 and DEMO2015 blanket modules were not split into different functional structures, but into layers (Fig. 3.31.). Such breeding blanket module segmentation is called Single-Module. In pictures arbitrary numbers mark the cells used in model. Layers from 79 to 122 correspond to the armor segment that is still composed mainly from tungsten, layers from 154 to 224, 4000 to 4002, 5001-5003 correspond to the first wall and vary greatly in terms of composition. Layers from 599 to 652, 4003 to 4011 and 5004-5015 represent breeder zone localization. The remaining layers represent backplate and manifold area.

In Figures 3.29-30 specific activities and decay heats in layers are presented along the module length. Activation characteristics correspond to different materials present in the layers.

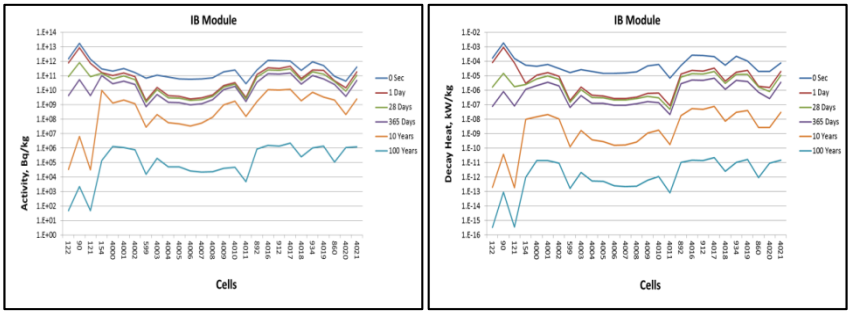

Fig. 3.29. Activity and decay heat along the blanket module length for DEMO 2017 WCLL blanket segments. Inboard Module.

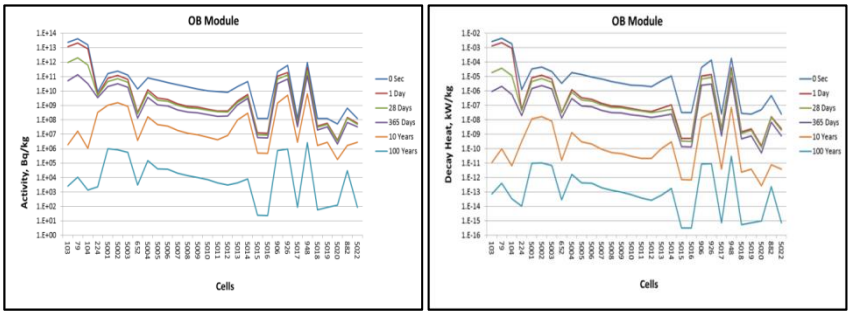

Fig. 3.30. Activity and decay heat along the blanket module length for DEMO 2017 WCLL blanket segments. Outboard Module.

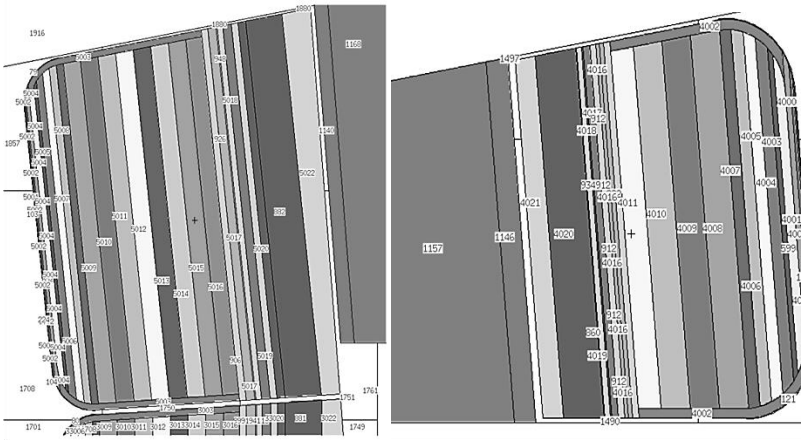

Fig. 3.31. 2017 WCLL breeder blanket modules. OB on the left and IB on the right.

For 2017 model, decay heat is the largest in the armor segment and 3 days after the end of reactor operation is above 2 kW/m^3, after a year decay heat still reaches values of 10 W/m^3 and above. The first wall, depending on localization, 2kW/m^3 and 10 W/m^3 radiological limits still exceeds respectively after 1 day and a half year period. For breeder zone relevant radiological limits are exceeded only briefly for a few seconds after the shutdown. Other structures do not exceed the radiological limits.

3.3.3. Activation Calculations of Fusion Relevant Structural Steels

In this section the examination of possible structural materials for DEMO nuclear fusion reactor is being carried out. Subject of this study is activation of reduced activation ferritic/martensitic and other steels that are used in the reactor design (for divertor, first wall or breeding blanket). Simulation of neutron irradiation in bulk material is being performed by using activation system program FISPACT with EAF-2010 nuclear data library. Neutron flux is selected in accordance with real neutron flux of the DEMO fusion reactor. After the irradiation certain properties of materials are being analyzed such as induced total activity, decay heat, gamma dose rate as well as possible ingestion and inhalation doses by released radionuclides.

Material selection is an important factor in nuclear fusion reactor design as some reactor's components will become radioactive in the process of operation due to interaction with neutrons generated during fusion processes. There are few approaches to resolve this issue. One of the possible solutions is material engineering. Having certain chemical compositions helps to significantly reduce the activity of materials. Reactor's construction materials must exhibit low activity, be mechanically strong, resistant to long exposures of high neutron and heat fluxes and be cost efficient. Among variety of materials that were created for these purposes in the last few decades, EUROFER 97-3 steel regarded as the get go material for European fusion program. Based on crystallinity stainless steels are classified to

austenitic, ferritic and martensitic. The goal of this study is to evaluate residual activity and decay heat after irradiation for variety of reduced activation ferritic and martensitic steels as some configurations of SS316 steel with regards to application in nuclear fusion.

For this study EUROFER 97, F82H, F82-IAE, JLF-1, Manet, Manet II, Optifer 1a, Optifer II, la12lc, la12talc, T91 and various configurations of 316 stainless steel were selected. Two extreme material composition configurations for EUROFER 97-3 were analyzed. In addition to optimal/achievable composition, samples with plentitude of possible impurities and no impurities were analyzed. All of these iron based alloys were considered for fusion reactor construction design (divertor, first wall or breeding blanket).

DEMO 2014 OB neutron flux was considered for this study (Fig. 3.20.). Long time exposure and a series of neutron irradiation pulses are considered. First irradiation sequence is 1841 day long with 0.3 MW m^{-2} load on the slab surface. Another sequence consists of 17 pulses: material is exposed to 1 MW m^{-2} load for 4 hours and after that it has 1 hour of cool down until repeat. Sequences are performed one after another with one hour delay.

Activity, dose rate and heat output of alloys are being examined. The period of interest spans up to 100 years after irradiation. Such length was selected taking into account previous studies that dealt with recycling of materials of fusion devices. For the analysis, period is divided into two parts:

- early period - covers the first year of cooling and calculated data might be useful for device operation, maintenance and decommissioning;

- late period - covers the last 50-100 year of cool-down and calculated data might be useful for disposal and recycling of the device materials.

Figures 3.32-33. show that F82H alloy exhibits lowest activity followed by Optifer II Optifer 1a and EUROFER 97 (target) in the late period. While in the early period EUROFER 97 has lowest activity followed by Optifer II and Manet 2.

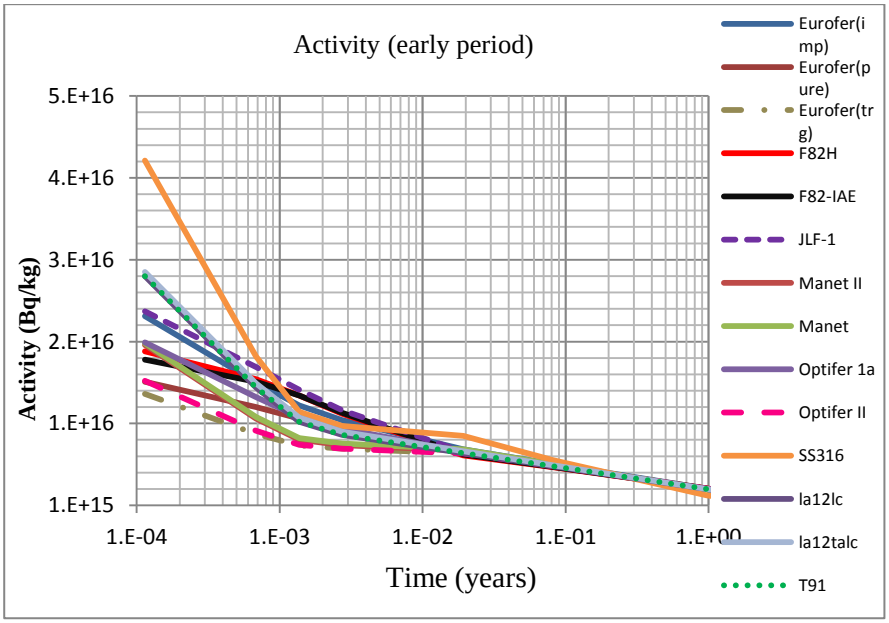

Fig. 3.32. Activity dependence on cool down time (early period).

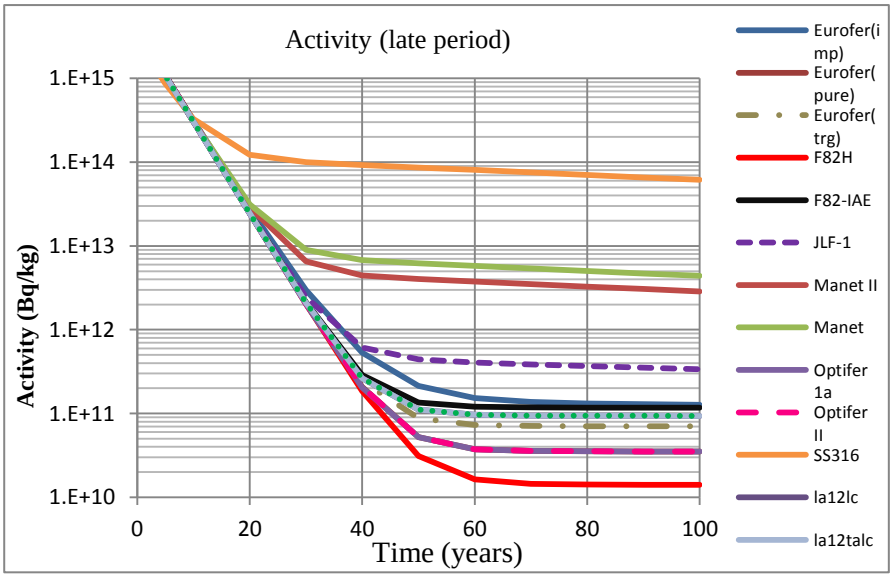

Fig. 3.33. Activity dependence on cool down time (late period).

The dose rate was calculated near the surface of the slab. Figures 3.34-35. show that the lowest dose rate in the early period corresponds to F82-IAE followed by F82H and EUROFER 97. In late period dose rate drop is very steep. EUROFER 97-3 with impurities exhibit worst characteristics followed by Manet and SS316.

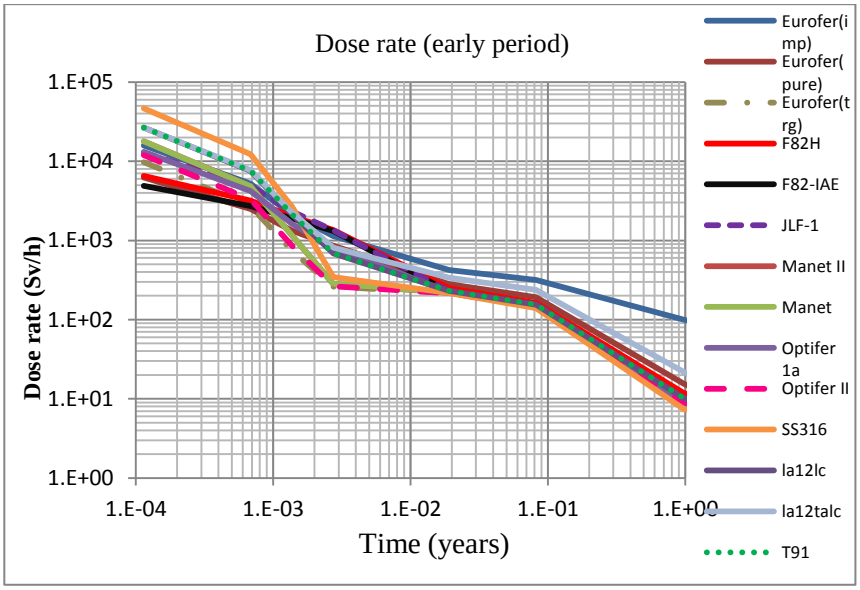

Fig. 3.34. Dose Rate dependence on cool down time (early period).

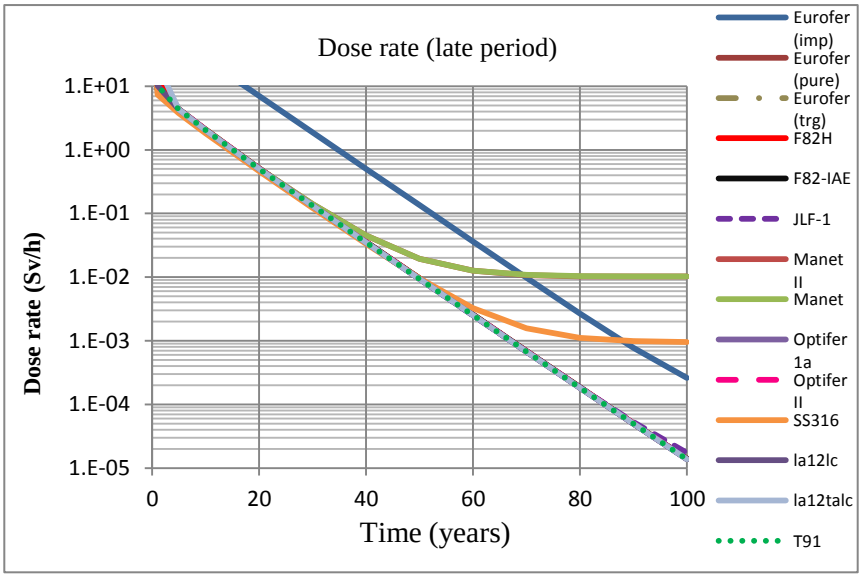

Fig. 3.35. Dose Rate dependence on cool down time (late period).

Heat output is shown in Figures 3.36-37. F82-IAE has the lowest heat output followed by F82H and EUROFER (target) in the early period. Lowest heat output in late period coincides with the value of F82H followed by Optifer II/ Optifer 1a and EUROFER (target).

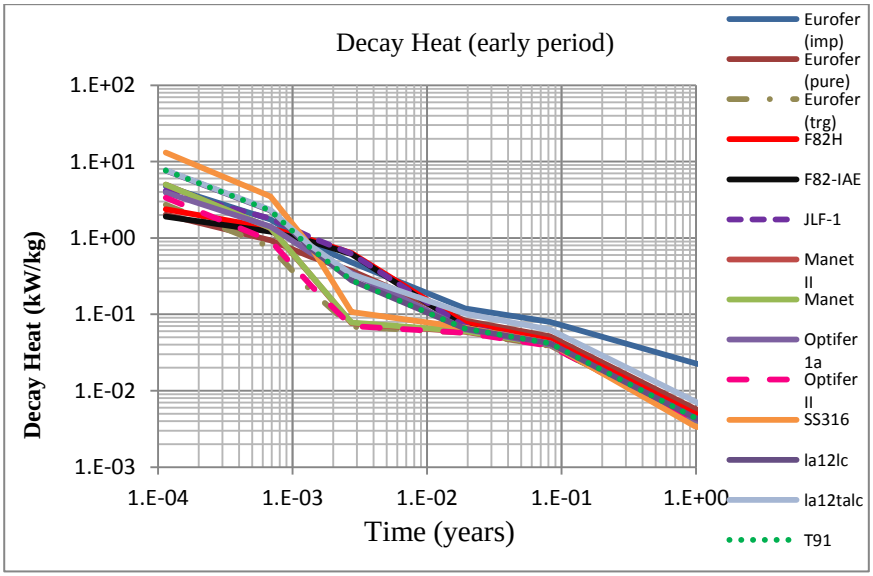

Fig. 3.36. Decay heat dependence on cool down time (early period).

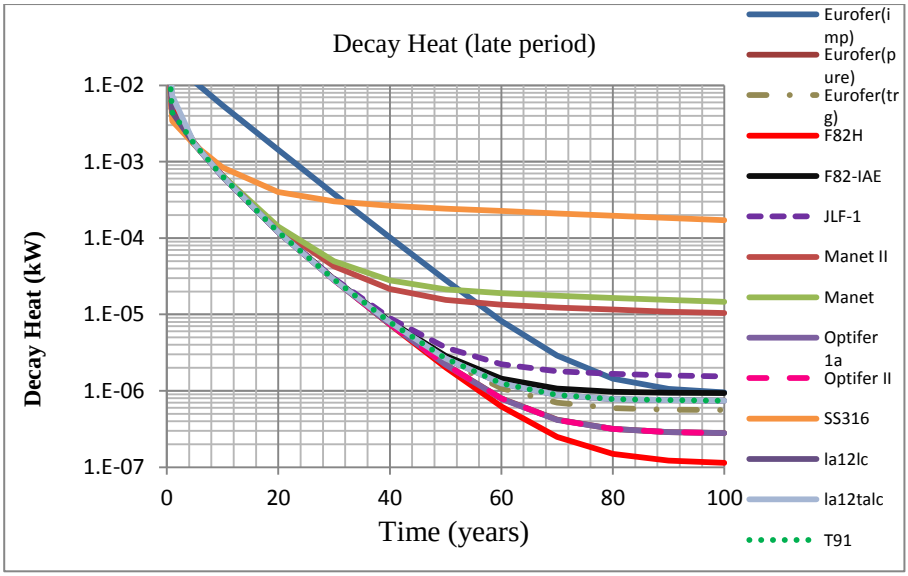

Fig. 3.37. Decay heat dependence on cool down time (late period).

Activity and dose rate are characteristics used to judge the potential hazard of an irradiated material. However, activity takes no account of the biological impact on human beings. Therefore FISPACT code includes tools to estimate the dose received by a man over his lifetime (50 years). Such estimation includes radiation protection calculation because radiation type has a different effect on human body as

well as the effect of radiation differs for different organs. These data were obtained from reports published by International Commission on Radiological Protection and the National Radiological Protection Board.

Ingestion and inhalation doses are needed for regulatory control and further decommissioning, recycling or disposal. Dosimetric calculations reconsider short-lived radionuclides and its daughter products, noble gasses and long-lived alpha emitters. Both ingestion and inhalation doses share similar tendencies – at the early period EUROFER 97 followed by Optifer II and Manet has the lowest doses, while in the late period F82H exhibit the lowest dose followed by Optifer II and EUROFER 97.

Figures 3.38-40 show the activities, decay heats and dose rates of 316 austenitic stainless steel configurations. While SS316 doesn't have as good characteristic as reduced activation alloys, it should still find some application in design of fusion devices. First of all, it is easier and cheaper to produce such materials in comparison to majority of reduced activation steels, secondly some construction elements are not heavily affected by neutrons. 316 Stainless steel material and other six configurations were analyzed. In graphs activity, decay heat and dose rate values are presented in percentage with regards to SS316. SS316 is a reference material and its value equal 100% at all times investigated. As for SS316 after 1 hour after the end of irradiation its activity is equal to $4.31 \cdot 10^{16}$ Bq/kg, dose rate equal to $4.6 \cdot 10^{4}$ Sv/h and decay heat equal to 13.1 kW/kg. In 10 years after the end of the irradiation respective values are equal to $3.27 \cdot 10^{14}$ Bq/kg, 1.82 Sv/h and $8.46\text{E} \cdot 10^{-4}$ kW/kg. In 100 years $6.16 \cdot 10^{13}$ Bq/kg, $9.54 \cdot 10^{-4}$ Sv/h and $1.72 \cdot 10^{-4}$ kW/kg.

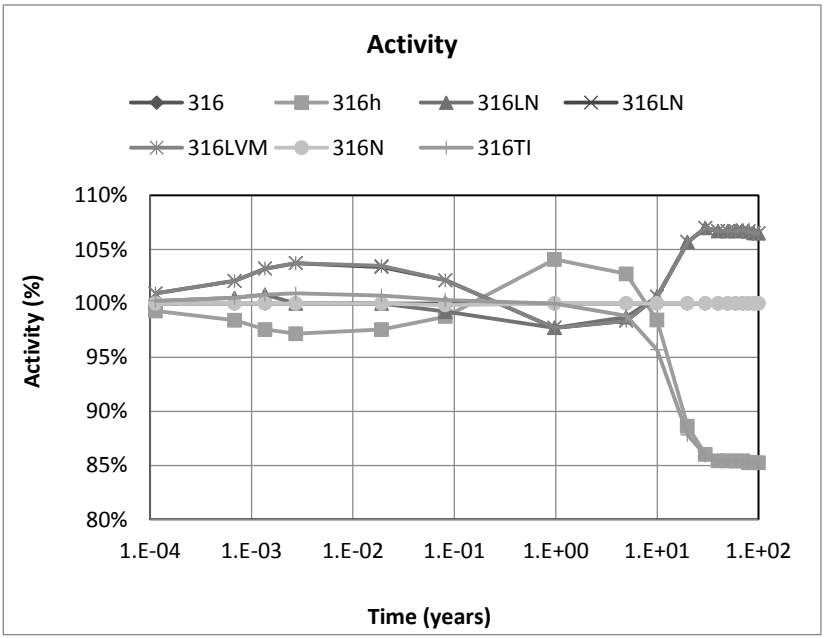

Fig. 3.38. Activity dependence on cool down time.

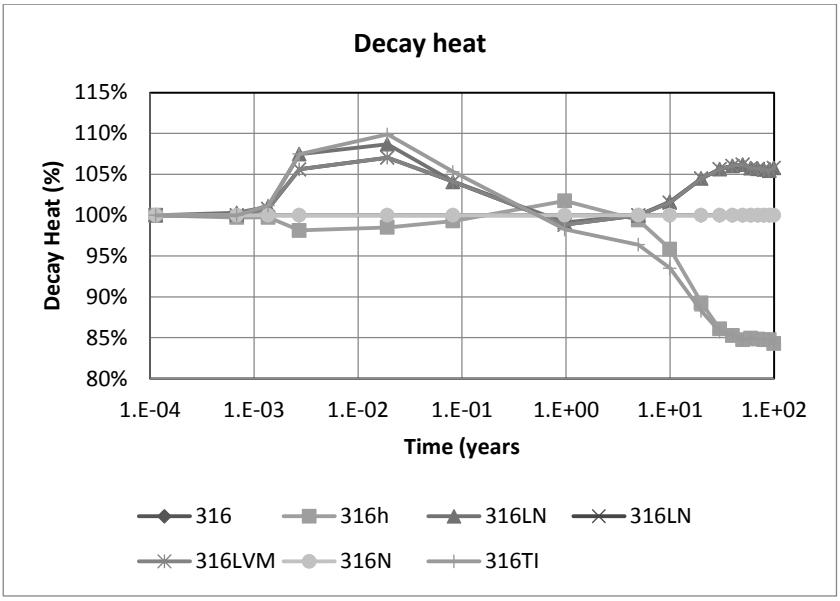

Fig. 3.39. Decay heat dependence on cool down time.

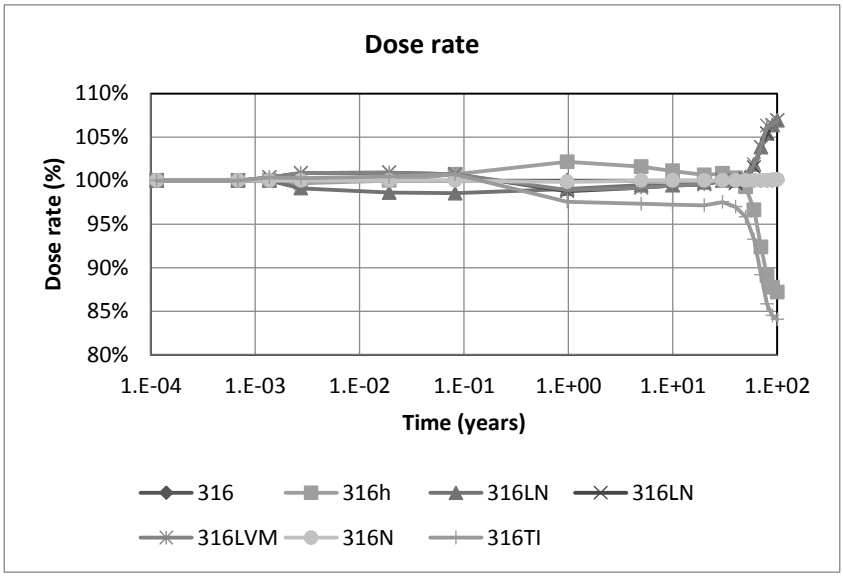

Fig. 3.40. Dose rate dependence on cool down time.

It is known that 316h has significantly higher carbon percentage ~ 0.1%, 316L is has lower carbon percentage ~ 0.03%, 316LN has lower carbon ~0.035% but higher nitrogen percentage ~0.1% , 316 LVM has lower carbon ~0.035% and lower

impurities percentage, 316N is enriched with nitrogen ~0.135% and 316Ti has titanium impurities ~0.7%. Compared with reduced activation steels variation in activity inventories for 316 stainless steel configurations are much smaller. Within the first 10 years they vary in 10 percent range and up to 20 percent after 100 years of cooldown. Main radionuclides in 316 type stainless steels were Mn-56, Cr-51, and Fe-55.

The activity of 316Ti and 316h is slightly lower in comparison to other investigated steels. The difference between the dose rates is insignificant. Heat output is also lower for the 316Ti, 316h type stainless steels. Both materials have higher fraction of carbon in their composition. Overall the difference in activation characteristics is relatively small and might be outweighed by the mechanical and economic factors.

3.3.4 Lithium Lead Flow Estimation in Breeder Blanket Module

This section is dedicated for calculations regarding the PbLi activation are being presented. Here DEMO operation assumed to be in pulse mode, which means that neutron irradiation last for 4 hours followed by 1 hour of cooldown. However PbLi circulate from blanket to tritium extraction system at different cycles. In addition to device irradiation scenario, simplified scenario for PbLi circulation was considered as well. It is assumed that PbLi cycle is 326 seconds long where for 235 seconds PbLi is located in the blanket, where irradiation is possible and 91 second in the tritium extraction system where there is no exposure.

After applying such scenario activity and decay heat values in comparison to just irradiation scenario were generally lower by ~28% (with 1-2 percent variation) which corresponds quite well to shorter exposure (irradiation time lower by ~28 %). For 0 and 1 second cooling intervals activity and decay heat values differ only by ~5 %. Furthermore Pb-207m and Pb-205m constitute for over 90 percent of activity while

PbLi is being irradiated. Values for tritium produced in the mixture also differ by roughly 28 %. As the objective of tritium extraction system is to remove tritium from PbLi, albeit with certain efficiency, tritium activity and decay heat values were excluded for further calculations.

There are two reasons why previous scenario can’t be applied outright for this particular DEMO blanket calculation. The first reason is that breeder zone segments in model used also contain fraction of nonmoving structures made of EUROFER. The second reason is that detailed irradiation scenarios require both large computation time and large computer data storage and also yields rather minor improvement in activation calculation results.

In order to better understand the impact of irradiation scenario three different irradiation modes were considered for 30 days. Continuous irradiation (utilized in simulating first 1888 days or irradiation in previous calculation), pulsed irradiation (4 hours irradiation and 1 hour of cooldown, corresponds to an actual device operation regime as well as being utilized to simulate last 10 days in previous

calculations) and 365s long PbLi cycle. The impact of irradiation wall loads and irradiation times between different scenarios were adjusted so it would not influence the comparison of the results (Fig. 3.41 and 3.42).

Both activity and decay heat values for different irradiation scenarios follow similar trends. At the end of irradiation and 1 second of cooldown PbLi cycle has ~35 % higher values than continuous scenario and ~10 % higher values that DEMO operation scenario. However with assumption that in actual scenario PbLi is being exposed 28% less, such difference shouldn't pose risk if conservative approach is assumed. The cooling period lasting from 5 minutes to 1 day is more pronounced in DEMO operation scenario, where the activity and decay heat values are higher from 8% to 2% and from 13% to 5 percent respectively. Such difference is likely caused by Pb-209 which has a 3.253 hours half-life.

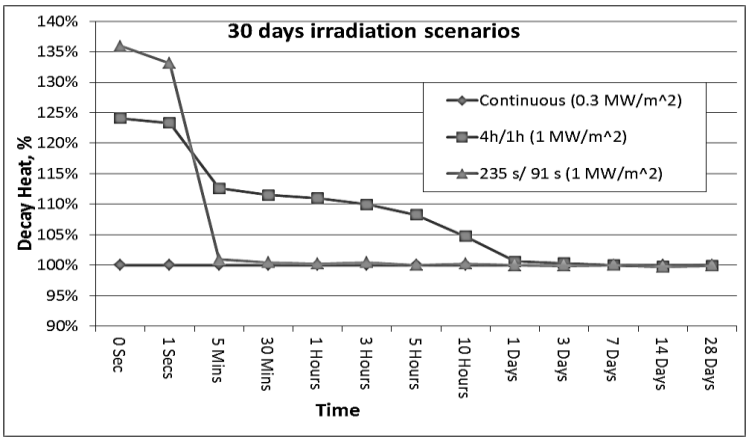

Fig. 3.41. Specific decay heat percentage values for different irradiation scenarios. Continuous irradiation scenario values were selected for reference.

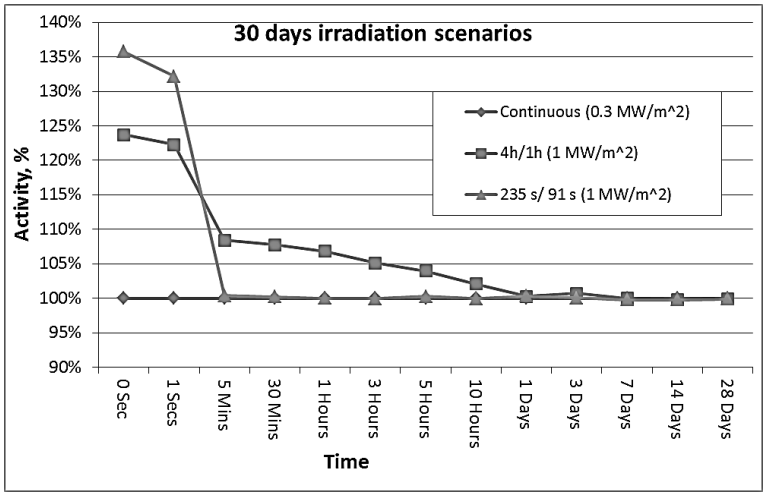

Fig. 3.42. Specific activity percentage values for different irradiation scenarios. Continuous irradiation scenario values were selected for reference.

To sum up, these results were obtained using DEMO 2017 WCLL heterogeneous MMS model. Activation characteristics of PbLi flow are mostly influenced by fast decaying nuclides in comparison to other possible irradiation scenarios. If PbLi cycle is not considered in DEMO Irradiation scenario, the expected activity and decay heat should be lower than calculated.

3.3.5 Nuclear Library Data Comparison

In this section nuclear results between different nuclear data libraries are being compared. The research objects are EUROFER 97-3 reduced activation steel, CuCrZr alloy and water. Simulation corresponds to previous DEMO 2015 calculations, where neutron spectrum (Fig. 3.20) is obtained for central outboard blanket localization and operation regime set for 1888 continuous 0.3 MW/m^2 followed by 10 pulse sequence (4 hour irradiation at 1 MW/m^2 and1 hour rest) shown in Fig. 3.43.

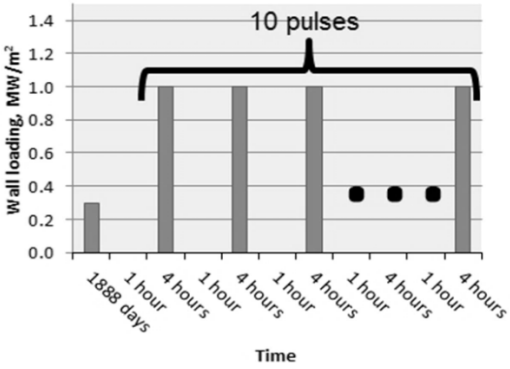

Fig. 3.43 irradiation scenario

Nuclear library comparison showed that there are significant variances in different databases for different time periods. No general tendencies were observed as differences in investigated activation characteristics can change substantially over different time periods. EAF-2010 nuclear library database was selected as a 100 % reference line for further percentage comparisons. For EUROFER 97-3 (Fig. 3.44-47.) significant differences start to show within 10 years after the end of irradiation with regards to activity.50 years after the irradiation the difference between EAF-2010 and JEFF 3.2 is more than 30 percent mostly due to variation in Nb-93m. Same radionuclide is responsible for differences in other library data as well. For decay heat and dose rate the differences are less evident, where the most noticeable change occur between the first day and first year of cooldown, where compared to EAF-2010 other data libraries has 5% and lower values for investigated

characteristics. Such difference is caused by Mn-54 which constitutes much more for EAF-2010 while W-187 is more pronounced in other data libraries.

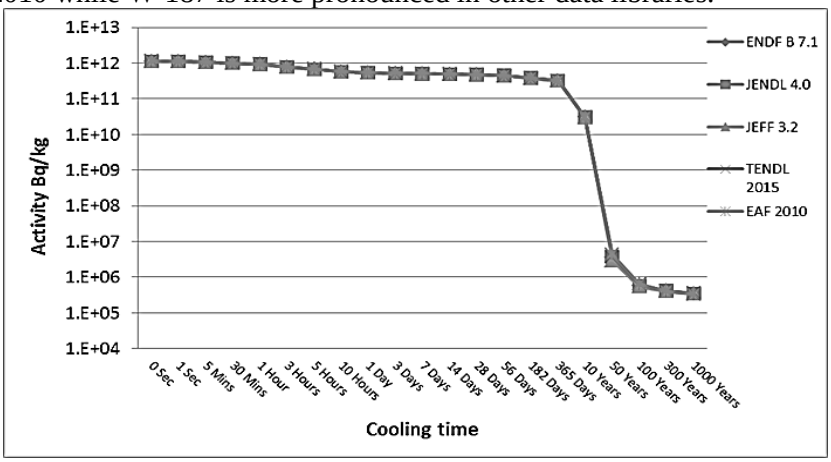

Fig. 3.44. EUROFER 97-3 specific activity.

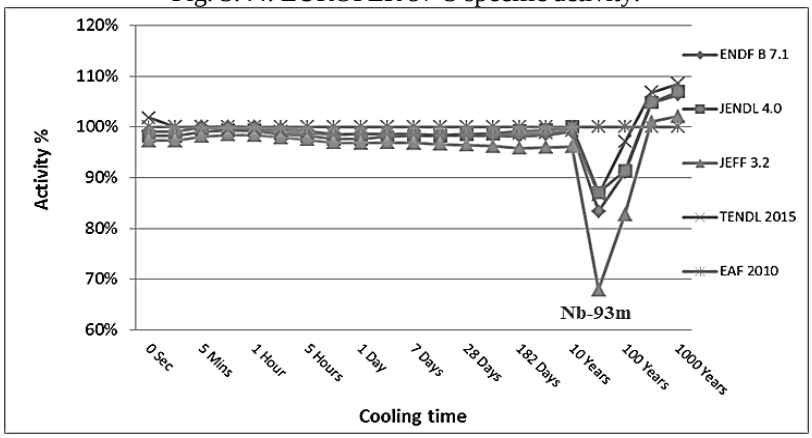

Fig. 3.45. EUROFER 97-3 activity comparison. EAF 2010 equal to 100% reference.

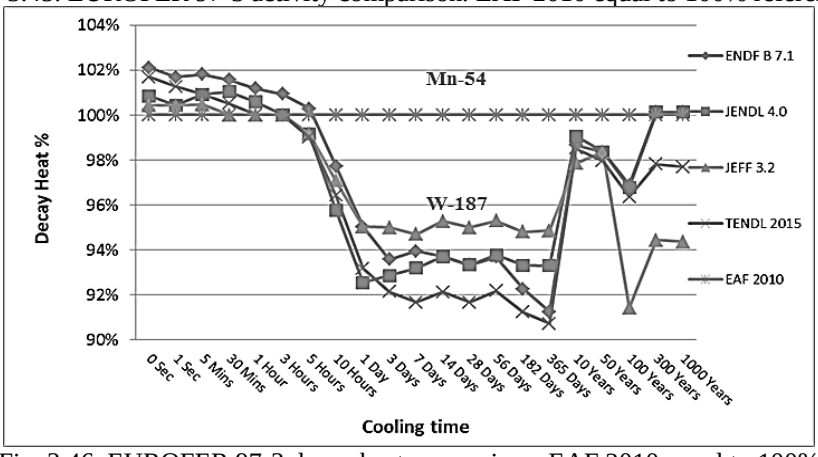

Fig. 3.46. EUROFER 97-3 decay heat comparison. EAF 2010 equal to 100% reference.

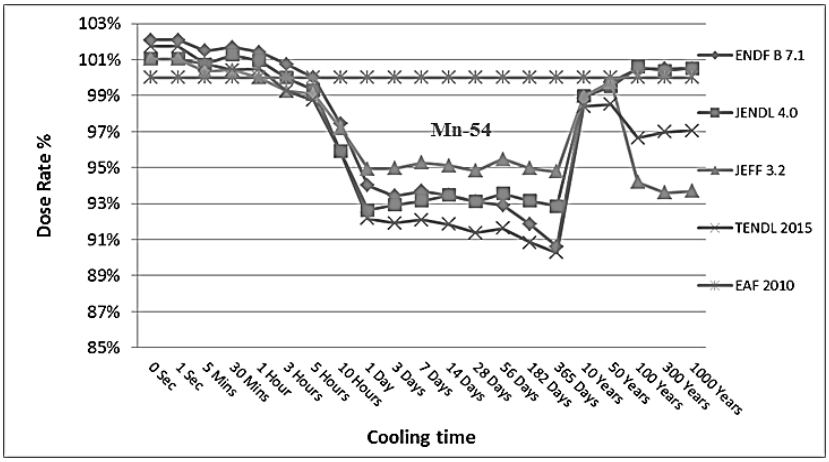

Fig. 3.47. EUROFER 97-3 dose rate comparison. EAF 2010 equal to 100% reference.

For CuCrZr alloy (Fig. 3.48-51.) the difference between EAF- 2010 and JEFF-3.2 activities reaches about 20 % 7 days after the end of irradiation and stay at similar level for almost 10 years. Differences in this time period are mainly caused by different amounts of Co-60 and Ni-63. For decay heat and dose rate principal radionuclide responsible for variations in values is Co-60.

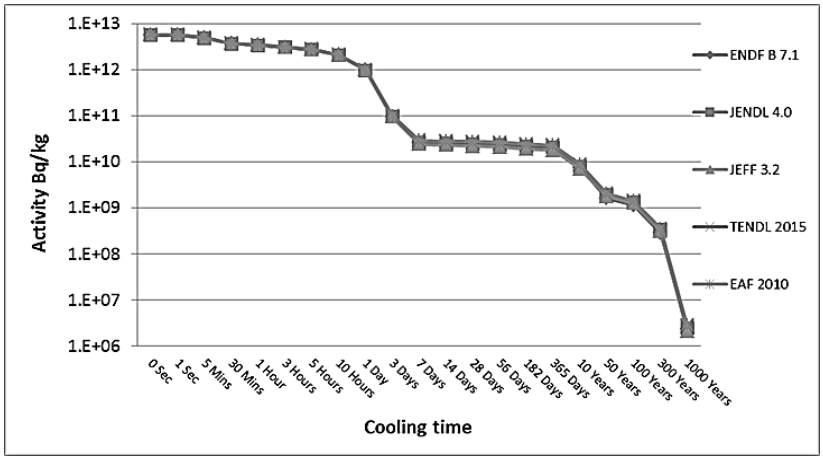

Fig. 3.48. CuCrZr specific activity.

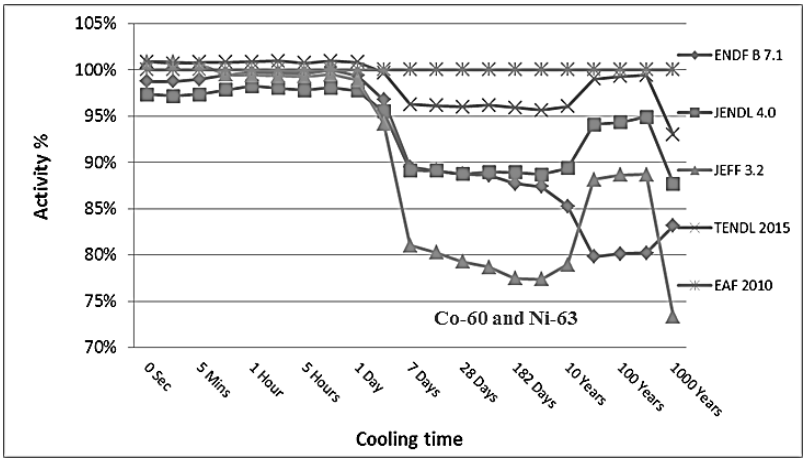

Fig. 3.49. CuCrZr activity comparison. EAF 2010 equal to 100% reference.

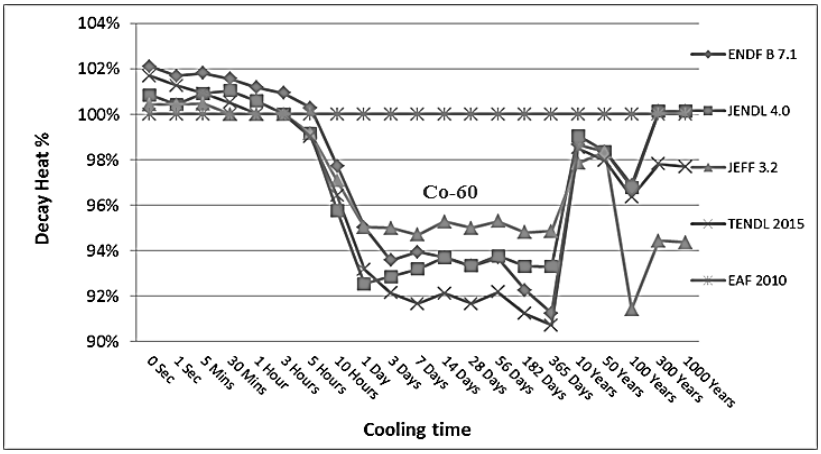

Fig. 3.50. CuCrZr decay heat comparison. EAF 2010 equal to 100% reference.

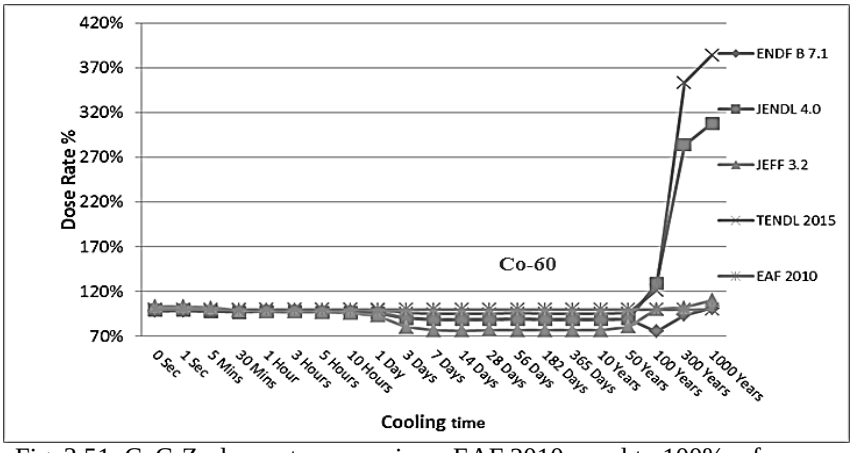

Fig. 3.51. CuCrZr dose rate comparison. EAF 2010 equal to 100% reference.

For water (Fig. 3.52-53.) the differences in activity and decay heat are more pronounced with exception of the first few minutes after irradiation where it ranges within 10 percent. Later on differences increase substantially due to different amount of H-3 C-14.In terms of activity there is EAF-2010 has 1000 times larger values that JEFF 3.2, 10 times larger values than ENDF 8.7.1 and 2 times larger values than TENDL 2015 and JENDL 4.0. For decay heat the percentages are lower but the trends are very similar. The dose rate is only relevant in the first few minutes after irradiation.

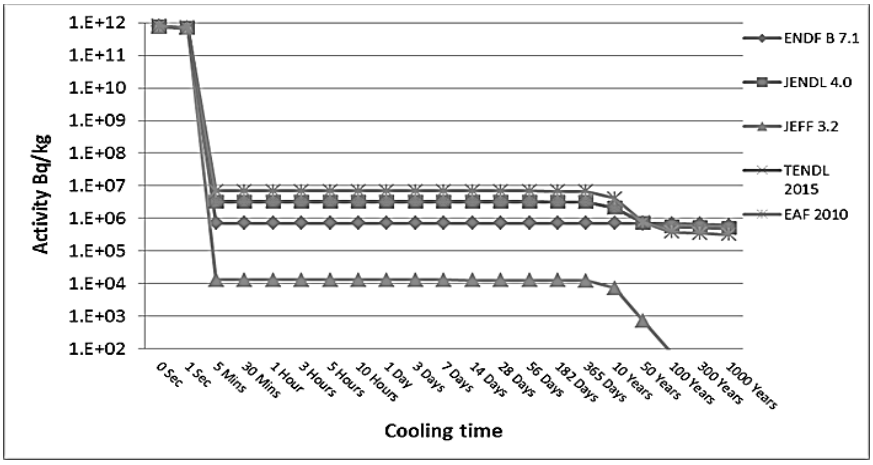

Fig. 3.52. water specific activity.

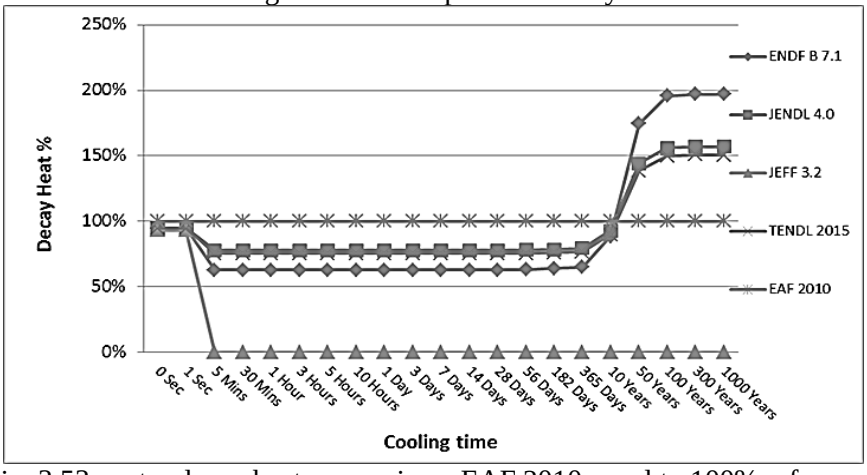

Fig. 3.53. water decay heat comparison. EAF 2010 equal to 100% reference.

EAF-2010 and TENDL 2015 are principal nuclear data libraries for European fusion research. For EUROFER and CuCrZr alloys activity, decay heat and dose rate characteristics for all nuclear data libraries tested were very similar in terms of radionuclide compositions.

Within one second after irradiation the difference between activation characteristics of different nuclear data libraries used was at most 7 percent between few certain cases. For later periods the differences between nuclear data library activation comparison increased, most notably in activation where in some cases it reached 30%. In case of water differences ranged from few times to few orders of magnitude after the first 5 minutes of cooldown.

3.3.6. Sensitivity Analysis of Neutron Spectrum

In this section sensitivity analysis was carried out for neutron spectra with respect to EUROFER 97-3 steel activation. Sensitivity analysis was performed with SUSA (Software for Uncertainty and Sensitivity Analyses) code (Kloos and Hofer 1999). Setup for this task corresponds to DEMO 2015 calculations for OB equatorial breeder blanket module (section 3.3.1). Sensitivity parameters are tied to 175 neutron groups. 100 new spectra were generated where each neutron group varies from 10 to -10 percent in comparison to original spectra. For sensitivity analysis it is considered that investigated neutron groups are not dependent from each other. Sensitivity analysis is performed using Spearman's rank correlation method. This method ranks every parameter in terms of its influence by comparing activity values calculated for each spectrum. The rank correlation shows which parameter has the highest impact. Correlation coefficients can vary from 1 to -1.

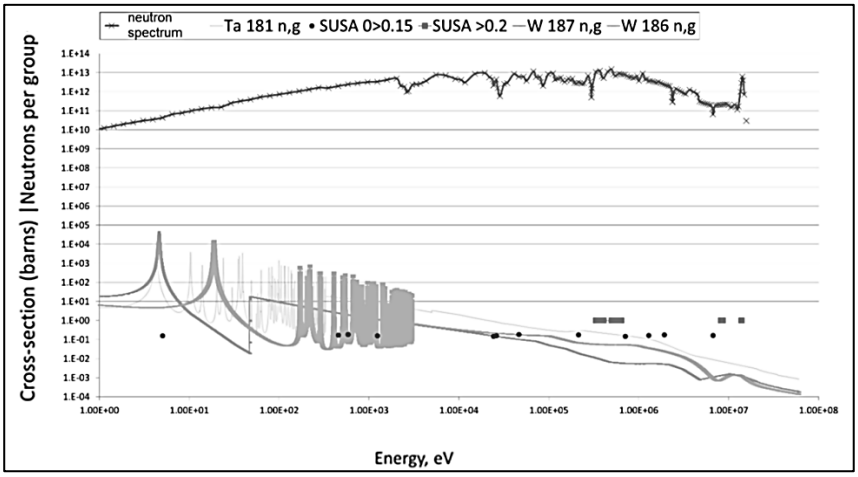

Fig. 3.54. Sensitivity analysis of EUROFER 97-3. Neutron spectra and cross sections TENDL 2015.

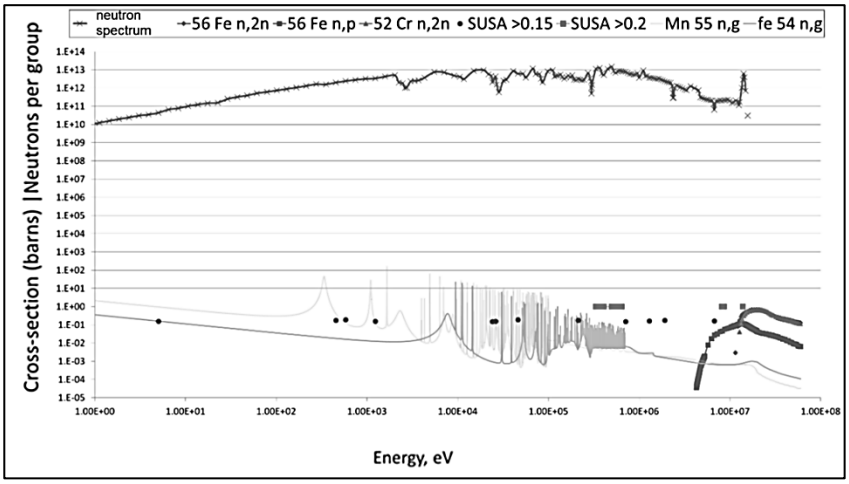

Fig. 3.55. Sensitivity analysis of EUROFER 97-3. Neutron spectra and cross sections TENDL 2015.

Due to large amount of investigated parameters (175 neutron energy groups), only values with correlation coefficient 0.15 and above will be examined. In Fig. 3.54-55. neutron spectra reaction cross-sections and correlation coefficients are superimposed on the same graph for EUROFER 97-3 material. Most coefficients correspond to certain neutron reaction, however there are some parameters that doesn't fit the particular data. Reasons for this might be unaccounted reactions, unforeseen decay events due to selected time period or just aggregation of multiple factors. However, most data does represent either cross-section peaks or peaks in impinging neutron numbers. The best agreement is presented for the 6^{th} and 4^{th} period element reactions. The 6^{th} period metals are most likely responsible for sensitivity in energy groups 7 (1.45 eV – 1.86 eV), 30, 31 (454 eV – 749 eV) and 49 (11.7 keV- 15 keV). Sensitivity in 54-105 (24.2 keV - 707 keV) energy groups correspond to resonance peaks in Mn-55, Fe-54, Cr-52 and Vn-51 neutron cross-sections and are tied to neutron capture (n, g) reactions. Sensitivity in 155-167 energy groups (8.6 MeV – 14.2 MeV) correspond to Fe-56, Cr-52, Mn-55 (n, 2n) and (n, p) high energy reactions. Group 167 characterizes typical DT fusion reaction as it covers energy interval from 13.8 MeV to 14.2 MeV.

So for this particular irradiation setup most sensitive neutron groups were determined. For EUROFER 97-3 three descriptive categories can be made:

- low energy groups that corresponds to the 6th period materials.
- medium energy groups that corresponds to the 4th period metals (n,g reactions).
- high energy groups (14MeV) that corresponds to the 4th period metals (n,p and n,2n reactions).

To sum up, sensitivity analysis results coincide with discrete energy levels of atoms and also depend on the activated material and interacting neutron amount.

This method could be used as auxiliary measure for neutron analysis in order to better grasp the activation tendencies of complex irradiation setups. However, for precise evaluation such method is not good enough as there are too many reactions to take into account as well as possible unforeseen decay events.

CONCLUSIONS

In this work neutron transport and material activation were analyzed in a close proximity of fusion relevant neutron sources in order to assess the neutron irradiation influence on the breeder blanket modules of DEMO nuclear fusion power plant concept. This study is based on multiple experiments designed to ensure successful operation and development of DEMO. JET experiments provide DEMO relevant neutron flux densities, while IFMIF-DONES is designed to match the lifetime activation of DEMO power plant. Consolidated results from neutron transport and material activation lead to the following conclusions:

1. Material activation caused by neutron irradiation from deuterium-tritium fusion is 10-50 times larger compared to deuterium-deuterium fusion in JET device in terms of Specific activity and dose rate. Specific activities and dose rates resulted from deuterium-deuterium fusion are affected more (up to ~30 %) by the change of irradiation sequence (from continuous to pulse mode) than from deuterium-tritium fusion.
2. Principal radionuclide production in IFMIF-DONES device (throughout the Test Cell) is governed by the high energy neutron reactions ((n, p), (n, 2n)) compared to DEMO (first wall). For SS316L(N)-IG Mn-56 is mainly produced from Fe-56 (n, p) (~54%) reaction in IFMIF-DONES and from Mn-55 (n, g) (~89%) in DEMO. Fe-55 is being produced in IFMIF-DONES from Fe-56 (n, 2n) (~92%) while the same reaction is only responsible for 58% of total radionuclide production in DEMO with Fe-54 (n, g) constituting (~39%). Cr-51 in IFMIF-DONES produced by Cr52 (n, 2n) (~67%) reaction, while in DEMO Cr-50 (n, g) is responsible for (~70%) of Cr-51. Activities in IFMIF-DONES retain relatively higher values compared to DEMO. After 1 day of cooling IFMIF-DONES retain ~80% of maximum achieved activity in steel compared to ~65% of DEMO. After 1 month of cooling the respective values are equal to ~63% for IFMIF-DONES and ~51% for DEMO with tendency to proportionally increase as the cooling period increases.
3. EUROFER 97-3 is a major contributor to the activation inventories in DEMO WCLL breeder blanket module with Mn-56, Cr-51 and Fe-55 as key radionuclides. It has the highest activity and decay heat values after 1 year of cooling till the remaining of the investigated time. Tungsten has the highest activity and decay heat within 1 year cooling period. W-187 and W-187 as key radionuclides in activated tungsten. Activity of PbLi peaks at the irradiation and retains high values for short period of time due to fast

decaying Pb-205m, Pb-203m and Li-8. H-3 produced in the breeder material is removed from the blanket.

4. After ~1/3 increase in fusion power and ~2/3 increase in vacuum vessel volume obtained breeder blanket module specific activity differences ranged from 2 to 15 times for armor, the first wall and breeder zone segments and from 10 to 100 times for the backplate, caps and manifold.
5. PbLi activation at the end of irradiation and within 1 second of cooldown is ~35 % and ~10 % higher in comparison to continuous and DEMO operation scenarios respectively when PbLi flow cycle scenario is assumed instead.
6. On the basis of sensitivity analysis, neutron energies ranging from 24.2 to 707 keV and from 8.6 to 14.2 MeV were determined to be the most significant in terms of activation in DEMO blanket module EUROFER-97-3 steel structure.

REFERENCES

1. A.FASSO, A.FERRARI, J.RANFT, and P.R.SALA. 2011. Fluka: a multi-particle transport code. Geneva: CERN.
2. ALLISON, J., et al. 2003. "Geant4—a simulation toolkit." Nuclear Instruments and Methods in Physics Research Section A: Accelerators, Spectrometers, Detectors and Associated Equipment 506: 250-303.
3. ANGELONE, M, et al. 2006. "Neutronics experiment for the validation of activation properties of DEMO materials using real DT neutron spectrum at JET." Fusion Engineering and Design 81: 1485-1490.
4. AUBERT, J, et al. 2018. "Status of the EU DEMO HCLL breeding blanket design development." Fusion Engineering and Design (https://doi.org/10.1016/j.fusengdes.2018.04.133).
5. BACHMANN , C, et al. 2018. "Overview over DEMO design integration challenges and their impact on component design concepts." Fusion Engineering and Design (https://doi.org/10.1016/j.fusengdes.2017.12.040).
6. BATISTONI, P, et al. 2015. "Benchmark experiments on neutron streaming through JET Torus Hall penetrations." Nuclear Fusion 55.
7. BATISTONI, P, et al. 2012. "Neutronics experiments for uncertainty assessment of tritium breeding in HCPB and HCLL blanket mock-ups irradiated with 14 MeV neutrons." Nuclear Fusion 52.
8. BOCCACCINI, L.V. 2014. "European DEMO breeding blanket design and development strategy in a roadmap to the realisation of fusion energy."
9. BOSH, H, and M HALE. 1992. "Improved Formulas for Fusion Cross-Sections and Thermal Reactivities ." Nuclear Fusion 32.
10. BOTH, J. P., A. MAZZOLO, O. PETIT, Y. PENELIAU, and B. ROESSLINGER. 2003. User Manual for Version 4.3 of the Tripoli-4 Monte-Carlo Method Particle Transport Computer Code. Saclay: CEA.
11. BROWN, D.A., M.B. CHADWICK, R. CAPOTE, et al. 2018. "ENDF/B-VIII.0: The 8th Major Release of the Nuclear Reaction Data Library with CIELO-project Cross Sections, New Standards and Thermal Scattering Data." Nuclear Data Sheets 148: 1-142.
12. BRYSK, H. 1973. "Fusion neutron energies and spectra." Plasma Physics 15.

13. CEPRAGA, D.G., G. CAMBI, M. FRISONI, and G.C. PANINI. 1998. ANITA-4: A Code for Material Irradiation Characterization in Fusion Neutron Spectra. ENEA.
14. CHEN , Z, et al. 2016. "Activation calculation and radiation analysis for China Fusion Engineering Test Reactor." Fusion Engineering and Design 109–111: 290-293.
15. CHEN, X., et al. 2012. "An overview of the welding technologies of CLAM steels for fusion application." Fusion Engineering and Design 87: 1639– 1646.
16. CISMONDI, F, et al. 2018. "Progress in EU Breeding Blanket design and integration." Fusion Engineering and Design (https://doi.org/10.1016/j.fusengdes.2018.04.009).
17. DANON, A, et al. 2003. "Heterogeneous austenite grain growth in 9Cr martensitic steels: influence of the heating rate and the austenitization temperature." Materials Science and Engineering 122-132.
18. DEL NEVO, A, et al. 2017. "WCLL breeding blanket design and integration for DEMO 2015: status and perspectives." Fusion Engineering and Design 124: 682-686.
19. EADE, T, et al. 2017. "Activation and decay heat analysis of the European DEMO blanket concepts." Fusion Engineering and Design 124: 1241-1245.
20. ERIKSSON, J, et al. 2016. "Calculating fusion neutron energy spectra from arbitrary reactant distributions." Computer Physics Communications 199: 40-46.
21. EURATOM. 2014. "Grant agreement number 633053 — EUROfusion." European Commission
22. EUROPEAN COMMISION. 2014. Communication From The Commission To The European Parliament, The Council, The European Economic And Social Committee And The Committee Of The Regions - A policy framework for climate and energy in the period from 2020 to 2030. 5644/1/14.
23. EUROPEAN UNION. 2017. "Energy balance sheets 2015 DATA." ISSN 1830-7558.
24. FEDERICI G. et al. 2016. "Overview of the design approach and prioritization of R&D activities towards an EU DEMO." Fusion Engineering and Design 109–111: 1464-1474.
25. FEDERICI, G, et al. 2019. "An overview of the EU breeding blanket design strategy as an integral part of the DEMO design effort." Fusion Engineering and Design 141: 30-42.
26. FISCHER, U, et al. 2005. "EU Blanket Design Activities and Neutronics Support Efforts." Fusion Science and Technology 1052-1059 .
27. FISCHER, U, et al. 2017. "Methodological approach for DEMO neutronics in the European PPPT programme: Tools, data and analyses." Fusion Engineering and Design 123: 26-31.
28. FISCHER, U, et al. 2005. "Nuclear data for fusion energy technologies: Requests, status and development needs." AIP Conference Proceedings 769: 1478-1485.
29. FISCHER, U, et al. 2018. "The role of nuclear data for fusion nuclear technology." Fusion Engineering and Design (https://doi.org/10.1016/j.fusengdes.2018.01.036.).
30. FISCHER, U , et al. 2019. "Neutronics of the IFMIF-DONES irradiation facility." Fusion Engineering and Design (https://doi.org/10.1016/j.fusengdes.2019.02.057).
31. FOREST, R. A. 2007. FISPACT-2007: User manual. Abingdon: EURATOM/UKAEA Fusion Association, Culham Science Centre.
32. Forrest, R. A. 2011. "Nuclear Science and Data Needs for Advanced Nuclear Systems." Energy Procedia 7: 540-552.
33. GAGANIDZE, E, and J AKTAA. 2013. "Assessment of neutron irradiation effects on RAFM steels." Fusion Engineering and Design 88: 118– 128.
34. GASPAROTTO M.et al. 2014. "Wendelstein 7-X—Status of the project and commissioning planning." Fusion Engineering and Design 89: 2121-2127.

35. GATU JOHNSON, M, et al. 2010. "Modelling and TOFOR measurements of scattered neutrons at JET." Plasma Physics and Controlled Fusion 52.
36. HERNÁNDEZ, F, et al. 2017. "A new HCPB breeding blanket for the EU DEMO: Evolution, rationale and preliminary performances." Fusion Engineering and Design 124: 882-886.
37. HIRSCH , R, and W RICE. 1974. "Nuclear Fusion Power and the Environment." Environmental Conservation 1: 251-262.
38. HODGSON, A. P. J., et al. 2015. "The Impact of Neutron Cross Section Group Structures on the Accuracy." Nuclear Science and Engineering 181: 1-8.
39. HOLTKAMP, N. 2009. "The status of the ITER design." Fusion Engineering and Design 84: 98-105.
40. HORTON L. et al. 2016. "JET experiments with tritium and deuterium–tritium mixtures." Fusion Engineering and Design 109–111: 925-936.
41. IAEA. 2007. Categorizing Operational Radioactive Wastes. Vienna: IAEA-TECDOC-1538.
42. IBARRA A., et al. 2014. "A stepped approach IFMIF/EVEDA towards IFMIF." Fusion Sci. Technol. 66: 252-259.
43. ICRP . 1991. 1990 Recommendations of the International Commission on Radiological Protection. ICRP Publication 60.
44. JABOULAY, J, et al. 2018. "Nuclear analysis of the HCLL "Advanced-Plus" breeding blanket." Fusion Engineering and Design (https://doi.org/10.1016/j.fusengdes.2018.05.052).
45. KEILHACKER, M. 1999. "High fusion performance from deuterium-tritium plasmas in JET." Nuclear Fusion 39: 209-234.
46. KEILHACKER, M., and M.L. WATKINS. 1999. "D-T experiments in the JET tokamak." Journal of Nuclear Materials 266: 1-13.
47. KIMURA, A. 2005. "Current Status of Reduced-Activation Ferritic/Martensitic Steels R&D for Fusion Energy." Materials Transactions 46: 394-404.
48. KLOOS, M, and E HOFER. 1999. SUSA Version 3.2. User's Guide and Tutorial. Garching: GRS.
49. KNASTER J., et al. 2016. "IFMIF, the European–Japanese efforts under the Broader Approach agreement towards a Li(d,xn) neutron source: Current status and future options." Nuclear Materials and Energy 9: 46-54.
50. KOLŠEK, A. et al. 2018. "Shutdown dose rate mitigation in the ITER upper ports." Fusion Engineering and Design https://doi.org/10.1016/j.fusengdes.2018.01.070.
51. KONDO, K, ET AL. 2014. "Neutronic analysis for the IFMIF EVEDA reference test cell and test facility." Fusion Engineering and Design 89: 1758-1763.
52. KONDO, K, ET AL. 2015. "Shielding performances analysis for the IFMIF test facility based on high-fidelity." Fusion Engineering and Design 98-99: 1998-2002.
53. KONING, A. J., et al. 2015. TENDL-2015: TALYS-based evaluated nuclear data library. https://tendl.web.psi.ch/tendl_2015/tendl2015.html.
54. KONING, A., et al. 2006. The JEFF-3.1 Nuclear Data Library, JEFF Report 21. Paris: OECD/NEA.
55. LAWSON, J. D. 1957. "Some criteria for a power producing thermonuclear reactor." Proceedings of the Physical Society B 70: 6.
56. LEE, S, et al. 2014. "Deuterium transport and isotope effects in type 316L stainless steel at high temperatures for nuclear fusion and nuclear hydrogentechnology applications." Current Applied Physics 14: 1385-1388.

57. LEE, Y. 2018. "Radiation shielding calculations for a 3D ITER benchmark model using TRIPOLI-4® Monte Carlo code." Fusion Engineering and Design (https://doi.org/10.1016/j.fusengdes.2018.03.036.).
58. LEICHTLE, D, et al. 2015. "Global shutdown dose rate maps for a DEMO conceptual design." Fusion Engineering and Design 98-99: 1524-1527.
59. LEICHTLE, D, et al. 2018. "The ITER tokamak neutronics reference model C-Model." Fusion Engineering and Design 136: 742-746.
60. LENGAR, I, et. al. 2016. "Radiation damage and nuclear heating studies in selected functional materials during the JET DT campaign." Fusion Engineering and Design 109-111: 1011-1015.
61. LEPPÄNEN, J, and KALTIAISENAHO T. 2016. "Expanding the Use of Serpent 2 to Fusion Applications: Shut-down Dose Rate Calculations." PHYSOR. Sun Valley.
62. LEPPÄNEN, J., et al. 2015. "The Serpent Monte Carlo code: Status, development and applications in 2013." Ann. Nucl. Energy 82: 142-150.
63. LIEW, S. L, L. P KU, and J. G KOLIBAL. 1986. "TFTR Basement Radiation Fluence Calculations and Comparisons with Measurements." Fusion Technology 10: 591-596.
64. LITAUDON, X. 2017. "Overview of the JET results in support to ITER." Nuclear Fusion 57.
65. LOPEZ ALDAMA, D, and R CAPOTE NOY. 2011. FENDL-3.0: Processing the Evaluated Nuclear Data Library for Fusion Applications. Vienna, Austria : IAEA.
66. MACFARLANE, R.E., and A.C. R.E. KAHLER. 2010. "Methods for Processing ENDF/B-VII with NJOY." Nuclear Data Sheets 111: 2739-2890.
67. MANN, F. M. 1989. "IFMIF, an accelerator-based neutron source for fusion components irradiation testing materials testing capabilities." Fusion Technology 15: 295-297.
68. MARTIN , B. 2009. Nuclear and Particle Physics: An Introduction. Wiley.
69. MARTONE, M, M ANGELONE, and M PILLON. 1994. "The 14 MeV Frascati neutron generator." Journal of Nuclear Materials 212: 1661-1664.
70. MORO, F, et al. 2018. "Neutronic analyses in support of the WCLL DEMO design development." Fusion Engineering and Design 136: 1260-1264.
71. MOTA, F, and J MOLLA. 2016. "Neutronic study of extended DONES irradiation module." Fusion Engineering and Design 109–111: 1212-1216.
72. Nave R., 2002 Hyperphysics http://hyperphysics.phy-astr.gsu.edu/hbase/NucEne/nucbin.html#c2. Accessed June 2018.
73. NI, M, et al. 2013. "Tritium supply assessment for ITER and DEMOnstration power plant." Fusion Engineering and Design 88: 2422-2426.
74. OTUKA, N., et al. 2014. "Towards a More Complete and Accurate Experimental Nuclear Reaction Data Library (EXFOR): International Collaboration Between Nuclear Reaction Data Centres (NRDC),." Nuclear Data Sheets 120: 272-276.
75. PACKER, L, et al. 2018. "Activation of ITER materials in JET: nuclear characterisation experiments for the long-term irradiation station." Nuclear Fusion 58.
76. PACKER, L, et al. 2017. "Status of ITER material activation experiments at JET." Fusion Engineering and Design 124: 1150-1155.
77. PALERMO, IOLE, RAQUEL GARCIA, MAURICIO GARCIA, and JAVIER SANZ. 2017. "Radiological impact mitigation of waste coming from the European fusion reactor DEMO with DCLL breeding blanket." Fusion Engineering and Design 124: 1257-1262.

78. PALERMO, IOLE, ROSARIA VILLARI, and ANGEL IBARRA. 2018. "Divertor options impact on DEMO nuclear performances." Fusion Engineering and Design 130: 32-41.
79. Palermo, Iole, Rosaria Villari, and Angel Ibarra. 2017. "Shutdown dose rate assessment with the Advanced D1S method for the European DCLL DEMO." Fusion Engineering and Design 122: 163-175.
80. PAUL, W, et al. 2017. "Tritium aspects of the fusion nuclear science facility." Fusion Engineering and Design (https://doi.org/10.1016/j.fusengdes.2017.04.099).
81. PEACOCK, N. J., et al. 1969. "Measurement of the Electron Temperature by Thomson Scattering in Tokamak T3." Nature 224: 488–490.
82. PEDERSEN T.S., et al. 2015. "Plans for the first plasma operation of Wendelstein 7-X." Nuclear Fusion 55.
83. PELOWITZ, D. B. 2013. MCNP6 User's Manual Version 1.0. Los Alamos: LANL .
84. PILLON, M, M ANGELONE, AND S SANDRI. 2011. "Measurements of Activation and Decay Heat Produced in Materials Irradiated with D-T Neutron and Comparison with EASY-2007 Code Predictions." Fusion Science and Technology 60: 687-691.
85. QIU, Y, ET AL. 2019. "Neutronics analyses for the bio-shield and liners of the IFMIF-DONES test cell." Fusion Engineering and Design (https://doi.org/10.1016/j.fusengdes.2019.01.064.).
86. RAPISARDA, D, et al. 2017. "Status of the engineering activities carried out on the European DCLL." Fusion Engineering and Design 124: 876-881.
87. REBUT, P. H., et al. 1992 . "The JET preliminary experiment." Plasma Physics and Controlled Fusion 34: 1749-1758.
88. ROMANELLI, F, et al. 2012. Fusion Electricity – A roadmap to the realisation of fusion energy. EFDA.
89. Rosen, L, and L Stewart. 1962. "Neutron-Induced Disintegration of Li6 and Li7." Phys. Rev. 126.
90. S., Ludwig. 2002. A Revision to ORIGEN2 - Version 2.2 . RSICC.
91. SANZ, J., CABELLOS O., and GARCÍA-HERRANZ N.. 2008. ACAB - Inventory code for nuclear applications. Madrid.
92. SARTORI, E. 1985. VITAMIN-J, A 175 Group Neutron Cross Section Library Based on JEF-1 for Shielding Benchmark Calculations. OECD NEA DATA BANK.
93. SEKI, Y., and H. IIDA. 1980. "Monte carlo calculation of first wall neutron flux in tokamak fusion reactor." Journal of Nuclear Science and Technology 301-304.
94. SHIBATA, K., et al. 2011. "JENDL-4.0: A New Library for Nuclear Science and Engineering." J. Nucl. Sci. Technol. 48: 1-30.
95. SIMAKOV, S. P., et al. 2012. "Status of the McDeLicious approach for the D-Li neutron source term modeling in ifmif neutronics calculations." Fusion Science and Technology 62: 233-239.
96. SMITH, R.D., and .PARISH T. A.. 1977. "STRUCTURE ACTIVATION IN AN EXPERIMENTAL POWER REACTOR." Proc of the Symp on Eng Probl of Fusion Res 1718-1722.
97. STORK, D, et al. 2014. "Developing structural, high-heat flux and plasma facing materials." Journal of Nuclear Materials 455: 277–291.
98. STORK, D, et al. 2014. "Materials R&D for a timely DEMO: Key findings and recommendations of the EU Roadmap Materials Assessment Group." Fusion Engineering and Design 89: 1586-1594.
99. STORK, D, and S Zinkle. 2017. "Introduction to the special issue on the technical status of materials for a fusion reactor." Nuclear Fusion 57.

100. SUBLET, J. CH. 2010. The European Activation File:EAF-2010 neutron-induced cross section library. Euratom/CCFE fusion association.
101. SUBLET, J.-C., EASTWOOD J., and MORGAN J.. 2016. THE FISPACT-II USER MANUAL. Abingdon: Culham Science Centre.
102. SUBLET, J.-CH. , et al. 2017. "FISPACT-II: An Advanced Simulation System for Activation, Transmutation and Material Modelling." Nuclear Data Sheets 139: 77-137.
103. IAEA 2001. Summary of the ITER Final Design Report . ITER EDA Documentation Series No 22: IAEA.
104. TASSONE, A, et al. 2018. "Recent Progress in the WCLL Breeding Blanket Design for the DEMO Fusion Reactor(." IEEE Transactions on Plasma Science 46: 1446-1457.
105. FUSION FOR ENERGY 2008. Technical Specifications EUROFER Material Database F4E-2008-GRT-010 (PNS-MD). Fusion for Energy.
106. TIAN K., et al. 2018. "Overview of the current status of IFMIF-DONES test cell biological shielding design." Fusion Engineering and Design (https://doi.org/10.1016/j.fusengdes.2018.03.043).
107. U.S. Energy Information Administration. 2017. "International Energy Outlook - 2017." DOE/EIA-0484.
108. VILLARI, R., et al. 2016. "Neutronics experiments and analyses in preparation of DT operations at JET." Fusion Engineering and Design https://doi.org/10.1016/j.fusengdes.2016.01.055: 109–111.
109. WENNINGER, R, et al. 2016. "The physics and technology basis entering European system code studies for DEMO." Nuclear Fusion 57.
110. WESSON, J. 1999. The Science of JET. Abingdon, Oxon.
111. WILSON, PAUL. n.d. http://alara.engr.wisc.edu/. Accessed 2018.
112. WU, YICAN. 2017. Fusion Neutronics. Singapore: Springer Nature.
113. YAMANISHI, T, et al. 2016. "Recent technical progress on BA Program: DEMO activities and IFMIF/EVEDA." Fusion Engineering and Design 109-111: 1272-1279.
114. YOUSSEF , M, et al. 1998. "Current Status of Reduced-Activation Ferritic/Martensitic Steels R&D for Fusion Energy Verification of ITER shielding capability and FENDL data benchmarking through analysis of bulk shielding experiment on large SS316/water assembly bombarded with 14 MeV ." Fusion Engineering and Design 42: 235-245.

PUBLICATIONS RELATED TO THE DISSERTATION

Publications in the journals included Clarivate analytics Web of Science database

1. Tidikas A., Stankūnas G. WCLL blanket module structure variation influence on neutron activation inventories (https://doi.org/10.1109/TPS.2018.2883482) // IEEE Transactions on Plasma Science. ISSN 0093-3813. eISSN 1939-9375. Vol. 47. Iss. 1. 2019. p. 874-877.
2. Stankūnas G.,Tidikas A., Pereslavstev P., Catalán J., Garcíac R., Ogando F, Fischer U. Activity inventories and decay heat calculations for a DEMO with HCPB and HCLL blanket modules// (http://dx.doi.org/10.1016/j.nima.2015.03.034) // Fusion Engineering and Design. ISSN: 0920-3796. 2016.
3. Stankūnas G., Tidikas A. Analysis of the wcll european DEMO blanket concept in terms of activation and decay heat after exposure to neutron

irradiaton (http://doi.org/10.2298/NTRP1703217S) // Nuclear Technology & Radiation Protection. ISSN 1451-3944. Vol. 32. No. 3. p. 217-221 2018

4. Stankūnas G., Tidikas A., Batistoni P., Lengar I., Jet Cintributors Analysis of activation and damage of ITER material samples expected from DD/DT campaign at JET (http://dx.doi.org/10.1016/j.fusengdes.2017.07.013) // Fusion Engineering and Design. ISSN 0920-3796. Vol. 125. 2017. p. 307–313 2017
5. Stankūnas G. , Čufar A., Tidikas A., Lengar I., Batistoni P. Activation inventories after exposure to DD/DT neutrons in safety analysis of nuclear fusion installations// Radiation Protection Dosimetry, https://doi.org/10.1093/rpd/ncx262 2018
6. Stankūnas G, Tidikas A., Fischer U., Activity inventories and decay heat generation of the Test Cell facility of IFMIF-DONES // Fusion Engineering and Design , ISSN 0920-3796, https://doi.org/10.1016/j.fusengdes.2018.03.040. 2018
7. Stankūnas G, Moro F., Tidikas A., Activity and decay heat calculations for the European DEMO WCLL breeder blanket module including activated PbLi flow // Fusion Engineering and Design , ISSN 0920-3796, https://doi.org/10.1016/j.fusengdes.2019.04.038. 2019

Papers in the proceedings of international conferences.

1. Tidikas A. Investigation of DEMO structural material characteristics induced by neutron irradiation // 12th international conference of young scientists on energy issues (CYSENI 2015), Kaunas, Lithuania, May 26-27, 2015. Kaunas: LEI, 2015. ISSN 1822-7554, p. 428-435.
2. Tidikas A., Stankūnas G. Neutron activation in water cooling systems of nuclear fusion devices // 13th Annual international conference of young scientists on energy issues (CYSENI 2016), Kaunas, Lithuania, May 26–27, 2016. Kaunas: LEI, 2016. ISSN 1822-7554. p. 332-340
3. Tidikas A., Stankūnas G. Influence of breeder blanket module size variation on neutron activation inventories // 14th Annual international conference of young scientists on energy issues (CYSENI 2017), Kaunas, Lithuania, May 25–26, 2016. Kaunas: LEI, 2016. ISSN 1822-7554.

List of presentations in the international conferences

1. Tidikas A. Investigation of DEMO structural material characteristics induced by neutron irradiation // 12th international conference of young scientists on energy issues (CYSENI 2015), Kaunas, Lithuania, May 26-27, 2015. Kaunas: LEI, 2015. ISSN 1822-7554, p. 428-435.
2. Tidikas, A. Radioactivity Assessment In Nuclear Fusion Reactors // Medical Physics in the Baltic States : proceedings of the 12th international conference on medical physics, Kaunas, Lithuania, 5-7 November, 2015 / Kaunas

University of Technology. Kaunas : Technologija. ISSN 1822-5721. 2015, p. 81-83.
3. Tidikas A., Stankūnas G. Neutron activation in water cooling systems of nuclear fusion devices // 13th Annual international conference of young scientists on energy issues (CYSENI 2016), Kaunas, Lithuania, May 26–27, 2016. Kaunas: LEI, 2016. ISSN 1822-7554. p. 332-340
4. Tidikas A., Stankūnas G. Neutron activation in heat transfer systems of nuclear fusion devices // 29th Symposium on Fusion Technology (SOFT 2016). 5-9 September 2016. Prague Congress Center
5. Stankūnas G. Tidikas A. Comparative Analysis of WCLL to Different European DEMO Blanket Concepts in Terms of Activation and Decay Heat after Exposure to Neutron Irradiation // 26th IAEA Fusion Energy Conference 7–22 October 2016 Kyoto, Japan
6. Stankūnas G. Tidikas A. and JET Contributors, Activity Inventories and Decay Heat of ITER Material Samples after Long Term Irradiations with 14 MeV Fusion Neutrons at JET // 9th IAEA Technical Meeting on Steady State Operation of Magnetic Fusion Devices, IAEA Headquarters, Vienna, Austria 20 - 23 March 2017
7. Stankūnas G., Cufar A., Tidikas A., Lengar I., Batistoni P. and JET Contributors, Activation Inventories and Material Damage After Exposure to DD/DT Neutrons in Safety Analysis of Nuclear Fusion Installations// Neutron and Ion Dosimetry Symposium (NEUDOS13), Kraków, Poland, 14 - 19 May 2017
8. Tidikas A., Stankūnas G. Wcll Blanket Module Structure Variation Influence On Neutron Activation Inventories// 27th IEEE Symposium on Fusion Engineering, Shanghai China, 4-8 June 2017
9. Stankūnas G., A. Tidikas, U. Fischer Activity inventories and decay heat generation of the TestCell facility of IFMIF-DONES The 13the International Symposium on Fusion Nuclear Technology ISFNT-13, 25-29 September 2017, Kyoto, Japan
10. Tidikas A. Application of sensitivity analysis in evaluation of aggregate cross-sections for irradiated EUROFER and CuCrZr alloys // 15th Annual international conference of young scientists on energy issues (CYSENI 2018), Kaunas, Lithuania, May 23–28, 2018. Kaunas: LEI, 2018. ISSN 1822-7554. p. 332-340

ANNEX

Material composition in %, with densities in g/cc. (table 3.1.2)

*** Al67O87N9**
AL 54.3562
O 41.85338
N 3.79042
DENSITY 3.70

*** Al68O84N12**
AL 54.82127
O 40.15656
N 5.02217
DENSITY 3.70

*** Al22O30N2**
AL 53.88522
O 43.57177
N 2.54301
DENSITY 3.70

*** Al23O28N5**
AL 54.50374
O 39.34536
N 6.1509
DENSITY 3.70

*** KU1**
SI 53
O 46.5
FE 0.12
AL 0.028
TI 0.01
CA 0.1
CR 0.002
LI 0.01
NA 0.03
K 0.2
DENSITY 2.21

*** Nb3Sn**
NB 11.1
TA 5.9
CU 78.5
SN 4.2
PB 0.15
ZN 0.15
DENSITY 7.8

*** Spinel**
O 45.07902
MG 16.89947
AL 38.0215
DENSITY 3.58

*** ZnS**
S 32.90305
ZN 67.09695
DENSITY 4.09

*** Al2O3**
AL 52.92507
O 47.07493
DENSITY 3.96

*** YAG**
AL 22.72635
O 32.34282
Y 44.93084
DENSITY 4.56

*** oxygen free CU**
CU 100
DENSITY 8.92

*** Al-Bronze**
AL 10.75
MN 0.5
NI 1.5
FE 4.0
CO 0.05
CU 83.2
DENSITY 7.45

*** KS-4V**
SI 53.016
O 46.515
FE 0.05
AL 0.055
TI 0.051
CA 0.04
CR 0.017
LI 0.016
NA 0.04
K 0.2
DENSITY 1.96

*** NbTi**
NB 53.9985
TI 46.9985
TA 0.002
O 0.001
DENSITY 6.0

*** JJ1**
FE 60.199
C 0.003
SI 0.52
MN 10
P 0.003
NI 12
CR 12
MO 5
N 0.2
CO 0.05
NB 0.025
DENSITY 8.0

*** SS316L(N)-IG**
FE 65.7436
C 0.012
MN 1.87
NI 12.15
CR 17.15
MO 2.36
B 0.0014
N 0.07
P 0.022
S 0.003
SI 0.31
TI 0.006
CU 0.231
NB 0.016
CO 0.047
TA 0.008
DENSITY 8.0

*** CuCrZr**
CU 99.1
CR 0.8
ZR 0.1
DENSITY 8.9

*** SS316L(N)**
FE 64.96
C 0.3
MN 2.0
NI 12.0
CR 17.0
MO 2.5
N 0.2
P 0.045
S 0.03
SI 1.00
CO 0.05
NB 0.02
DENSITY 8.0

*** SS304 Borated 1.25%**
FE 64.96
C 0.06
MN 2.0
NI 9.25
CR 19.0
MO 2.5
N 0.1
P 0.045
S 0.03
SI 0.75
CO 0.05
NB 0.01
TA 0.005
B 1.25
DENSITY 8.0

*** Alloy 660**
FE 52.74
C 0.06
P 0.03
S 0.02
AL 0.2
B 0.005
MN 2.0
NI 25.5
CR 15.0
MO 1.25
V 0.3
SI 0.75
TI 2.15
DENSITY 7.98

*** Beryllium S-65C grade**
BE 99.397
O 0.4
AL 0.03
C 0.07
FE 0.05
SI 0.03
NI 0.01
CU 0.01
U 0.003
DENSITY 1.848

*** SS316L**
FE 64.73
C 0.3
MN 2.0
NI 12.0
CR 17.0
MO 2.5
N 0.1
P 0.045
S 0.03
SI 0.75
CO 0.2
NB 0.1
TI 0.1
TA 0.15
DENSITY 7.99

*** XM-19**
FE 56.835
NI 12.5
CR 22.0
MO 2.25
MN 5.0
SI 0.75
C 0.03
S 0.03
N 0.3
P 0.045
V 0.2
CO 0.05
TA 0.01
DENSITY 7.88

Material composition in % with densities in g/cc. (table 3.1.4)

* Al-Bronze	* INCONEL 718	* SS304 Borated 1.16%	* EF973	* Alloy 660
AL 8.73	FE 17.291	FE 66.8075	FE 88.8220	FE 52.9
MN 0.18	NI 52.5	C 0.08	C 0.105	C 0.032
NI 4.96	CR 19	MN 0.74	N 0.035	P 0.01
FE 4.26	CU 0.2	NI 12.5	MN 0.55	S 0.001
SI 0.01	MO 3.05	CR 18.39	NI 0.01	AL 0.28
ZN 0.016	NB 5.125	N 0.026	CR 9.0	B 0.0059
CO 0.0005	C 0.06	P 0.016	O 0.001	MN 1.5
CD 0.0005	MN 0.3	S 0.0005	B 0.001	NI 25.4
NB 0.0005	P 0.01	SI 0.31	NB 0.005	CR 15.1
TA 0.0005	S 0.01	CO 0.05	CU 0.003	MO 1.23
PB 0.0005	SI 0.3	B 1.16	AL 0.004	V 0.27
SN 0.005	TI 0.9	DENSITY 8.0	CO 0.005	SI 0.49
CU 81.8365	AL 0.5		TI 0.001	TI 2.26
DENSITY 7.45	CO 0.75	* CuCrZr	MO 0.003	CO 0.004
	B 0.004	CU 99.15	SI 0.026	CU 0.03
*316LN TF	DENSITY 8.192	CR 0.75	V 0.2	PB 0.00005
FE 65.34		ZR 0.1	W 1.1	DENSITY 7.98
C 0.015	* 316IG	DENSITY 8.9	P 0.0015	
MN 1.8	FE 65.5736		S 0.003	* Alloy 660 div
NI 12.5	C 0.012	* XM-19	TA 0.12	FE 52.74
CR 17.0	MN 1.80	FE 56.585	DENSITY 7.87	C 0.06
MO 2.5	NI 12.25	NI 12.5		P 0.03
N 0.16	CR 17.15	CR 22.0	* SS316L	S 0.02
P 0.03	MO 2.50	MO 2.25	FE 65.472	AL 0.2
S 0.02	B 0.0014	MN 5.0	C 0.02	B 0.005
SI 0.6	N 0.07	SI 0.75	SI 0.6	MN 2.0
CO 0.05	P 0.022	C 0.03	MN 1.8	NI 25.5
DENSITY 8.0	S 0.003	S 0.03	P 0.03	CR 15.0
	SI 0.31	N 0.3	S 0.008	MO 1.25
* W	TI 0.006	P 0.04	CR 17.25	V 0.3
W 99.9707	CU 0.231	V 0.2	NI 12.5	SI 0.75
FE 0.0002	NB 0.016	CO 0.05	MO 2.25	TI 2.15
NI 0.005	CO 0.047	TA 0.01	CO 0.07	DENSITY 7.98
SI 0.01	TA 0.008	NB 0.2	DENSITY 7.99	
C 0.0003	DENSITY 8.0	DENSITY 7.88		
O 0.01				
N 0.0038				
DENSITY 19.11				

Material composition of DEMO WCLL breeder blanket.

EUROFER 97-3	wt% [10^{-2}g/g]	PbLi	wt% [10^{-2}g/g]	Tungsten	wppm [10^{-6}g/g]
Fe	balance	Pb	balance	W	Balance
B	0.001	Ag	0.001	Ag	10
C	0.105	Cu	0.001	Al	15
N	0.04	Nb	0.001	As	5
O	0.001	Pd	0.001	Ba	5
Al	0.004	Zn	0.001	Ca	5
Si	0.026	Fe	0.005	Cd	5
P	0.002	Cr	0.005	Co	10
S	0.003	Mn	0.005	Cr	20
Ti	0.001	Mo	0.005	Cu	10
V	0.2	Ni	0.005	Fe	30
Cr	9	V	0.005	K	10
Mn	0.55	Si	0.01	Mg	5
Co	0.005	Al	0.01	Mn	5
Ni	0.01	Bi	0.02	Na	10
Cu	0.003	Sn	0.02	Nb	10
Nb	0.005	W	0.02	Ni	5
Mo	0.003	Li	0.62	Pb	5
Ta	0.12			Ta	20
W	1.1			Ti	5
				Zn	5
				Zr	5
				Mo	100
				C	30
				H	5
				N	5
				O	20
				P	20
				S	5
				Si	20
Density	7.87 g/cc		9.54 g/cc		19.24 g/cc

Material composition of reduced activation steels in %

Material	Fe	C	Mn	Ni	Cr	O	B	W	Nb	Al	P	Ti	Mo	N	Si	V	S	TA	others
EUROFER (pure)	90.285	0.09	0.2		8.5			1.0						0.015		0.15		0.05	
EUROFER 97	90.46	0.11	0.4		9									0.03					
EUROFER (impure)	88.137	0.12	0.6	0.005	9.5	0.01	0.001	1.2	0.001	0.001	0.005	0.01	0.005	0.045	0.005	0.25	0.005	0.09	Cu 0.005 Co 0.005
F82H	89.898	0.093	0.17		7.5			2.01						0.006		0.14	0.16	0.023	
F82-IAE	89.5	0.1	0.1		8.0			2.0						0.05	0.1	0.2			
JLF-1	88.12	0.1	0.45		9.0			2.0						0.05	0.08	0.2			
MANET	86.3085	0.14	0.75	1	10.8		0.002		0.14		0.005		0.77		0.37	0.19	0.0045		
MANET 2	87.1505	0.1	0.75	0.65	10.3				0.14		0.0045		0.57		0.14	0.19	0.0045		
Optifer 1a	88.769	0.1	0.5		9.3		0.006	1.0						0.015	0.06	0.25			
Optifer 2	89.664	0.125	0.5		9.1		0.006							0.015	0.04	0.25			
La12lc	88.73	0.09	1.1		9.0			0.7						0.04	0.03	0.3		0.01	
LA12talc	88.64	0.09	1.1		9.0			0.7						0.04	0.03	0.3		0.1	
T91	89.31	0.1	0.4	0.13	8.2				0.01				1.0	0.05	0.5	0.3			
SS316	61.895	0.03	2.0	14.0	18.0						0.045		3.0		1.0	0.03			

Compositions of SS316 type steels in %.

Material	Fe	C	Mn	Ni	Cr	P	Ti	Mo	N	Si	S
SS316	61.865	0.06	2.0	14.0	18.0	0.045		3.0		1.0	
SS316H	65.055	0.1	2.0	12.0	17.0			2.5	0.045	1.0	0.03
SS316L	60.14	0.35	2.0	15.0	19.0	0.45		3.0		1.0	0.03
SS316LN	60.8	0.03	2.0	14.5	18.5	0.25		3.0	0.1	0.75	0.1
SS316LVM	59.96	0.03	2.0	15.0	19.0	0.25		3.0		0.75	0.01
SS316N	61.71	0.08	2.0	14.0	18.0	0.045		3.0	0.135	1.0	0.03
SS316Ti	62.27	0.08	2.0	12.0	18.0	0.45	0.7	3.0		0.75	0.03

IFMIF-DONES shielding materials. Concrete and water composition presented in atom number per 1/kg. Steel composition is presented in percentage. Densities are presented in g/cc.

*** Concrete**		***Steel**	*** Water**	
H1	1.88E+24	C 0.03	H1	1.82E+25
H2	1.08E+20	MN 1.8	H2	3.66E+21
O16	1.24E+25	NI 12.25	O16	3.65E+25
O17	4.46E+21	CR 17.5	O17	1.46E+22
O18	2.27E+22	MO 2.5	DENSITY 1.0	
SI28	5.12E+23	N 0.07		
SI29	2.51E+22	P 0.025		
SI30	1.60E+22	S 0.01		
CA40	1.04E+24	SI 0.5		
CA42	6.60E+21	CU 0.3		
CA43	1.35E+21	TA 0.01		
CA44	2.03E+22	TI 0.1		
CA46	3.73E+19	B 0.001		
CA48	1.67E+21	NB 0.1		
MG24	1.85E+23	CO 0.05		
MG25	2.25E+22	AL 0.05		
MG26	2.39E+22	O 0.002		
AL27	5.25E+23	K 0.0005		
S32	2.53E+22	BI 0.0008		
S33	1.97E+20	V 0.004		
S34	1.08E+21	ZR 0.002		
S36	4.74E+18	AG 0.0002		
FE54	3.10E+23	CD 0.0002		
FE56	4.69E+24	SN 0.002		
FE57	1.06E+23	SB 0.0005		
FE58	1.39E+22	BA 0.0005		
TI46	5.88E+22	W 0.001		
TI47	5.19E+22	PB 0.0008		
TI48	5.03E+23	FE 64.6895		
TI49	3.62E+22	FE 64.6895		
TI50	3.40E+22	DENSITY 7.93		
CR50	8.90E+20			
CR52	1.65E+22			
CR53	1.84E+21			
CR54	4.49E+20			
MN55	2.17E+22			
V50	9.39E+19			
V51	3.67E+22			
DENSITY 3.4				

Radionuclide composition of DEMO 2015 WCLL OB equatorial breeder blanket module.

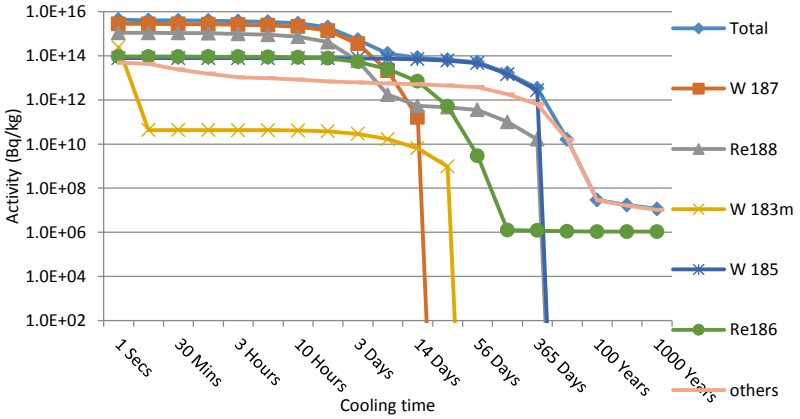

Fig 4.1. Specific activity of armour segment.

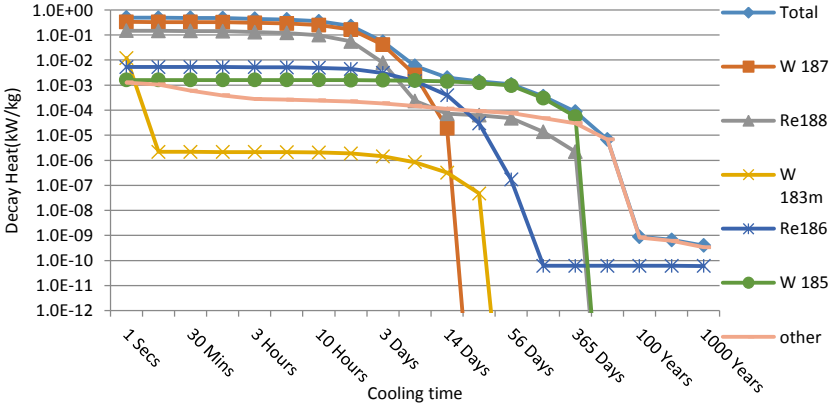

Fig 4.2. Specific decay heat of armour segment.

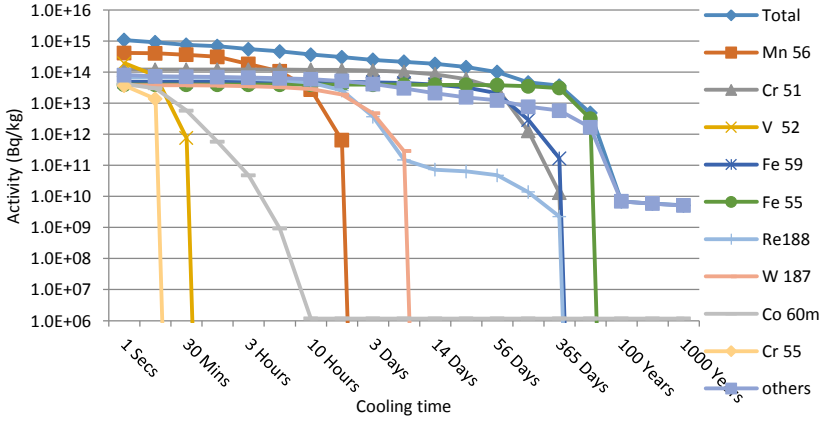

Fig 4.3. Specific activity of first wall segment.

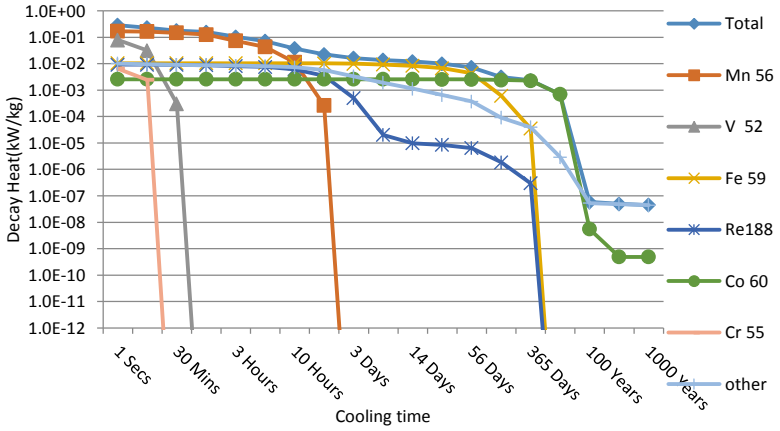

Fig 4.4. Specific decay heat of first wall segment.

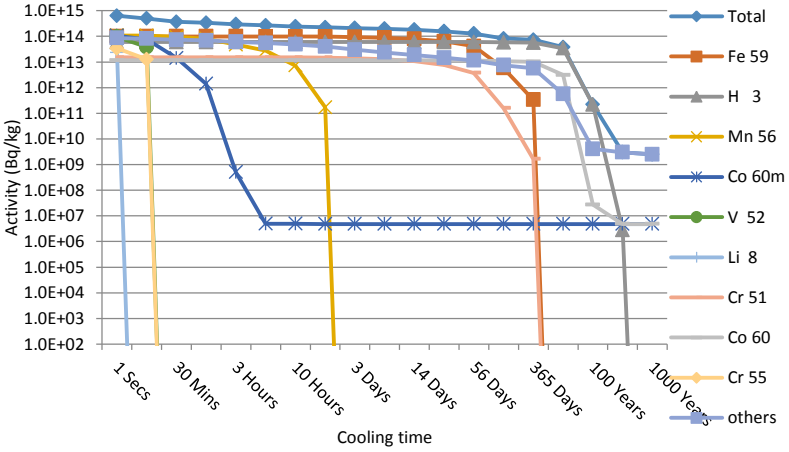

Fig 4.5. Specific activity of breeder zone segment.

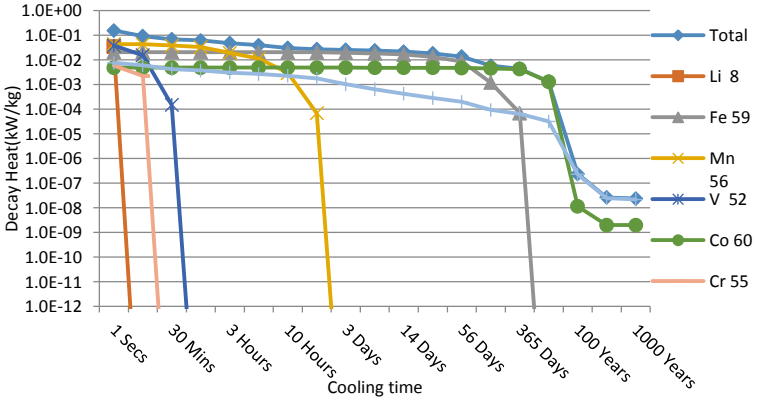

Fig 4.6. Specific decay heat of breeder zone segment.

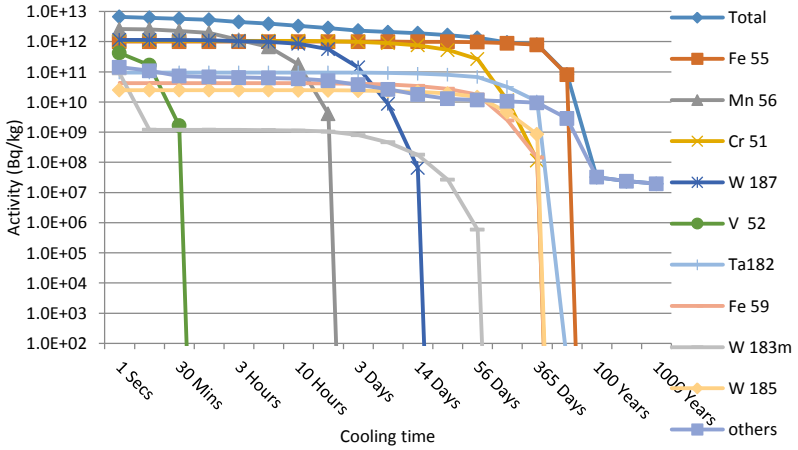

Fig 4.7. Specific activity of caps segment.

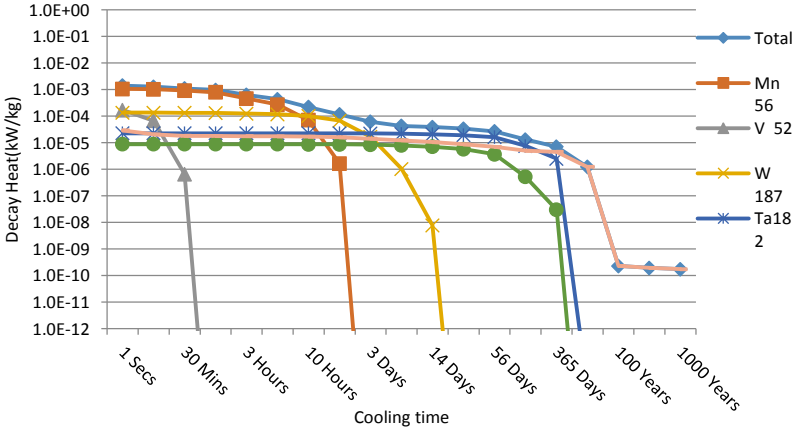

Fig 4.8. Specific decay heat of caps segment.

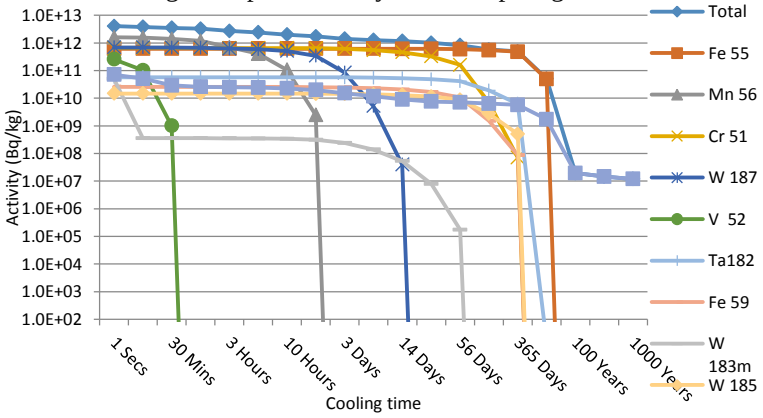

Fig 4.9. Specific activity of backplate segment.

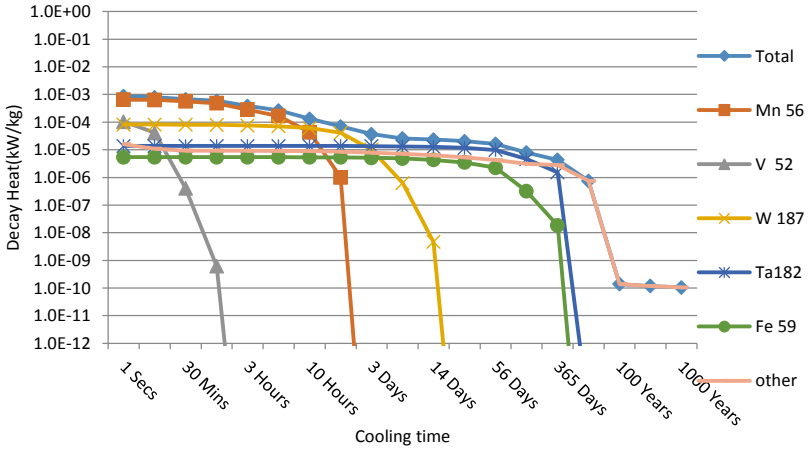

Fig 4.10. Specific decay heat of backplate segment.

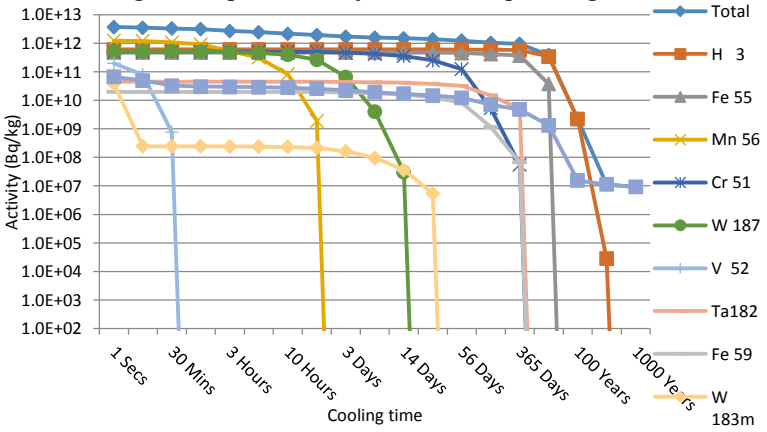

Fig 4.11. Specific activity of manifold segment.

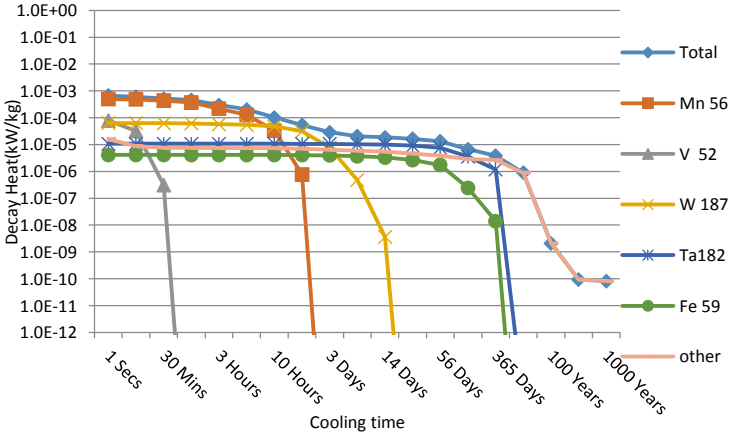

Fig 4.12. Specific decay heat of manifold segment.

SL344. 2019-07-02, 12,5 leidyb. apsk. l. Tiražas 12 egz. Užsakymas 151 .
Išleido Kauno technologijos universitetas, K. Donelaičio g. 73, 44249 Kaunas
Spausdino leidyklos „Technologija“ spaustuvė, Studentų g. 54, 51424 Kaunas